1-1-2014

Development of Specific and Potent Î±-Helical Inhibitors and Probes of Cysteine Proteases

Nataline Meinhardt
University of Pennsylvania, nataline.meinhardt@gmail.com

Development of Specific and Potent Î±-Helical Inhibitors and Probes of Cysteine Proteases

Abstract
Cysteine proteases are of great scientific and pharmaceutical interest due to their diverse roles in cellular processes and diseases. However, it has been difficult to design inhibitors for use in determining their individual roles due to the conserved active site. Interestingly, each protease has an endogenous inhibitor that forms an α-helix at the prime side of the active site. We developed a new method for stabilizing α-helices using natural amino acids that allowed us to make small peptides into α-helical inhibitors. We were then able to use structure based design to turn these α-helices into specific inhibitors and probes for use in understanding the proteases' roles in various diseases and cell processes. The use of α-helices has further implications as a new method of creating investigative tools for understanding proteases. new method of creating investigative tools for understanding proteases.

Degree Type
Dissertation

Degree Name
Doctor of Philosophy (PhD)

Graduate Group
Biochemistry & Molecular Biophysics

First Advisor
Doron C. Greenbaum

Keywords
alpha-helices, cysteine proteases, inhibitors, structure-based design

Subject Categories
Biochemistry

DEVELOPMENT OF SPECIFIC AND POTENT α-HELICAL INHIBITORS AND PROBES OF CYSTEINE PROTEASES

Nataline Meinhardt

A DISSERTATION

in

Biochemistry and Molecular Biophysics

Presented to the Faculties of the University of Pennsylvania

in

Partial Fulfillment of the Requirements for the

Degree of Doctor of Philosophy

2014

Supervisor of Dissertation

_____

Doron Greenbaum, Ph.D., Assistant Professor of Pharmacology

Graduate Group Chairperson

_____

Kate Ferguson, Ph.D., Associate Professor of Physiology

Dissertation Committee

Ronen Marmorstein, Ph.D., Professor of Biochemistry and Biophysics

James Shorter, Ph.D., Associate Professor of Biochemistry and Biophysics

E. James Petersson, Ph.D., Assistant Professor of Chemistry

Rahul Kohli, MD, Ph.D., Assistant Professor of Biochemistry and Biophysics

Scott L. Diamond, Ph.D., Arthur E. Humphrey Professor of Chemical and Biomolecular Engineering, Bioengineering

Scott Sieburth, Ph.D., Professor of Chemistry, Temple University

DEVELOPMENT OF SPECIFIC AND POTENT α-HELICAL INHIBITORS AND PROBES OF CYSTEINE PROTEASES

ACKNOWLEDGMENT

The work presented in this thesis is the result of hard work and support, both scientifically and otherwise, of a number of individuals. I'd like to first thank my advisor, Doron, for his guidance and help in developing this project and bringing it to fruition. I'd also like to thank the members of the Greenbaum laboratory and of the laboratories of all of our collaborators. Each and every one of you has fostered a unique and enthusiastic scientific community. I have appreciated all of my experiences and everything I have learned during my time with you.

I'd like to thank each member of my committee, Drs. Ronen Marmorstein, Rahul Kohli, James Petersson, and Jim Shorter. Through the years you have all been incredible in helping me organize my ideas and focus my ambitions. I'd also like to thank Drs. Scott Sieburth and Scott Diamond for being available on short notice to attend my defense and present insightful questions. I am grateful for the support and funding provided by the Biochemistry and Molecular Biophysics Graduate Group and the Chemistry-Biology Interface Training Grant.

I'd like to thank my both my immediate family, my parents, Steven and Sarah, and my brothers, Nick and Steve, and my extended family. You have always been there to support me and help me in whatever endeavor I choose. I'd like to thank my friends, especially Pat, Cathy, Nikki, Nathaniel, Vonni, Annie, Jenny, and Heather. You have always been there for me, and yes, we are effing awesome. Finally, I'd like to thank my boyfriend, Bruce. I am more thankful for you than words can express. Thank you everyone for all you have done for me.

ABSTRACT

DEVELOPMENT OF SPECIFIC AND POTENT α-HELICAL INHIBITORS AND PROBES OF CYSTEINE PROTEASES

Nataline Meinhardt

Doron Greenbaum, Ph.D.

Cysteine proteases are of great scientific and pharmaceutical interest due to their diverse roles in cellular processes and diseases. However, it has been difficult to design inhibitors for use in determining their individual roles due to the conserved active site. Interestingly, each protease has an endogenous inhibitor that forms an α-helix at the prime side of the active site. We developed a new method for stabilizing α-helices using natural amino acids that allowed us to make small peptides into α-helical inhibitors. We were then able to use structure based design to turn these α-helices into specific inhibitors and probes for use in understanding the proteases' roles in various diseases and cell processes. The use of α-helices has further implications as a new method of creating investigative tools for understanding proteases.

TABLE OF CONTENTS

LIST OF TABLES

LIST OF ILLUSTRATIONS

CHAPTER 1: Introduction

1.1 Introduction to Cysteine Proteases

Cysteine proteases are enzymes that cleave peptide bonds using a catalytic dyad consisting of cysteine and histidine.[1] The cysteine/histidine pair forms a thiolate-imidazolium ion pair in which the thiolate ion nucleophilically attacks the carbonyl carbon in the peptide bond.[2] This nucleophilic attack results in a thioester which is subsequently hydrolyzed There are multiple cysteine protease families. We are most interested in the papain superfamily, which is the largest of the cysteine protease families identified to date.[3] The papain superfamily is named after the protease papain which was first isolated from the papaya. We are specifically interested in calpain-1 and cathepsins L, S, and K due to the presence of α-helices from the endogenous inhibitor or prodomain at each respective protease active site.

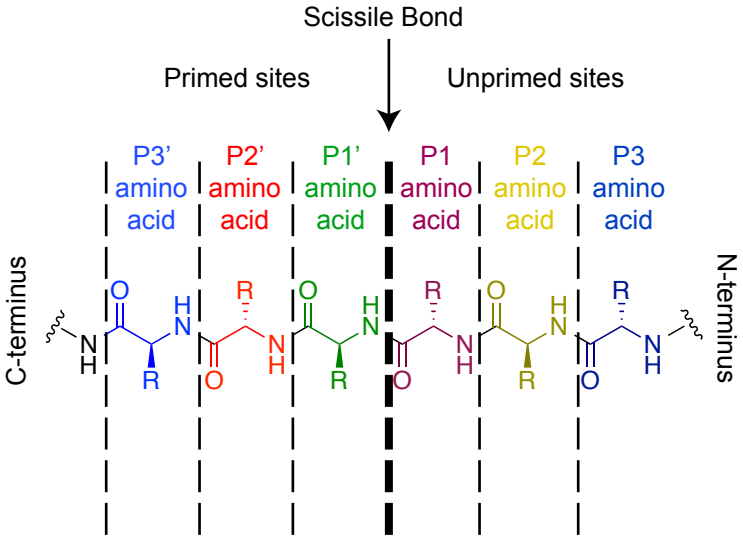

Figure 1.1. Model of substrate association nomenclature.[4,5]

Specificity of proteases usually relies on recognition of the amino acids around the scissile bond generally the three amino acids amino- or carboxyterminal to the scissile

bond.[6] Substrate amino acids are denoted by the letter P and enzyme substrate binding pockets are designated S; both are numbered according to their relative position to the scissile bond.[4,6] This numbering has both prime (P' or S') and unprimed (P or S) denotations where the unprimed side is N-terminal to the scissile bond, while the prime side is C-terminal to the scissile bond (Figure 1.1).[4] One of the main points of interest is the S1' site which is a well defined pocket that can bind hydrophobic ring systems for π-π stacking against a tryptophan.[1]

1.2 Cysteine Protease Regulation and Cellular Location

Proteases are regulated through a number of different mechanisms and located in a number of different cell types and various subcellular compartments within the cell. Calpain is regulated by both spatial, through relocation to the cell membrane, and temporal controls, through calcium flux and the endogenous, proteinaceous inhibitor calpastatin. Calpain-1 is a cytoplasmic protein generally found in all cells where it plays a role in proteolytic cleavage of the cytoskeleton.[7] Other calpains are found in specific cells, such as calpain-3 which is primarily located in skeletal muscle.[8]

Cathepsins are regulated by changes in pH and by the endogenous prodomain, which is cleaved upon activation but can still function as an inhibitor.[9] Cathepsins are synthesized as an inactive proenzyme that is converted to active enzyme through autoproteolytic cleavage.[10] Procathepsin is processed at low pH, hence cysteine cathepsins are normally found in acidic cellular compartments, i.e. in lysosome and endosomes.[10,11] Cathepsin L is generally found in all cells while cathepsin K is found in osteocytes, and cathepsin S is almost exclusively found in antigen-presenting cells, B lymphocytes, and dendritic cells.[3,11-13]

Cysteine cathepsins are suggested to function in lysosomal protein degradation where they cleave a wide assortment of substrates.[6,10] However, data increasingly supports the idea that cathepsins also function in extralysosomal activity such as at the plasma membrane or in the extracellular milieu.[6] One such example of a cathepsin with extralysosomal activity is cathepsin K which is found in the bone resorption pit. The resorption pit has a low pH and this has led to the proposal that processing of the proenzyme may actually occur in this location.[11] Due to their wide variety of locations cysteine proteases are involved in a number of diseases and cell functions

1.3 Cysteine Protease Cellular Function and Role in Disease

Cysteine proteases play critically important roles in cellular functions and disease. Cathepsin L functions to break down proteins in the lysosome and is involved in epidermal and cardiac homeostasis, prohormone processing, and autophagy.[6] Cathepsin S is found primarily in the lysosome in antigen-presenting cells where it is involved the processing of the invariant chain, the chaperone molecule, of the MHC II complex.[12-14] Cathepsin K is excreted to the bone resorption pit where it plays a role in bone remodeling by breaking down collagen fibers in osteoclast mediated bone resorption.[11] Calpains are found in the cytoplasm and are known to breakdown cystoskeletal proteins, especially spectrin. As such they are suggested to play a role in cell migration and apoptosis.[7]

Due to their roles within the cell, misregulation of cysteine proteases, either gain or loss of function, has been associated with numerous diseases.[15] Cathepsin S has been suggested to be involved in rheumatoid arthritis, multiple sclerosis, asthma, and psoriasis.[13] Cathepsin S also has elastase activity and subsequently has been implicated in

the pathogenesis of cardiovascular diseases like atherosclerosis and abdominal aortic aneurysm.[13] Increased production of cathepsin S is also related to tumor progression and angiogenesis of cancer and consequently, an adverse outcome.[16] Cathepsin L contributes to cancer cell proliferation, tumor growth, and resistance to therapy.[6,17] Excessive cathepsin K activity associated with degradation of collagen fibers leads to osteoporosis and osteoarthritis.[18] Calpains contribute to secondary degeneration after acute cellular stress such as myocardial ischemia, cerebral ischemia, or traumatic brain injury.[19,20] Hyperactivation of calpain is also correlated with amyloid diseases such as Huntington's disease, Parkinson's disease, and Alzheimer's disease.[21-23]

1.4 Prior Inhibitors of Cysteine Proteases

Due to their role in disease there has been much interest in designing inhibitors of cysteine proteases. Most inhibitors are substrate mimetics that competitively block the active site of the protease by blocking substrate turnover.[24] Often the inhibitors contain a peptide sequence with an additional reactive electrophilic moiety or 'warhead'.[17] This warhead covalently binds the catalytic cysteine either reversibly or irreversibly depending on the reactive group.[17,24]

There are a number of different warheads used for cysteine protease inhibitors. Some early inhibitors used an epoxysuccinate, diazomethyl ketone, or fluoromethyl ketone to covalently and irreversibly react with the active site cysteine.[5,16,25] The irreversibility and high potency of these inhibitors led to many off-target effects and possible metabolic consequences.[16,24] Thus, efforts have shifted to develop reversible inhibitors. A few examples of the reversible warheads have been α-ketoamides[16], nitriles[26], and azepanones[27,28].

There has been investigation into the variation of the warhead moiety, however these inhibitors have primarily focused on binding to pockets on the unprime side of the enzyme. Many of the issues associated with inhibitor development have been due to the inability to achieve selectivity due to the similarity of these unprimed side P1-P3 binding pockets of papain family cysteine protease active sites.[5] Inhibitors design has even been extended as far as the P4 pocket in an effort to increase selectivity among the family.[5,16,24,27,28]

In addition to synthesized inhibitors, cysteine proteases also have endogenous inhibitors. As mentioned earlier, the cathepsins are synthesized containing a proregion that acts as an endogenous inhibitor (Figure 1.2). *In vitro* studies have shown that the isolated propeptides retain their inhibitory activity and act as competitive tight binding inhibitors of the mature enzymes.[29] The propeptides demonstrate some selectivity but not absolute specificity.[9] Calpain, on the other hand, is not synthesized as a zymogen but relies on calcium binding for activation. However, calpain does have an endogenous proteinaceous inhibitor called calpastatin (Figure 1.2). In contrast to the cathepsin prodomains, calpastatin is absolutely specific for calpain. Interestingly, a trait all of these endogenous inhibitors share is a unique α-helix that sits at the active site blocking substrate binding.[3,11,29,30] This α-helical structure and prime side binding present a unique avenue for cysteine protease inhibitor development.

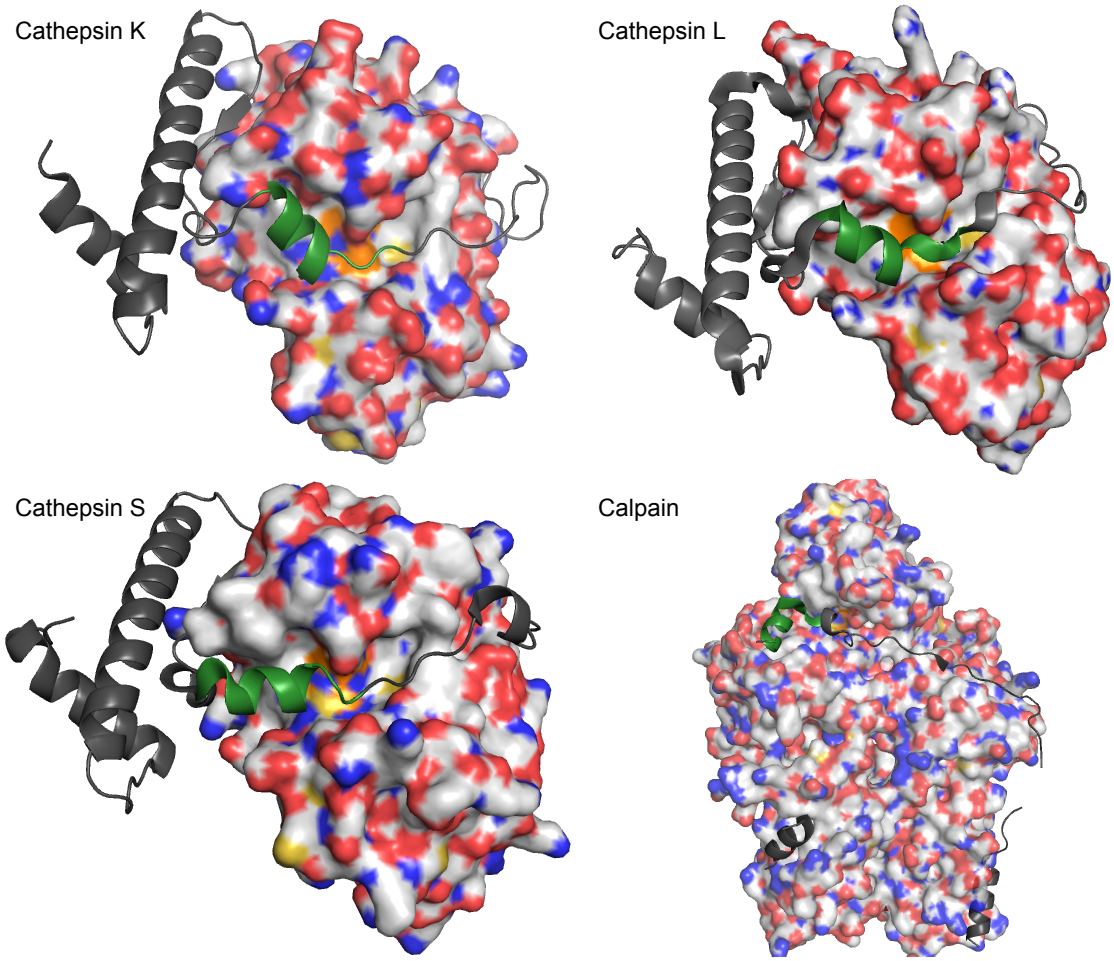

Figure 1.2. Structures of zymogen cathepsins and calpastatin bound calpain. Zymogen forms of the cathepsins have a prodomain that functions as an endogenous inhibitor while calpain has an endogenous inhibitor called calpastatin. All of these endogenous, proteinaceous inhibitors have an α-helix, denoted in green, that sits at the prime side of the active site, depicted in orange. (Cathepsin K:1BY8, Cathepsin L:1CS8, Cathepsin S:2C0Y, Calpain: 3BOW).[3,11,29-31]

1.5 α-Helix Stabilization Strategies

The α-helices in the endogenous cysteine inhibitors present an interesting avenue for protease inhibitor development. Previously, α-helices have been synthesized as peptide mimetics of larger proteins, however when a small segment is excised from the parent protein it tends to lose its secondary structure. This loss of secondary structure results in reduced efficacy, permeability, and proteolytic stability.[32] Thus, to increase the

activity of these inhibitors, various techniques have been used to stabilize the α-helices prior to binding to the enzyme.

A number of different methods have been utilized for α-helix stabilization; one of the most widely utilized is the ring closing olefin metathesis. This method was first suggested by Blackwell *et al.*, and it effectively introduces non-native carbon-carbon bond constraints.[33] However, this initial work of Blackwell *et al.* did not show an enhancement of α-helical stability but rather the creation of a 3_{10} helix.[33] The Verdine laboratory improved upon this technique by using unnatural amino acids with R or S stereochemistry, i.e. $S_{i,i+4}S$, $R_{i,i+4}R$, $R_{i,i+4}S$, $R_{i,i+7}S$, etc., and alkyl tethers of varying length (Figure 1.3).[32,34] They found that α-helical stabilization increased as the ring size of the macrocyclic cross-link is increased.[34] They subsequently named this technique hydrocarbon 'stapling'.[32,34]

A similar method for α-helix stabilization is the hydrogen bond surrogate developed by the Arora group. Hydrogen bond surrogates use the ring closing metathesis to create alkyl linkages that mimic the length and location of the hydrogen bond.[35-38] Due to the close mimicking of the hydrogen bond location this alkyl linker is on the 'inside' of the helix and does not block or remove solvent-exposed molecular recognition groups (Figure 1.3). The hydrocarbon stapling, by comparison, is on the 'outside' of the helix and uses the R-groups from two amino acids (Figure 1.3). A variation of the hydrogen bond surrogate contains a thioether instead of a double bond.[39] The reaction conditions for this linkage are milder than ring closing metathesis, and the activity of the resulting α-helices are not affected.[39] A downside of the hydrogen bond surrogate is that it uses the

amino terminus of the peptide in the linkage preventing the addition of a warhead at the N-terminus.

Another side chain stapling method using mild linking conditions is the oxime linker developed by Haney *et al*. (Figure 1.3).[40,41] The usefulness of this method is that not only can the peptide be linked in aqueous conditions but the linking strategy is reversible in water allowing for a dynamic mixture of linked and unlinked peptides.[41] A negative aspect of this reversibility though is the unlinked moiety leaves itself open to proteolytic cleavage.

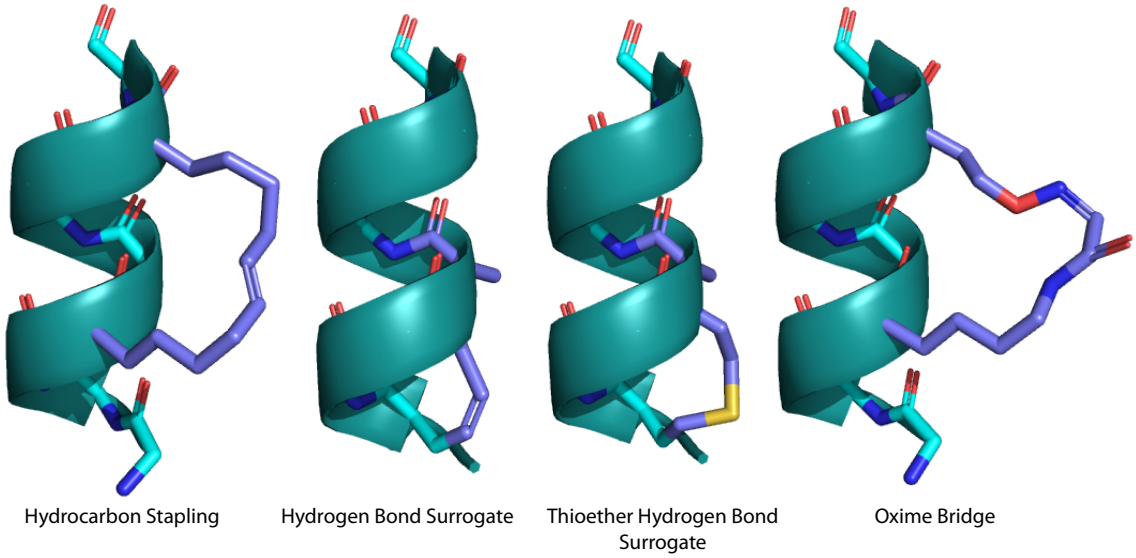

Figure 1.3. Side chain and backbone linkages stabilize α-helices. Both the hydrocarbon stapling and oxime bridge create tethers using amino acid side chains while the hydrogen bond surrogate creates a bond mimicking the backbone hydrogen bond.[31]

While the hydrocarbon stapling, hydrogen bond surrogate, and oxime linker methods have been used with good success, each method requires the incorporation of unnatural amino acids. A technique that doesn't involve unnatural amino acids or harsh conditions involves the use of cysteine residues that nucleophilically attack halogenated

aromatics. Timmerman *et al.* first used this method to stabilize single, double, and triple loops rather than α-helices (Figure 1.4).[42] Muppidi et al. adapted the technique to stabilize α-helices using a biphenyl motif to link two cysteines in an *i*, *i*+7 conformation, opposed to the *i*, *i*+4 conformation used in the other linking strategies (Figure 1.4).[43]

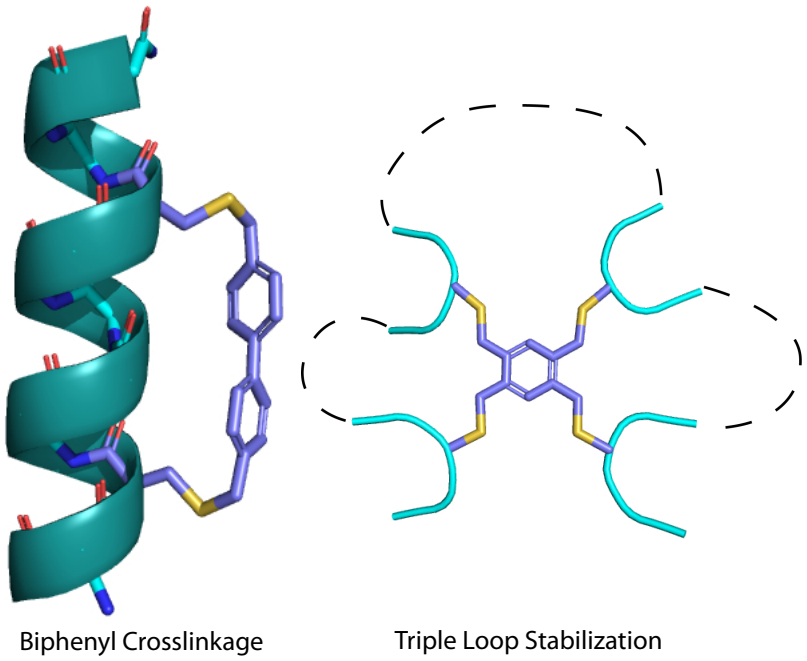

Figure 1.4. Aromatic linkers stabilize loops and α-helices via thioether bonds. These linkers have been used to stabilize multiple loops as well as α-helices.[31]

These different techniques of α-helical stabilization have been used to develop inhibitors, however these molecules have primarily been inhibitors of protein-protein interactions.[44] These α-helical inhibitors include the stabilized BH3 domain of the Bcl-2 family of proteins to inhibit Mcl-1 as a possible anti-cancer agent[45], a stabilized α-helix from the NR coactivator peptide 2 to inhibit estrogen receptor α (ERα) for development of potential therapeutics for breast and endometrial cancer and osteoporosis[46], stabilized

α-helical p53 peptide to inhibit Mdm2 as a cancer therapy[35,47], and a stabilized Jun-based inhibitor that binds to cFos as a step toward developing small molecule drugs for cancer and inflammatory diseases.[48] These stabilized α-helices have been demonstrated to be specific and potent inhibitors of their respective protein-protein interactions.

Some of the endogenous inhibitors and prodomains of cysteine proteases also have α-helices that bind to the respective protease. Based on the success of the α-helical inhibitors of protein-protein interactions and the presence of α-helical secondary structures in the prodomains of the cathepsins and the endogenous inhibitor of calpain-1, it can be postulated that a stabilized α-helix based may also be a good protease inhibitor.

CHAPTER 2: Development of α-Helical Calpain Probes by Mimicking a Natural Protein-Protein Interaction

2.1 Introduction

The primary goal of this work was to design and synthesize α-helical inhibitors as well as activity-based probes of human calpain, a calcium-regulated cysteine protease involved in a myriad of normal and pathological biological processes.[49-60] Although there has been considerable interest in the design of α-helical peptides for the study of protein-protein/receptor-ligand interactions and drug design, to our knowledge, there has been no work to date investigating α-helices as protease inhibitors.

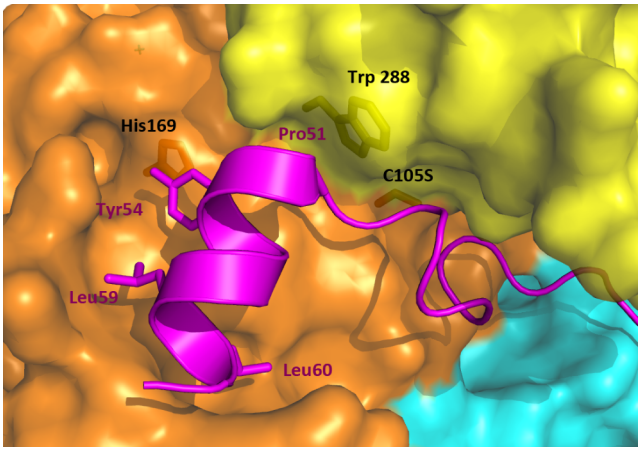

Figure 2.1. X-ray crystal structure of the calpain 2-calpastain complex (PDB ID: 3BOW). Key residues on the inhibitor, calpastatin, (purple) and calpain-2 (black) are labeled.

The text of this chapter has been published. Reprinted with permission from Jo *et al.* Development of α-Helical Calpain Probes by Mimicking a Natural Protein-Protein Interaction. J Am Chem Soc, 2012. 134(42). Copyright 2014 American Chemical Society.

Inhibitor design for this class of enzyme has historically focused on the use of peptidomimetics that fit into the active site cleft in a substrate-like manner and utilize covalent, reversible or irreversible reactive groups to react with the active site cysteine.[61-68] The problems with this approach are twofold: 1) the papain superfamily has a highly conserved active site cleft, which complicates identification of peptidomimetic side chains that differentially bind to individual enzymes, and 2) small peptides do not bind well to calpains.

To overcome this problem we took inspiration from the recent co-crystal structure of calpain with its endogenous protein inhibitor, calpastatin and from calpain inhibitors containing constrained scaffolds or macrocycles.[30,69-72] Calpastatin is unstructured in solution; however, upon binding to active calpain it drapes across the entire protein and undergoes structural rearrangements to form three α-helices that contact three different domains of the enzyme. One of these α-helices binds adjacent to the prime side of the active site cleft (Figure 2.1), forming a number of energetically favorable interactions between apolar sidechains that become buried upon complex formation. We therefore hypothesized that this α-helical motif would provide increased specificity via its unique binding mode since the helix avoids the highly conserved region of the active site while still inhibiting substrate access to the active site cleft.

This two-turn α-helix represents a ten-residue peptide. Previous work indicated that small peptides were poor inhibitors of calpains.[7,73] We corroborated this idea by determining that the minimal calpastatin fragment peptide that formed the two-turn α-helix (IPPKYRELLA) did not inhibit calpain (K_i >100 μM). We reasoned that the entropic cost of forming an α-helix from a random coil limited the ability of small

peptides to inhibit the enzyme; thus we decided to design a stabilized version of this peptide to minimize unfavorable conformational entropy.

Several strategies have previously been developed for α-helix stabilization involving main- or side-chain modifications including: disulfide bond formation,[74-76] hydrogen bond surrogates,[77,78] ring closing metathesis,[33,79-81] cysteine alkylation using α-haloacetamide derivatives[82] or biaryl halides,[43] lactam ring formation,[83-89] hydrazone linkage,[90] oxime linkage,[91] metal chelation,[92,93] and "click" chemistry.[94,95] Of the different methods used to stabilize these structures, the inclusion of a semi-rigid cross-linker[96-104] has been particularly successful, and is explored herein.

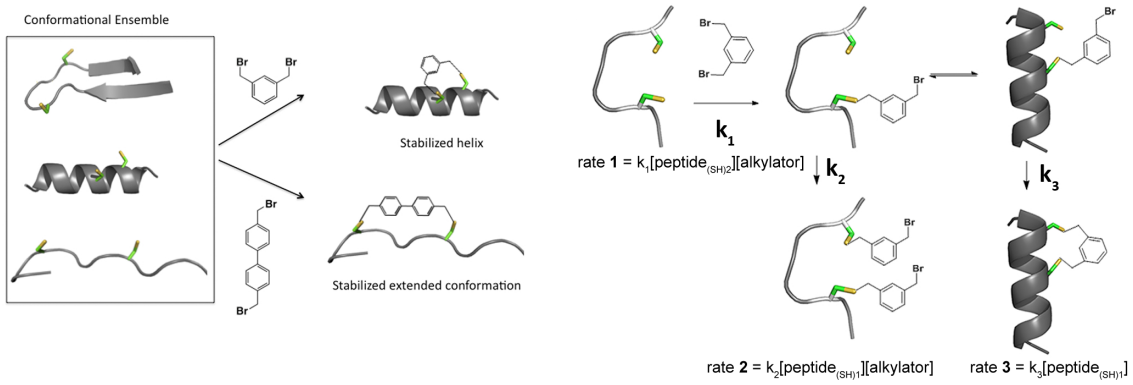

Figure 2.2 Conformational restriction via crosslinking (left). Kinetic "selection of the fittest" reaction. Hypothetical rate constants are denoted by k_1, k_2, and k_3 (right).

2.2 Results and Discussion

2.2.1 Design of template-constrained cyclic peptides stabilizing an α-helix conformation.

Peptides are intrinsically flexible chains, which rapidly interconvert among a large ensemble of conformations, including canonical secondary structures (α-helices,

reversed turns, β-hairpins, etc.). Generally, only one of these conformations is required to bind a given receptor/enzyme, and very large changes in affinity (>10^4) can be realized by simply restricting the structure to a single conformational state.

We were particularly interested in conformational restriction via cysteine alkylation[105-108] for its chemical stability, selectivity, cost effectiveness, and ease of introduction via standard mutagenesis into recombinantly expressed peptides or proteins or by solid-phase peptide synthesis. Importantly, a number of structurally diverse thiol reactive crosslinkers are also commercially available. Thus, we envisioned that the bioactive conformation of a given peptide could be stabilized by identification of the optimal cysteine crosslinker from screening a library of crosslinkers on a peptide with two cysteines anchored in appropriate positions. We refer to α-helical peptides stabilized in this manner as template-constrained peptides.

Figure 2.2 (left) shows the fundamental concept of template-constrained cyclic peptides, in this case accomplished *via* sidechain-to-sidechain cyclizations. To do this, a pair of cysteine residues is installed at appropriate positions in order to stabilize a local conformation. Here, we placed the cysteine residues at *i, i+4* positions, because this spacing brings two thioether residues into proximity when in the α-helix. In a series of parallel reactions we react the peptide with an indexed array of different crosslinking agents. Bis-alkylators with sufficient reactivity to alkylate thiols will cleanly form cyclic peptides, if the macrocycle can be formed in a low-energy conformation that matches one of the low-energy conformations of the peptide. For example, a meta-xylyl group, which matches the inter-thiol distance of the cysteine sidechains when in an α-helical conformation, should stabilize this helical structure. By contrast, the much longer

distance of the 4,4'-biphenylmethyl group would not be consistent with the α-helical conformation, and would instead favor formation of a more extended conformation. Thus, depending on the template, it should be possible to stabilize any one of a number of conformations.

We use a kinetic "selection of the fittest" method, to screen for only those linkers that help select stable, low-energy conformations over more strained conformations. The kinetic scheme for cyclization requires two steps (Figure 2.2, right): The first step involves the second-order alkylation of the dithiol-peptide, which depends on the concentration of both the alkylating agent and the peptide (rate **1** = $k_1[peptide_{(SH)2}][alkylator]$). The rate of this reaction depends on the chemical nature of the alkylator, but to the first approximation is largely independent of the peptide structure, which is largely in a random coil in the linear form. Once mono-alkylated, the second-order process of reacting with a second equivalent of the alkylating agent (rate **2** = $k_2[peptide_{(SH)1}][alkylator]$) will compete with the desired first-order cyclization process (rate **3** = $k_3[peptide_{(SH)1}]$). (Solvolysis reactions of the mono-alkylated product also compete with cyclization.) The cyclization reaction depends on the ability of the peptide to reach a stable, strain-free conformation as it enters the transition state for cyclization, which we presume is geometrically similar to the product for large macrocyclic rings such as those formed here. Thus, the ratio of bis-alkylated to mono-alkylated compound provides a quantitative measure of the ease of cyclization that is dependent on the conformation of the cyclic form of the peptide. Bis-alkylation is dependent on the concentration of the peptide while cyclization is independent of this parameter, therefore it is possible to select for the most efficient crosslinkers by simply running the reaction at

a fixed peptide concentration with increasing concentrations of bis-alkylators and examining the product distribution by mass spectrometry.

In summary, the current method of template-constrained thioether cyclization involves several steps: 1) Screening for cross-linking agents with appropriate reactivity and ability to form cyclic products under favorable conditions with nearly equimolar amounts of peptide and bis-alkylator. 2) Examining bis-alkylator "hits" with increased stringency, using higher molar concentrations of alkylators in large excess of the peptide. This step should provide template-constrained peptides with relatively strain-free conformations. 3) Testing the template-constrained peptides to determine which have been stabilized in the appropriate conformation. This can easily be accomplished by circular dichroism (CD) spectroscopy for an α-helix. 4) Finally, determining the impact of stabilizing the helix on the ability of the peptide to bind to a protein known to recognize the sequence in a helical conformation.

To explore template-constrained cyclization to stabilize α-helices in aqueous solution, we used the model peptide **1 (**sequence: Ac-YGGEAAREACARECAARE-$CONH_2$) which was similar to the FK-4 peptide previously described (Table S2.1 Supporting Information).[109] The model peptide exhibited a low to moderate level of helicity without any stabilization.

Scheme 2.1. Helix stabilization via screening of 24 crosslinkers.

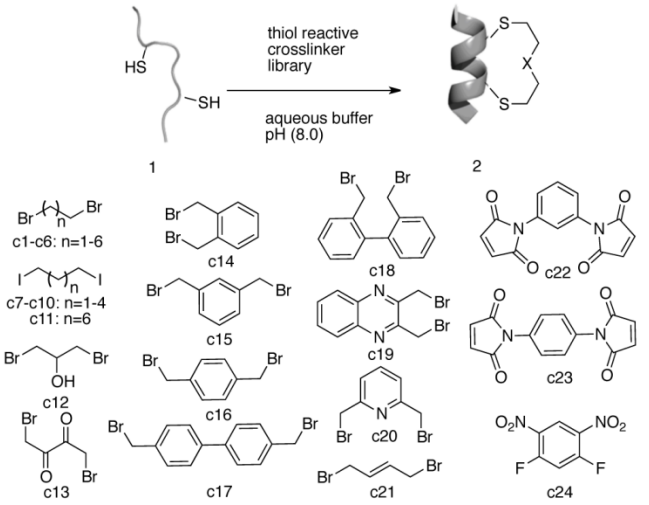

We screened twenty-four crosslinkers for cys-thioether macrocyclizations. The crosslinkers included alkyl bromides **c1-c6**, **c12,** and **c13**, alkyl iodides **c7-c11**, benzyl bromides **c14-c20**, allyl bromide **c21**, maleimides **c22** and **c23** and an electrophilic difluoro-benzene **c24** (Scheme 2.1). The initial screening reaction was performed in a 96-well plate format to identify crosslinkers that react with cysteine thiols under mild conditions (bicarbonate buffer, pH = 7.5 to 8.0) at room temperature. The crude reaction mixture was analyzed by MALDI-TOF mass spectrometry to identify any crosslinker that was a "hit". Additional HPLC profiling can characterize product distribution.

Product distribution was analyzed using MALDI-TOF and revealed that cysteine alkylation did not occur when simple alkyl halides **c1-c12** were used; only intramolecular disulfide bond formation due to oxidation was observed to occur.[110] Even when the leaving group was changed from bromide to the more reactive iodide **c7-c11** alkylation reactions failed under these aqueous conditions. The crosslinking reaction with 1,4-dibromo 2,3-butanedione **c13** produced a complex mixture of products. Crosslinking reactions with the maleimide crosslinkers **c22-c23** also resulted in a mixture of epimeric

products that were further complicated by hydrolysis of the imide (Figure S2.1 Supporting Information). Reactions using 1,5-difluoro-2,4-dinitrobenzene **c24** resulted in a similar complex mixture of products. For the biaryl derivatives **c17, c18**, predominantly unreacted peptide was detected (MALDI-TOF and HPLC) accompanied by traces of the desired, cyclized product (Figures S2.1 and S2.2 Supporting Information).

The cleanest macrocyclization resulted from the reaction[111,112] with benzylic/allylic halides **c14-c16** and **c19-c21,** which provided the major peak of the cyclization product as seen by MALDI-TOF and HPLC trace analysis (Figures S2.1 and S2.2 Supporting Information). We then tested the crosslinker "hits" **c14-c16** and **c19-c21** under the conditions designed to increase the rate of bis-alkylation over cyclization (by increasing the concentrations of alkylating agent and peptide in solution). HPLC analysis of the "selection of the fittest" showed that the 1,3-bis(bromomethyl) benzene (α,α'-dibromo-*m*-xylene) crosslinker **c15** and 2,6-bis(bromomethyl)pyridine crosslinker **c20** gave the cleanest formation of the desired macrocycle (Figure S2.3 Supporting Information). By contrast, crosslinking with allyl crosslinker **c21** produced multiple peaks. It is interesting that the *m*-xylene crosslinker **c15** was most successful crosslinker out of the three α,α'-dibromoxylenes **c14-c16**, considering that all the three alkylating agents have relatively different reactivity profiles (ortho>meta>para).[106]

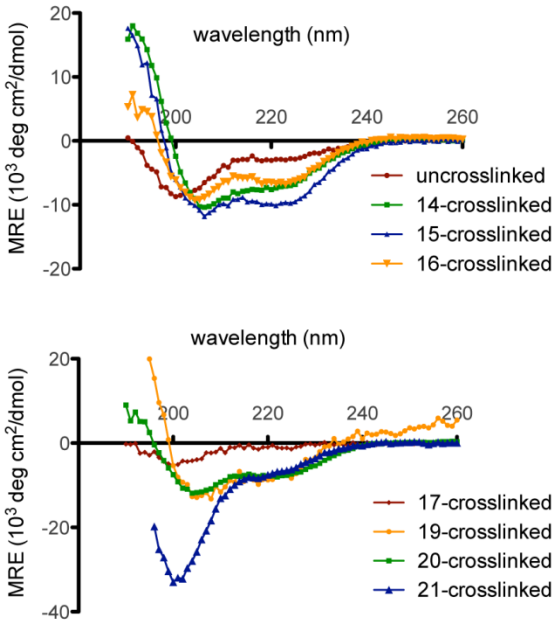

Figure 2.3. CD spectra of the model peptide and the crosslinked peptides in phosphate buffer [50mM, pH=7.0, 25 ^{o}C].

We next evaluated the CD spectra of these selected template constrained cyclic peptides to determine the effect of the template on their coil-helix equilibria (Figure 2.3). The determination of secondary structure was complicated somewhat by the fact that the spectra are generally interpreted using the intensity of θ_{222}, which requires knowledge of the concentration[113], generally by measuring the absorbance of an N-terminal Tyr residue. Some of our linkers contain aromatic groups that could absorb at 278 nm and complicate concentration determination. Therefore, we use dry weight to estimate the concentration, which results up to a 25% error in concentration determination (assessed by comparing gravimetric versus spectrophotometric determination of peptides containing Tyr chromophores and lacking other groups). Because θ_{222} is not accurately measured, we therefore interpret the data largely based on the shape of the spectra, particularly the ratio of the peak shape and relative intensities of the two exciton-coupled

π-π' bands at 190 nm and 208 nm relative to that of the n-π' band near 222 nm.[114] The three xylene-based crosslinkers **c14-c16** all showed an increase of the helicity in the CD spectroscopy analysis. Notably, the *m*-xylene based crosslinker **c15** showed the most increase in helicity followed by *o*-xylene **c14** and finally *p*-xylene **c16**.

Interestingly, the CD spectrum of the crosslinked peptides by crosslinkers **c17** and **c21** showed some structural differences from those seen using the xylene crosslinkers. As expected, the 4,4'-biphenyl (**c17)** crosslinked peptide showed little helicity, likely due to destabilization of the α-helix and stabilization of an extended conformation of the peptide because the end-to-end length of the biphenyl template is much longer than the typical α-helix pitch. Likewise, peptide crosslinked with the butenyl derivative **c21** showed a CD spectrum with a deep minimum near 200 nm, similar to that of the random coil (Figure 2.3). It would be interesting to test whether this peptide**,** after the reduction of the double bond, could stabilize a 3_{10} helix as shown in the Grubbs's work[33]. This crosslinker could be an alternative to ring closing metathesis (RCM) stapling and subsequent double bond reduction strategy.

Heterocyclic templates were also capable of stabilizing the α-helix. 2,3-quinoxaline **c19** and 2,6-pyridine **c20** crosslinked peptides showed CD spectra similar to those of the *o*-xylene **c14** and *m*-xylene **c15** crosslinked peptides (Figure 2.3).

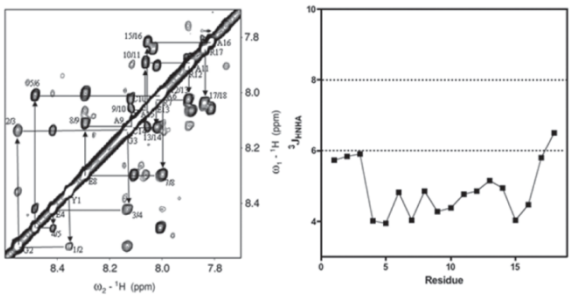

Figure 2.4. NMR of *m*-xylyl c15-constrained cyclic peptide (left). NOE sequential walk of backbone amide region of NOESY (250 ms) for the peptide. The cross peaks are labeled as NH(*i*)/NH(*i* + 1) $^3J_{NH-HA}$ coupling as function of residue (right). The small $^3J_{NH-HA}$(<6Hz) and strong sequential NH-NH NOEs denote helix formation in the peptide.

NMR spectroscopy experiments demonstrate that the cyclic template restraint strongly stabilized the helical conformation within the macrocyclic ring, and that the helix extended towards the C-terminus of the peptide (Figure 2.4). Typical stepwise NH(i)/NH(i + 1) NOE connections were observed from the first residue to the last residue, which are indicative of a helical conformation. Closer inspection showed that the cross-peak intensity became stronger after the residue 6, suggesting that the crosslinked region in the helix was more organized than frayed region of the N-terminus, which included two glycines. Furthermore, $^3J_{NH-HA}$ coupling was evaluated by the INFIT (inverse Fourier transformation of in-phase multiplets) procedure.[115] The J coupling constant is a good indicator of secondary structure. It is generally averaged to ~7 Hz if the residue is in a random coil or in equilibrium between different structures. It is less than 6 Hz if it is in α-helical structure and is larger than 8 Hz if the secondary structure is a β-sheet. Our J coupling constant was mostly below 6 Hz suggesting an α-helical structure. In addition, the chemical shift index of α-H strongly demonstrated helix formation even in the fraying N-terminus. Secondary chemical shifts which were

calculated by subtracting the experimental values from the intrinsic values and clearly showed the effect of the crosslinker. The most dramatic changes were observed on Cys10, Ala11, Arg12 and Cys14, influenced in part by the anisotropy effect from the benzene ring in the crosslinker (Figure S2.4 Supporting Information).

2.2.2 Application of *i, i+4 m*-xylene crosslinker-based stabilization for calpain inhibitor design.

Turning back to calpain inhibitor design we chose to use the calpastatin fragment IPPKYRELLA (previously shown to be inactive against calpain) as the backbone since this sequence, in the context of full-length calpastatin, forms a two-turn helix in the prime side of the active site of calpain-1 as shown in figure 1. Three different sets of double cysteine mutants, **3a-c,** along with their *m*-xylene crosslinked partners, **3a-c,** were synthesized (Figure 2.5, Table S2.3 Supporting Information). Cysteine locations were chosen by both visual inspection and virtual alanine scanning mutagenesis (Table S2.2 Supporting Information) so as not to disturb key interactions at the protein-helix interface, which includes Pro51 (inhibitor) ring stacking against Trp288 (calpain) and Tyr54 (inhibitor) H-bonding to His169 (calpain) as shown in Figure 1.

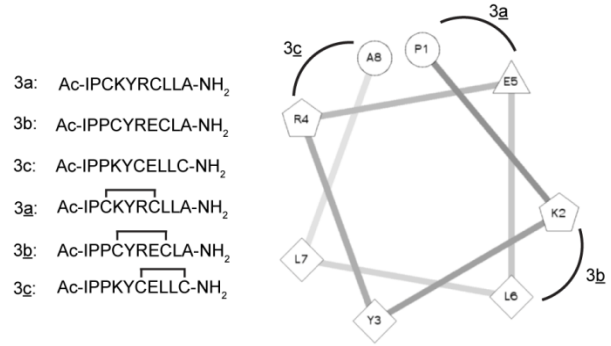

Figure 2.5. Sequence of double cysteine mutants (3a, 3b, and 3c) and their crosslinked counterparts (3a, 3b, and 3c) (left). A helical wheel representation to indicate the crosslinked regions (right).[116] ⌐¬ denotes the *m*-xylyl c15 crosslinking between the cysteines.

Next, the difference in structural changes as a result of cysteine crosslinking was examined via CD spectroscopy (Figure 2.6).[113,117] The helical content of the uncrosslinked peptides was low in the absence of added trifluoroethanol (TFE), so the experiments were conducted in the presence of 40% TFE.[118] CD analysis revealed a clear trend whereby all unlinked peptides showed little secondary structure, while the crosslinked peptides demonstrated varying degrees of α-helicity. Peptide **3c** showed the greatest helicity after crosslinking, followed by **3b**, while **3a** showed negligible helicity after crosslinking. The lack of increased helicity for **3a** may be due to the fact that it lacks the proline that is frequently found as an helix initiator of an α-helix.[119] A possible salt bridge between the glutamic acid and lysine may also be enhancing helical content in **3c**.[120-122] Thus, we believe that the primary sequence of the peptide as well as the crosslinker can influence the final helical content of the product peptide.

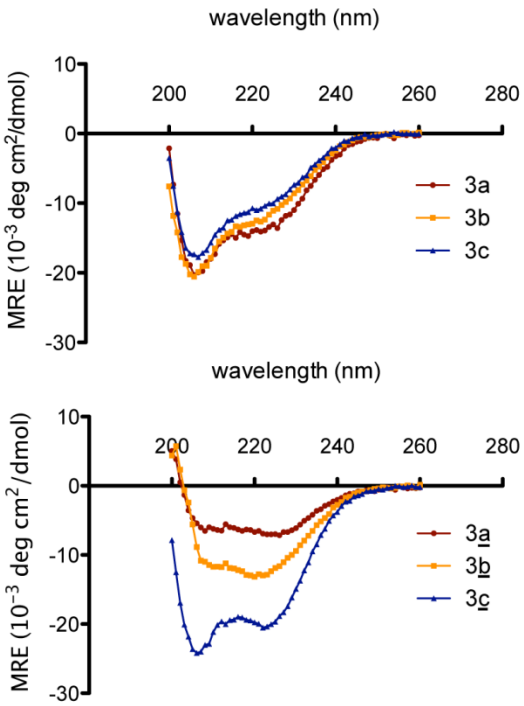

Figure 2.6. CD spectra of uncrosslinked peptides 3a-c (top) and crosslinked peptides 3a-c (bottom), [~125 μM peptide, 50 mM Tris (pH 7.5), 40% TFE]. Crosslinked peptide 3c demonstrates the greatest helical content. (See Figures S2.5 and S2.6 in Supporting Information for CD analysis without 40% TFE.)

The inhibitors, both crosslinked and uncrosslinked, were tested for their ability to inhibit calpain-1 (Table 2.1, Figure S2.7 and S2.9 Supporting Information). No appreciable inhibition (K_i >100 μM) of calpain-1 was observed for the uncrosslinked peptides **3a-c**. These results corroborate previous reports stating that the minimum length of a standard calpastatin derived peptide needed to achieve reasonable calpain inhibition is 27 amino acids long.[123] However, the crosslinked peptide, **3c**, which is only 10 amino acids long, showed good inhibition of calpain-1 in the low micromolar range (Table 2.1, Figure S2.9 Supporting Information). Furthermore, a trend relating higher helical content (Figure 2.6) positively correlated with better inhibition of calpain-1 (Table 2.1). This trend is likely directly related to helical content stabilized by the crosslinker **c15**,

although it is also possible that the crosslinker itself could contribute to enzyme recognition of the inhibitor.

Peptide	**3a**	**3b**	**3c**	**3a**	**3b**	**3c**
Calpain-1 (μM)	>100	>100	>100	>100	95.6 ± 25.5	10.2± 2.9

Table 2.1 K_i against calpain-1. [124] The calpain assay was done as described in Materials and Methods.

Kinetic studies were then performed to understand the mechanism of **3c** inhibition of calpain-1; standard Michaelis-Menten and Lineweaver-Burke analysis showed that **3c** behaved as a competitive inhibitor (Figure 2.7, Figure S2.10 and Table S2.4 Supporting Information). These results are consistent with the idea that **3c** binds to the α-helix binding site in the primed side of the active site of calpain and physically blocks substrate binding, and subsequently proteolysis, as predicted from the initial co-crystal data (Figure 2.1).

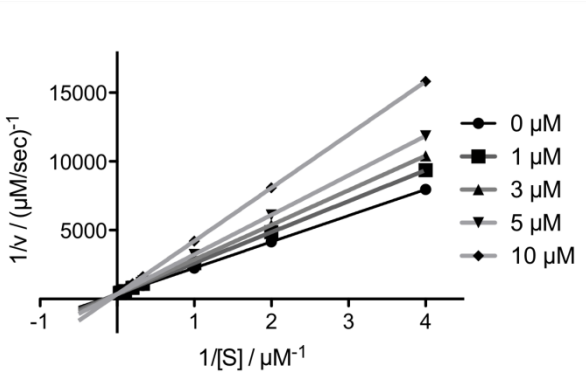

Figure 2.7. Lineweaver-Burke analysis shows that calpain inhibitor 3c to be a competitive inhibitor. Lineweaver-Burke plot was constructed from standard Michaelis-Menten kinetics.

There has been considerable difficulty in achieving good selectivity within the papain superfamily of enzymes as these enzymes contain highly conserved active

sites.[30,125] To determine whether the helical inhibitor **3c** was specific for calpain we tested it against a set of canonical papain family cysteine proteases including: papain, cathepsin B and cathepsin L (Table 2.2, Figure S2.11 Supporting Information). Significantly, no inhibition (K_i> 100 μM) was observed using the crosslinked peptide **3c** against papain or cathepsin B. The inhibitor was about four fold more potent against calpain over cathepsin L (K_i=39.9 ± 1.09 μM). These results indicate that this α-helical motif may represent a uniquely selective binding element for inhibition of calpains and further validates our structure-based approach. Furthermore, structure activity relationship studies of these helical inhibitors may result in a more potent and specific inhibitors of calpain and also shed some light on to how the calpastatin helix interacts with human calpains.

Enzyme	Calpain-1	Papain	Cathepsin B	Cathepsin L
3c (μM)	10.2 ± 2.9	>100	>100	39.2 ± 1.1

Table 2.2. The K_i of crosslinked inhibitor 3c against other papain family proteases.

The crosslinking reaction was performed with the crosslinker **c15** and the three peptides in aqueous buffer system. However, in instances where there are multiple cysteines, we believe that solid-phase cysteine crosslinking could be useful for selective crosslinking. To this end, we tested the on-resin crosslinking the peptide **3c**. Fmoc-Cys(Mmt)-OH was used instead of Fmoc-Cys(Trt)-OH and selective deprotection of specific cysteine side chains was achieved by 1% TFA/DCM treatment while the peptide was still resin bound.[126,127] (See the Materials and Methods). The same kinetic results were achieved with on resin crosslinked inhibitor.

Based on our initial success with a stabilized, α-helical-based inhibitor of calpain we next endeavored to develop an activity-based probe (ABP) specific for calpains. ABPs are complementary chemical tools to traditional genomic and proteomic techniques; ABPs are used for identification of enzymatic targets and to evaluate dynamics of enzyme activity regardless of levels of expression.[128-133] This is important because in many cases translation and transcription do not correlate with enzyme activity[134]; this is especially true for calpains as their proteolytic activity is finely regulated post-translationally by intracellular calcium levels. Basic ABP design includes a mechanism based inhibitor, a specificity element, and a tag (Figure 2.8, top). In this case, the crosslinked peptide **3c** was used for the specificity element and the succinyl epoxide functions as the warhead group that reacts with the cysteine thiol. This warhead has been established to react in a mechanism dependent manner only with active papain family proteases[135]. Three dipeptide linkers (NM-01, 02, and 03) of different lengths and rigidities were chosen via visual inspection in PyMOL[31] based on the crystallographic structure of calpastatin-bound calpain 2 (PDB code 3BOW).[30] Lastly, we chose to use either biotin or fluorescein isothiocyanate (FITC) as a tag.

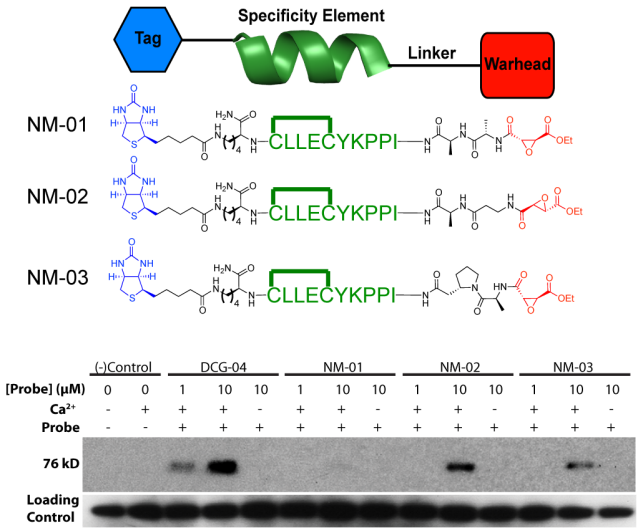

Figure 2.8. Design of a calpain specific ABP (top). ABPs contain a mechanism based inhibitor, specificity element, and tag. Only the chemical structures ABPs containing a biotin tag are shown here. ⌐¬ denotes the *m*-xylyl c15 crosslinking between the cysteines. ABP binding to calpain-1 (bottom). The linker length and rigidity between the crosslinked peptide and succinyl epoxide was evaluated via reaction with calpain-1 *in vitro*. A five-carbon backbone, flexible linker appears optimal. Loading control lanes beneath the panel show Western blot analysis using anti-calpain-1.

We used three different amino acid sequences as linkers: alanine-alanine, β-alanine-alanine, and alanine-β-homoproline, (NM-01, NM-02, and NM-03, respectively) (Table S2.5 Supporting Information). NM-01 is the shortest linker by one carbon but has similar flexibility as NM-02. NM-02 and NM-03 should cover a similar distance between the helix and succinyl epoxide, however the β-homoproline provides more rigidity than the β-alanine.

To evaluate the best linker, we initially tested biotinylated versions of either NM-01, -02, or -03 on purified, activated calpain-1 at two concentrations, 1 and 10 μM, and on unactivated calpain at 10 μM (Figure 2.8, bottom). Each ABP was added to purified calpain (pH 7.0), followed by the addition of calcium to activate the enzyme. The probe was allowed to react for 20 min. at room temperature. No calcium addition was used as a

control to demonstrate that labeling only occurred with active calpain, and DCG-04, a pan-papain family cysteine protease ABP[135], was used as a positive control as it is known to label calpains. Samples were analyzed by SDS PAGE electrophoresis; proteins were transferred to PVDF membrane and analyzed by western blot for biotin using streptavidin-HRP. Our results show that two ABPs, NM-02 and NM-03, labeled calpain in an activity dependent manner, which indicated that an extra carbon in the amino acid backbone of the linker was necessary for the epoxide to react with the active site cysteine (Figure 2.8). The intensity of the bands in the blot suggested that the use of the linker β-alanine-alanine resulted in the most potent probe (NM-02) (Figure 2.8, bottom). The ABP with the alanine-β-homoproline linker (NM-03) also bound to calpain but the rigidity in the linker induced by the pyrrolidine ring in homoproline may have contributed to less labeling. These results further support our hypothesis that the helix is binding at the active site as measurements of the probe visualized in PyMOL[31] show that a β-alanine-alanine linker would position the epoxide at the correct distance from the active site cysteine.

The presence of the succinyl epoxide warhead could reduce the specificity of the inhibitor due to its reactivity against most papain family active site cysteines. However, based on the previous kinetic studies, we reasoned that if the crosslinked peptide bound to the enzyme followed by a covalent reaction between the warhead and the active site cysteine, the ABPs had a high probability of being specific for calpain despite the addition of this reactive warhead. To investigate the specificity of NM-02, we tested a FITC tagged NM-02 against calpain-1 and calpain-2, and a panel of papain family proteases including papain, cathepsin B, and cathepsin L (Figure 2.9). FITC-NM-02 was

added in increasing concentrations to either papain, cathepsin B, or cathepsin L and allowed to react for 20 min. at room temperature. Labeled enzymes were analyzed by SDS-PAGE and were visualized using a flatbed fluorescent scanner (Typhoon). We found that even at 10 μM, NM-02 did not bind to any of the other papain family cysteine proteases, which was in good agreement with the K_i (Table 2.2) determined in the binding studies of the crosslinked peptide **3c**. This further suggests that NM-02 is specific for calpain at concentrations that would be appropriate for protease labeling experiments.

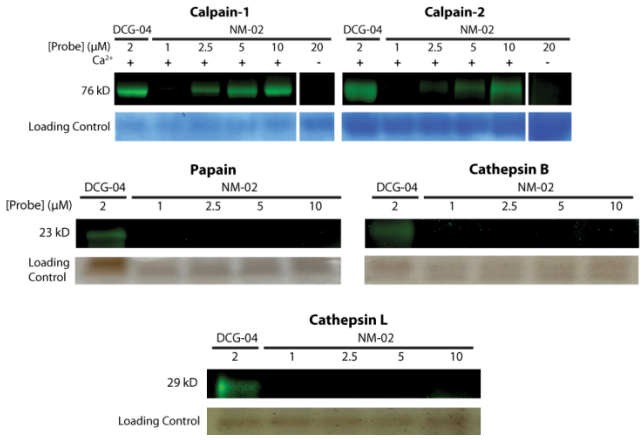

Figure 2.9. FITC-NM-02 as a calpain specific ABP. We tested FITC- NM-02 (probe) *in vitro* against purified calpain-1, calpain-2, papain, cathepsin B, and cathepsin L. Only active calpain-1 and -2 are labeled and both are increasingly labeled with increased amounts of probe. Papain, Cathepsin B, and Cathepsin L are not labeled by NM-02. Loading control lanes beneath each panel show colloidal blue staining or silver staining of the respective gel.

2.3 Conclusions

In summary, we have demonstrated a simple screening of inexpensive, commercially available crosslinkers on an *i*, *i*+4 double cysteine mutant peptide to identify the best crosslinker to stabilize an α-helix. We identified five crosslinkers that increase α-helical character. Out of these five crosslinkers, dibromo-*m*-xylene, **c15**,

reacted in a simple, one-pot reaction, both in solution and on solid-phase, with the cysteine side chain and best increased the helicity of the peptide.

We have also applied this helix stabilization method to mimic a protein-protein interaction between a protease and its endogenous protein inhibitor to create, to our knowledge, the first active site directed, α-helical inhibitor of a protease. Importantly, we demonstrate that this inhibitor is shows good potency and high specificity for calpains over other highly similar cysteine proteases.

Lastly, we show that we can use the α-helical inhibitor as a scaffold to create an activity-based probe for examination of calpain activity. We determined that a β-amino acid is needed in the linker to bridge the gap between the helix and the active site cysteine. Furthermore it appeared that the ABP, NM-02, retained specificity for calpains over closely related cathepsin proteases. Given this specificity, we hope that these inhibitors and probes will allow for future studies of calpain function in multiple biological systems. We believe that the methodology used to stabilize this α-helical inhibitor will be another useful technique for α-helix stabilization for use in multiple biological applications.

2.4 Materials and Methods

2.4.1 Crosslinker Screen:

To each well of a black round-bottomed 96-well plate (polypropylene) 90 μL of the stock solution, a peptide solution (0.114 mM) in NH_4HCO_3 buffer (12mL, 50 mM, pH=8.0), treated with TCEP (1M solution in the same NH_4HCO_3 buffer, 1.1 eq.) at room temperature (rt) for 1 h was added. Then 10 μL of the freshly prepared alkylating agent

solution (1.5 mM in anhydrous DMF, 1.5 eq.) was applied to the well at rt and stirred for 2 h under protection from light. MALDI spectra were taken to monitor reaction progress and more alkylating agent was added if needed. The reaction was quenched by addition of 5% HCl which resulted in acidic conditions (pH=3-4). If necessary, 100 μL of ether was added to dissolve the excess reagent and organic byproducts into the organic layer. The ether layer could be removed by pipetting. MALDI spectra were taken from the sample in the remaining aqueous solution mixture. (Performed by H. Jo.)

2.4.2 "Selection of the fitness" Screen:

Screens were performed in 1.5 mL microcentrifuge tubes. 1 mL of the stock peptide solution (1mM) in NH_4HCO_3 buffer (50mM, pH=8.0) was pre-treated with TCEP as described above and incubated for 1 h. Then, 100 μL of the concentrated alkylating agent solution (250mM or saturated solution in anhydrous DMF) was added and shaken for 2 h under protection from light. The reaction was quenched by the addition of 5% HCl which resulted in acidic conditions (pH=3-4) and purified by Reverse Phase HPLC. (Performed by H. Jo.)

2.4.3 Crosslinking with the unpurified peptide:

The lyophilized crude peptide solution (app. 3-5mg/mL) in NH_4HCO_3 buffer (100mM, pH=8.0) was treated with TCEP (1.5 eq.) and stirred for 1 h. The alkylating agent in DMF (app. 3eq) was added to the solution and shaken for the 2 h. The reaction was quenched by adjusting the pH of the mixture to slightly acidic conditions through the addition of 0.5 N HCl or TFA. The crude mixture was either purified by HPLC or lyophilized for the next step.

2.4.4 Preparation of crosslinked peptides 3c from model peptide 3c by solid-phase peptide crosslinking:

The uncrosslinked peptide **3c** was similarly prepared on the CLEAR^{TM} Rink Amide MBHA resin using the standard Fmoc peptide synthesis protocol (See Supporting Information). Fmoc-Cys(Mmt)-OH was used for cysteine for ease of deprotection. After the final coupling and cooling down to room temperature, the resin was washed with NMP(x3) and DMF(x3) followed by DCM(x3). The resin was then treated with 1% TFA solution in DCM for 10 min then washed with dichloromethane. This process was repeated until the solution lost its yellow color, which indicated the complete removal of Mmt protecting group. Then, the resin was washed with hexane and dried. After re-swelling in DMF, a solution of α,α'-dibromo-*m*-xylene (2 eq.) in DMF and DIPEA (4 eq) was added. Alternatively, the resin was re-swollen in NH_4HCO_3 buffer (pH=8.0, 100 mM) for 1 h, a solution of α,α'-dibromo-*m*-xylene (5 eq.) in a minimal volume of DMF was added. The solution was stirred for 3 h at room temperature. The solvent was then removed and the resin was washed thoroughly with DMF. The Fmoc group on *N*-terminus was removed by treatment with 20% piperidine in DMF and acetylated by Ac_2O and DIPEA. The cleavage/deprotection was done using TFA/thioanisole/EDT/anisole (90/5/3/2). The crude mixture was purified by reverse phase HPLC.

2.4.5 CD spectroscopy:

Peptide solutions were prepared at ~50 μM in 50 mM phosphate buffer (pH 7.0) without TFE. The molar concentration of the peptide determined was by the weight (after lyophilization of the HPLC fractions) with consideration for molecular weight increase due to the presence of TFA salt for basic residues (Lys, Arg) as well as hydration (average 10%). Concentrations of the uncrosslinked peptides were determined by

absorbance of Tyr residue at 280 nm with an extinction coefficient of 1280 M^{-1} cm^{-1}.[136] Circular dichroism studies were conducted at 25˚C on a JASCO J-810 spectropolarimeter equipped with a Peltier temperature control unit.

2.4.6 NMR spectroscopy:

The peptide sample was prepared with peptide concentrations of 2 mM in 0.6 mL of 9:1 v/v water/D_2O mixture in 50 mM sodium phosphate, pH 5.5. All spectra were recorded at 10 ^oC on a Bruker Avance III 500 MHz spectrometer equipped with a cryogenic probe. All 2D homonuclear spectra were recorded with standard pulse sequences.[137] Spectra were processed and analyzed using the programs nmrPipe[138] and XEASY,[139] respectively. (See Supporting Information.) (Performed by Y. Wu.)

2.4.7 Protease Activity Assays:

Peptides were evaluated for ability to bind and subsequently inhibit the cysteine proteases using standard proteolytic fluorescence activity assays. Inhibition was assayed using a standard donor-quencher strategy using a previously published peptide substrates.[62,140,141]

Enzyme concentration for Calpain-1 was 25 nM. Enzyme concentration for papain was 25 nM. Enzyme concentrations for cathepsin B and cathepsin L was 3 nM. Calpain and papain buffer contained 10 mM dithiothreitol (DTT), 100 mM KCl, 2 mM EGTA, 50 mM Tris-HCl (pH 7.5), and 0.015% Brij-35. Substrate concentration for calpain and papain was 0.25 μM H-Glu(Edans)-Pro-Leu-Phe-Ala-Glu-Arg-Lys(Dabcyl)-OH (K_m calculation in Supporting Information, Figures S2.8 and S2.10).[62,140,141] Cathepsin buffer contained 10 mM DTT, 500 mM sodium acetate (pH 5.5), and 4 mM EGTA.[62,140,141] Substrate concentration for the cathepsins was 0.25 μM Z-FR-Amc. Calpain was activated by the injection of $CaCl_2$ to a final concentration of 5 mM. Papain

and cathepsin assays were activated by the addition of the substrate via a multichannel pipette. Varying concentrations of inhibitor, 1-100 μM, were used for each assay. All assays were done at a total well volume of 100 μL in 96-well plate, and each well contained a separate inhibitor concentration. Fluorescence was read in a Berthold Tri-Star fluorimeter. The excitation wavelength was 380 nm and the emission wavelength was 500 nm for H-Glu(Edans)-Pro-Leu-Phe-Ala-Glu-Arg-Lys(Dabcyl)-OH. The excitation wavelength 351 nm and emission wavelength was 430 nm for Z-FR-Amc.

2.4.8 Kinetic analysis of Calpain-1 by 3c:

To identify inhibition type we used standard Michaelis-Menten treatment. Initial velocities (obtained from the linear segment of the progress curves) were plotted against substrate concentration.[142] Due to the linearity of the first segment of the progress curve we believe that autoproteolysis during the first 500 seconds was not substantial enough to prevent the use of simple Michaelis-Menten kinetics, i.e. loss of enzyme did not change the velocity enough to cause it to deviate from linearity and incorporation of this additional complex would severely complicate the kinetics. Velocities were determined in RFU/sec then converted to μM/sec using the conversion factor 1386 RFU/μM. The conversion factor was obtained by the total hydrolysis of the substrate H-Glu(Edans)-Pro-Leu-Phe-Ala-Glu-Arg-Lys(Dabcyl)-OH in a known concentration by papain. To avoid weighting errors we used the values of K_m^{app} and V_{max}^{app} determined directly from the non-linear least-squares best fits of the untransformed data and put these values into the reciprocal equation:

$$\frac{1}{v} = \left(\frac{K_m}{V_{max}} \times \frac{1}{[S]}\right) + \frac{1}{V_{max}}.$$ [142]

We then plotted the resulting reciprocal velocities against the respective reciprocal substrate concentrations.

2.4.9 Determination of IC_{50} against Enzymes:

IC_{50} curves were generated identifying the initial rate of the enzyme at each inhibitor concentration from the respective progress curves. The conversion factor (1386 RFU/μM) was obtained by the total hydrolysis of the substrate H-E(Edans)-PLFAER-K(Dabcyl)-OH in a known concentration by papain. Initial velocities were converted from RFU/sec to μM/sec. Fractional activity was calculated by dividing the initial velocity at each inhibitor concentration by the initial velocity of the uninhibited enzyme. Data obtained up to 500 seconds was used for the initial rate calculation. The initial rate was then plotted against the log of the inhibitor concentration, and IC_{50} was calculated by GraphPad Prism.

2.4.10 Activity Based Probe Linker Experiments:

Experimental conditions included 10 mM dithiothreitol (DTT), 1.5 μg calpain, 100 mM KCl, 2 mM EGTA, 50 mM Tris-HCl (pH 7.5), 0.015% Brij-35, and either 1 μM or 10 μM of biotinylated probe (DCG-04, NM-01, NM-02, NM-03). Calpain was activated by the addition of calcium (3.33 μM of 50 mM $CaCl_2$) to a final concentration of 8.3 mM in tubes containing either 1 μM or 10 μM ABP. For the negative control, water, instead of $CaCl_2$, was added to the calpain solution containing 10 μM probe. Probes were allowed to bind to the calpain for 20 minutes at room temperature. The reaction was stopped by the addition of 10 μL NuPage® LDS Running Buffer (Life Technologies, Grand Island, NY). 10 μL of each labeled enzyme was loaded on a 10% Bis-Tris NuPAGE® gel (Life Technologies, Grand Island, NY) and separated via gel electrophoresis for 1.5 h, 140 V. The bands were then transferred to a PVDF membrane

at 30 V for 70 min. The membrane was blocked and blotted using the Vectastain® Elite® ABC kit (Vector Laboratories, Burlingame, CA). Kodak film was exposed to the membrane and developed.

2.4.11 ABP Labeling Experiments:

Buffer conditions for calpain and papain experiments were 10 μM dithioreitol (DTT), 100 mM KCl, 2 mM EGTA, 50 mM Tris-HCl (pH 7.5), and 0.015% Brij-35. 1.5 μg calpain-1 or 6 μg calpain-2 (calpain-2 was not as active) was used. (For labeling experiments greater concentrations of enzyme were used for ease of visualization of the enzyme on stained gels.) Buffer conditions for cathepsin experiments were 10 μM DTT, 500 mM sodium acetate (pH 5.5), and 4 mM EGTA. 1.5 μg of each cathepsin was labeled.[62,140,141] Probes were allowed to bind for 20 min. at room temperature. Labeled enzymes were separated via gel electrophoresis on 10% (calpain, papain) or 12% (cathepsins) Bis-Tris NuPAGE® gels for 1 hr, 140 V. A Typhoon Fluorescent Imager was used for FITC visualization of the probe bound enzyme. Following fluorescent scanning the gels were colloidal blue stained (calpain-1 and calpain-2) or silver stained (papain, cathepsin B, and cathepsin L) to demonstrate that the same amount of enzyme had been used in all lanes. (See Supporting Information).

CHAPTER 3: Development of Potent and Specific Inhibitors and Quench Activity Based Probes for Calpain-1

3.1 Introduction

Calpain-1 is a cysteine protease involved in a number of cell processes such as cell migration and apoptosis and diseases states such as amyloid diseases and secondary cell death after acute cellular stress.[19-23] There has been substantial interest in designing inhibitors and probes of calpain-1 in order to investigate the role it plays in these diseases. However, a large hurdle to overcome in the development of these investigative tools is the conserved active site of the papain family cysteine proteases. Endogenous inhibitors and substrates can be good starting points for the development of specific inhibitors. Calpain has an absolutely specific endogenous inhibitor called calpastatin and a commercially available fairly specific substrate.[30,69,140,143] Either one or both of these molecules can be starting points for the development of new calpain inhibitors and probes to investigate the role calpain plays in both cellular function and disease.

We have previously developed a small ten amino acid two-turn α-helical potent and specific inhibitor for calpain based on the endogenous inhibitor calpastatin. We further were able to add an epoxysuccinic warhead to the inhibitor to create a specific activity based probe. However, there are still improvements to be made to create a more potent and specific inhibitor and probe.

3.2 Results and Discussion

3.2.1 Alanine Scanning Mutagenesis to Identify Residues Important for Enzyme Binding

To improve upon the ten amino acid inhibitor, alanine scanning was performed to identify important residues for binding to the enzyme and to identify where mutations in

the ten amino acid peptide could be introduced (Table S3.1 Supporting Information). Alanine scanning mutagenesis involves mutating each amino acid in the peptide to alanine to identify how each amino acid affects the potency and specificity of the inhibitor.

	Inhibitor	Calpain-1 (μM)
3c	IPPKY**C**ELL**C**	10.2 ± 2.9
3d	APPKY**C**ELL**C**	65.6 ± 20.5
3e	IAPKY**C**ELL**C**	13.7 ± 4.4
3f	IPAKY**C**ELL**C**	27.4 ± 5.6
3g	IPPAY**C**ELL**C**	17.7 ± 5.6
3h	IPPKA**C**ELL**C**	>100
3i	IPPKY**C**ALL**C**	28.9 ± 9.1
3j	IPPKY**C**EAL**C**	30.9 ± 9.2
3k	IPPKY**C**ELA**C**	25.2 ± 7.9

Table 3.1 Alanine Scanning Mutagenesis. K_i for each alanine mutant against calpain-1.

Alanine scanning mutagenesis identified isoleucine and tyrosine as the most important residues for inhibitor binding to calpain due to the substantial loss of potency in each of these mutants (Figure S3.1, Table S3.2 Supporting Information). This result correlates the findings in a β–Alanine scanning study done by Betts *et al*., which identified this isoleucine to be important for inhibition in the 27 amino acid calpastatin derivative.[123,144] The aliphatic chain of the isoleucine projects into the prime side cleft to form a hydrophobic interaction with Ala101 and Leu102.[30] Further mutational studies reinforce the hypothesis that the branched aliphatic side chain is necessary for retaining potency as a Ile→Leu mutation has no effect upon calpain inhibition or specificity, while a mutation to a similar sized branched polar side chain, Ile→Gln, did reduce the potency (Figure S3.2, Tables S3.3 and S3.4 Supporting Information).

Tyrosine appears to be fitting into a cleft lined with E164 and H169 suggesting that it might be forming electrostatic interactions with either glutamate or histidine or π-π stacking interactions with the H169. A mutation of tyrosine to Ala(4,4'-biphenyl) resulted in no change in K_i while a benzyl tyrosine mutation caused an increase in K_i suggesting that ring stacking may play a larger role in potency than electrostatics (Figure S3.2, Table S3.3 and S3.4 Supporting Information). It must be acknowledged, though, that these results are not conclusive as both mutant side chains are substantially larger than the tyrosine side chain, and subsequently steric hindrance could also play a role. These groups were introduced because it was thought that they might fit into the large cleft where the tyrosine resides and create more interactions between the inhibitor and enzyme.

Alanine mutations of the N-terminal proline, P^1, and lysine, **3e** and **3g** respectively, have no effect on inhibitor potency suggesting that these are key locations for potential mutations. The P^1 residue stacks against Trp288.[30] Mutating this proline to an aromatic residue could increase the π-π interactions with tryptophan thereby increasing the binding affinity. Interestingly, P^1 is also important for specificity. The alanine mutant **3e** resulted in a substantial decrease in specificity, especially against cathepsin L (Table S3.2 Supporting Information). The proline was mutated to pentafluorophenylalanine, *pfF*, **4a**, which decreased the K_i by half while retaining the same specificity for calpain over cathepsin L and improving specificity against cathepsin S (Table 3.2, Figure S3.3 and Table S3.5 Supporting Information).

The lysine residue of inhibitor **3c** sits between calpain residues Glu164 and Gln290. Increasing electrostatic interactions in this region may be accomplished by

mutating the lysine to a more positive residue such as arginine. The guanidinium group on the arginine may also enable multiple hydrogen bonds to these surrounding residues. This Lys→Arg mutation, **4b**, results in a decrease in K_i to 5 μM (Table 3.2). Similarly to the pentafluorophenylalanine mutation the Lys→Arg mutation also resulted in an increase in specificity against cathepsin L and S (Table 3.2, Figure S3.3 and Table S3.5 Supporting Information).

Interestingly, when these two mutations are combined, **4c**, the potency of the inhibitor is lost (Table 3.2, Figure S3.3 and Table S3.5 Supporting Information). This loss of potency could suggest that one or both of the mutations change the orientation of the α-helical inhibitor in the prime side of the active site creating clashes between the inhibitor and enzyme.

All other alanine mutations resulted in 3-fold loss of potency of the inhibitor. This loss of potency could be due to a loss of α-helicity, reduction of binding interactions, or a change in binding orientation because of the change in the amino acid side chain.

	Inhibitor	Calpain-1 (μM)	Cathepsin L (μM)	Cathepsin S (μM)
4a	I*pfF*PKY**C**ELL**C**	5.1 ± 1.9	22.2 ± 1.1	>100
4b	IPP*R*Y**C**ELL**C**	5.3 ± 2.0	37.9 ± 1.1	35.9 ± 1.1
4c	I*pfF*P*R*Y**C**ELL**C**	37.1 ± 11.6	NT	NT

pfF=pentafluorophenylalanine; NT=Not Tested

Table 3.2 Mutant calpain-1 inhibitors. K_i for each mutant inhibitor for calpain-1. Each single mutant had improved potency against calpain-1, however the double mutant had reduced potency against calpain-1.

3.2.2 Increasing Potency Through Increasing Peptide Length

Peptide **3c** was modeled after a two-turn α-helix that binds at the calpain active site in the endogenous calpain inhibitor calpastatin. Previous studies demonstrated that the shortest, effective, non-stabilized inhibitor was 27 amino acids. The Anagli group demonstrated that truncating the inhibitor from the N-terminus resulted in a sequential

decrease in inhibition.[123] The shortest, non-stabilized fragment tested was 19 amino acids long and had an IC_{50} of 1.8 ± 0.016 μM. From this information, it was hypothesized that lengthening the inhibitors would also result in an increase in inhibition, while the stabilization of the α-helix would still allow the inhibitor to be substantially shorter than the previous calpastatin fragments.

To evaluate this hypothesis, inhibitors of varying lengths were synthesized. During the development of the calpain probe, a linker of alanine and β-alanine was added between the α-helical inhibitor and the epoxysuccinic acid warhead. This linker lengthened the peptide to a 12 amino acid peptide, **5a**, however these additional amino acids did not increase the potency of the inhibitor (Table 3.3, Figure S3.4 and Table S3.6 Supporting Information). This lack of increased potency may be due to the absence of side chains that interact with the enzyme. Therefore, the calpastatin amino acid sequence was used to extend the inhibitor. The first lengthened inhibitor, **5b**, was 13 amino acids and had a K_i of 5.3 ± 1.9 μM (Table 3.3, Figure S3.4 and Table S3.6 Supporting Information). Further analysis of the unstabilized 13-mer supports the idea that additional enzyme contacts help overcome the free energy needed for binding, however, 13 amino acids is not long enough to get good inhibitory activity (Tables S3.7 and Table S3.6 Supporting Information). Extending the inhibitor to 17 amino acids, **5c**, creates an inhibitor slightly shorter than the shortest non-stabilized inhibitor tested by Betts et. al.[123] This inhibitor extends past the active site into the unprimed side of the enzyme where leucine interacts with the P2 pocket.[30,69] It includes the loop over the active site and resulted in an inhibitor with a K_i of 3.6 ± 1.7 μM (Table 3.3, Figure S3.4 and Table S3.6 Supporting Information).

Finally, **5d** was synthesized where the glycine was mutated to phenylalanine resulting in a removal of the loop over the active site and subsequent increase in the number of N-terminal interactions. This inhibitor results in a K_i of 1.2 ± 1.3 μM which is very similar to the IC_{50} from the unstabilized 19-mer (Table 3.3, Figure S3.4 and Table S3.6).[123] These results imply that stabilizing the α-helix does improve inhibitor potency.

	Inhibitor	Calpain (μM)	Cathepsin L (μM)	Cathepsin S (μM)
5a	βAAIPPKY**C**ELL**C**	10.7 ± 3.5	42.0 ± 1.3	38.4 ± 1.1
5b	EVTIPPKY**C**ELL**C**	5.3 ± 1.9	69.6 ± 1.5	31.3 ± 1.2
5c	LGKREVTIPPKY**C**ELL**C**	3.6 ± 1.7	>100	31.5 ± 1.1
5d	LFKREVTIPPKY**C**ELL**C**	1.3 ± 1.3	10.7 ± 1.1	41.5 ± 4.5

Table 3.3 Calpain-1 inhibitors of increasing peptide length. The K_i of each calpain-1 inhibitor of increasing length. The potency of the inhibitors tends to increase with longer peptides, however the presence of side chains seems to influence the potency.

Lengthening the stabilized peptide into the unprimed region does have an effect upon potency, however simple length addition does not implicitly increase potency, sequence also seems to have an effect upon K_i.

3.2.3 Developing Quench Probes

Previously, an activity based probe or ABP was created by adding a fluorophore tag, amino acid linker, and electrophilic warhead to the stabilized α-helical inhibitor. This ABP binds only active enzyme and was fairly specific for calpain. However, the attachment of a fluorophore tag means that there will always be substantial background fluorescence, which could interfere with visual identification of proteases.[145-147] One way to overcome the background fluorescence is through the use of a quench probe. A quench probe contains a donor fluorophore and a quencher, which absorbs fluorescence in the same wavelength range that the donor emits. Upon binding to the enzyme this quencher is removed and the enzyme can then be visualized by the fluorophore.[145-147]

Our proposed method for removing the quencher from the probe post enzyme binding was to attach a cleavable sequence to the N-terminus of the α-helical inhibitor. The results of the lengthening studies suggest that the inhibitor can be extended at the N-terminus with little detriment to potency, and in some cases may actually increase potency. Previously, no cleavage product could be isolated from peptide **5d** after cleavage assays suggesting that simply laying across the enzyme active site is not sufficient for proteolysis by calpain. The addition of the substrate sequence rather than the calpastatin inhibitor sequence ensured that the quencher is actually cleaved from the inhibitor.

The initial substrate sequence chosen was Pro-Leu-Phe-Ala-Ala-Arg because this sequence has been determined to be a preferred calpain-1 substrate sequence.[143] The scissile bond is found between the phenylalanine and alanine. This substrate sequence was added to the N-terminus of the α-helical inhibitor for a final amino acid sequence of Pro-Leu-Phe-Ala-Ala-Arg-Ile-Pro-Pro-Lys-Tyr-Cys-Glu-Leu-Leu-Cys-Lys (**6a)**. The lysine was added at the C-terminus for future fluorophore addition similar to the ABP developed previously. Initial analysis of this substrate/inhibitor found that it was also cut between the phenylalanine and alanine demonstrating that this was a potentially good sequence for the quench probe.

Studies found that the addition of a charged residue at the C-terminus negatively affected enzyme binding, thus the location of the fluorophore had to be moved closer to the N-terminus (Figure S3.5, Tables S3.58 and S3.9 Supporting Information). We used Edans and Dabcyl as the donor and quencher respectively. This is the same donor/quencher pair found in the commercially available substrate (sequence: NH_2-

Glu(Edans)-Pro-Leu-Phe-Ala-Glu-Arg-Lys(Dabcyl)-OH; Dabcyl is attached to a lysine and Edans is attached to a glutamate.) In both peptides the quencher is at the N-terminus. We synthesized two peptides with donor fluorophores at different positions. In one quench probe the donor was situated between the substrate sequence and inhibitor sequence, Lys(Dabcyl)-Pro-Leu-Phe-Ala-Ala-Arg-Glu(Edans), **6c**. In the other quench probe, the donor was within the substrate sequence, Lys(Dabcyl)-Pro-Leu-Phe-Ala-Glu(Edans)-Arg, **6d** (Figure S3.10 Supporting Information). Pymol modeling suggests that this residue side chain may face the solvent rather than the enzyme making this location amenable for donor fluorophore attachment (Figure S3.6 Supporting Information).[31]

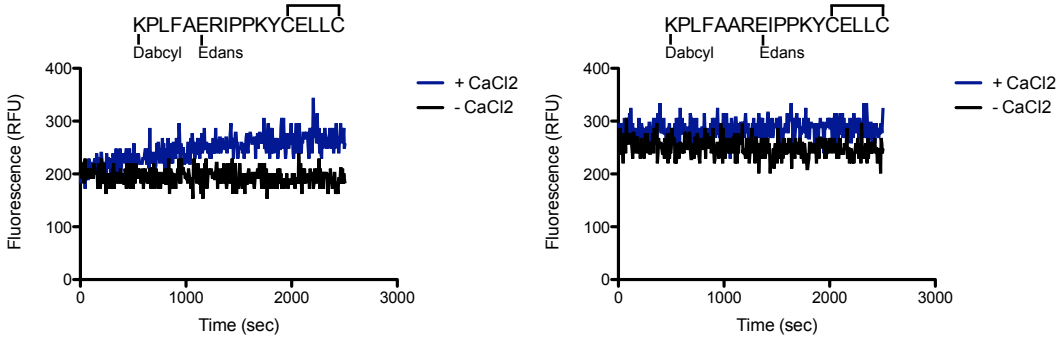

Figure 3.1. Proteolytic cleavage of the quench probe. (left) The quench probe with the donor situated in the middle of the substrate sequence. (right) The quench probe with the donor situated between the substrate sequence and inhibitor sequence.

Results from proteolytic cleavage assays show that the quench probe with the donor in the middle of the substrate undergoes greater proteolytic cleavage than the probe with the donor between the substrate and inhibitor as evidenced by the larger increase in fluorescence (Figure 3.1). Although, post assay HPLC analysis indicates that both probes

are cleaved between the phenylalanine and alanine. The discrepancy in the proteolysis of the substrate portions of the probes is likely due to differences in where the scissile bond fits across the active site in relation to the α-helix fitting into the prime side cleft. The extra amino acid between the substrate sequence and α-helix may cause the scissile bond to not fit properly at the active site cysteine residue. The preferred sequence, K(Dabcyl)-Pro-Leu-Phe-Ala-Glu(Edans)-Arg, is also desirable as the Pro-Leu-Phe-Ala-Ala-Arg substrate sequence is also cleaved by cathepsin L.

Finally, we used the calpain mutations previously identified to create a more potent inhibitor post proteolytic cleavage. We synthesized quench probe peptides with the preferred substrate sequence, Lys(Dabcyl)-Pro-Leu-Phe-Ala-Glu(Edans)-Arg, and three different inhibitor sequences, the **3c** inhibitor sequence (**6d**), the Pro→pentafluorophenylalanine mutation (**6e**), and the Lys→Arg mutation (**6f**). We then tested all quench probe peptides and the commercially available substrate in a proteolytic cleavage assay (Figure 3.2, Table S3.10 Supporting Information).

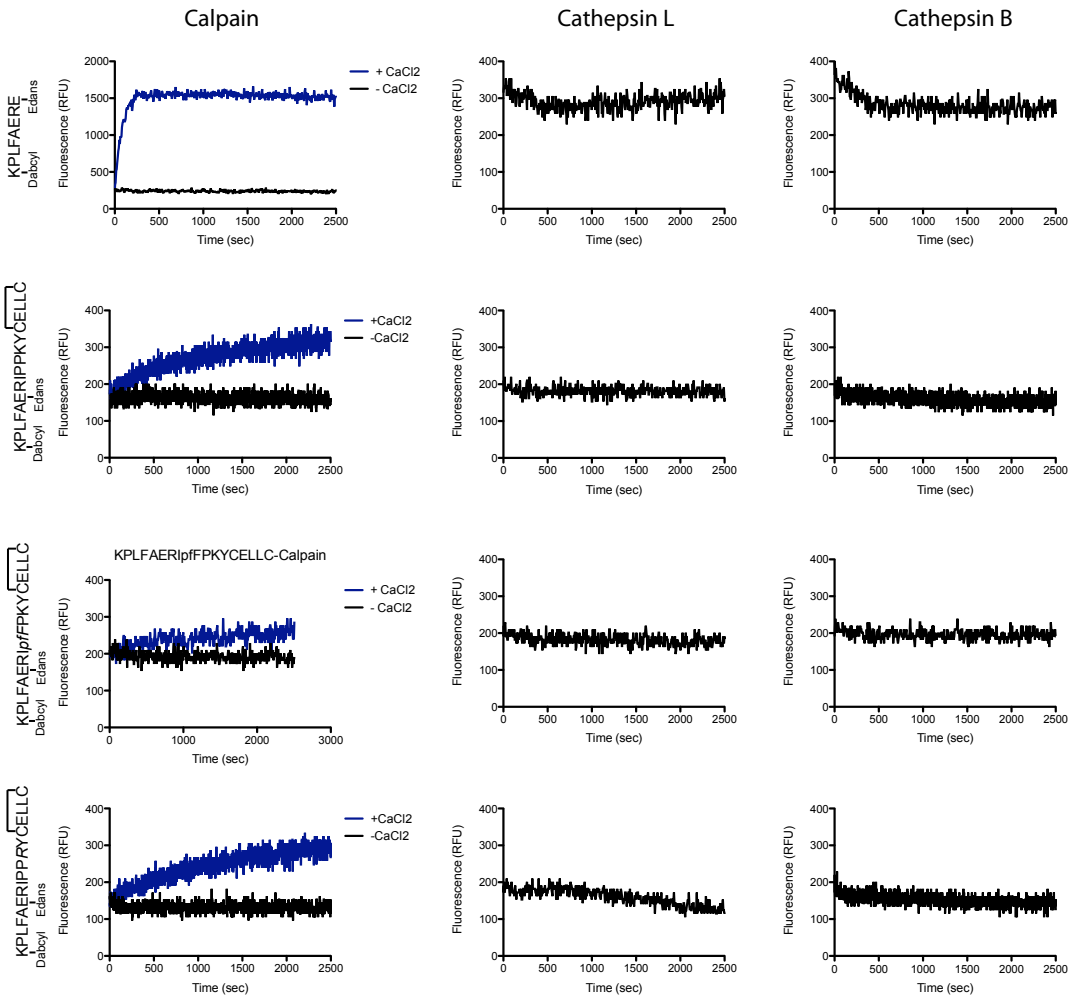

Figure 3.2. Quench probe and commercial substrate cleavage by calpain-1, cathepsin L, and cathepsin B.

We found that both quench probes **6d** and **6e** have similar fluorescence increases while quench probe **6f** has about half the fluorescence increase (Figure 3.2). This lack of fluorescence increase is likely due to an impurity in the purified product where there appeared to be a moiety with a double linker attachment that could not be separated from the single linker peptide. This impurity decreases the cleavable concentration.

Furthermore, it could be interacting with the enzyme. Satisfyingly, though, none of the quench probes are cleaved by cathepsin L or cathepsin B.

For inhibition analysis the quench probes were synthesized without the donor/quencher fluorophores and tested against calpain-1, cathepsin L, and cathepsin B. Peptide **6g**, Pro-Leu-Phe-Ala-Glu-Arg-Ile-Pro-Pro-Lys-Tyr-Cys-Glu-Leu-Leu-Cys, and peptide **6h**, Pro-Leu-Phe-Ala-Glu-Arg-Ile-*pfF*-Pro-Lys-Tyr-Cys-Glu-Leu-Leu-Cys, had the same potency as their respective original inhibitors (Table 3.4, Figure S3.7 and Table S3.10 Supporting Information). Peptide **6h** is also extremely specific for calpain-1 over both cathepsin L and cathepsin B. Peptide **6i**, Pro-Leu-Phe-Ala-Glu-Arg-Ile-Pro-Pro-Arg-Tyr-Cys-Glu-Leu-Leu-Cys, had a decrease in potency (Table 3.4, Figure S3.7 and Table S3.10 Supporting Information). Similar to the double mutant, **4c**, the decrease in potency could be associated with a change in orientation of the helix due to the arginine mutation that further changes how the substrate sits across the active site.

	Inhibitor	Calpain	Cathepsin L	Cathepsin B
6a	PLFAERIPPKY**C**ELL**C**	11.4 ± 3.7	6.4 ± 1.3	65.2 ± 1.3
6b	PLFAERI*pfF*PKY**C**ELL**C**	5.6 ± 2.1	48.6 ± 1.2	64.7 ± 1.4
6c	PLFAERIPP*R*Y**C**ELL**C**	16.9 ± 5.5	17.0 ± 1.2	>100

pfF=pentafluorophenylalanine

Table 3.4 Quench Probes as Inhibitors. The K_i for each quench probe (without fluorophores) against canonical cysteine proteases.

3.3 Conclusion

Alanine scanning mutagenesis identified two residues that are important for inhibitor binding to calpain-1 and two residues that could be mutated to enhance potency. Structure based design allowed us to propose mutations to increase potency, peptides **4a** and **4b**. Each of the proposed mutations resulted in an increase in potency. Further

analysis into lengthening the inhibitor demonstrated that additions to the N-terminus can increase potency. Finally, each aspect culminated in the development of a potent quench probe, **6h**, that is only cleaved by calpain-1 and specifically inhibits calpain-1, not cathepsin L or cathepsin B.

3.4 Materials and Methods

3.4.1 Crosslinking with the unpurified peptide:

The lyophilized crude peptide was dissolved in DMF (conc~1-5 mM) with 2% triethylamine. The alkylating agent, α,α'-dibromo-m-xylene (1.5 eq.), was added to the solution and shaken for the 2 h. The crude mixture was purified via HPLC.

3.4.2 Protease Activity Assays:

Peptides were evaluated for ability to inhibit cysteine proteases using standard proteolytic fluorescence activity assays. Inhibition was assayed using a standard donor-quencher strategy with previously published peptide substrates.[62,140,141]

Enzyme concentration for Calpain-1 was 25 nM. Enzyme concentration for cathepsin B and L was 3 nM, and cathepsin S was 5 nM. Calpain buffer contained 10 mM dithiothreitol (DTT), 100 mM KCl, 2 mM EGTA, 50 mM Tris-HCl (pH 7.5), and 0.015% Brij-35. Substrate concentration for calpain-1 was 0.5 μM NH_2-Glu(Edans)-Pro-Leu-Phe-Ala-Glu-Arg-Lys(Dabcyl)-OH.[62,140,141] Final substrate concentration for the cathepsins was 0.5 μM Z-FR-Amc. Cathepsin L buffer contained 10 mM DTT, 500 mM sodium acetate (pH 5.5), and 4 mM EGTA.[62,140,141] Cathepsin B buffer contained 10 mM DTT, 100 mM sodium acetate (pH 5.5), 0.01% Triton X-100, and 4 mM EGTA. Cathepsin S buffer contains 10 mM DTT, 100 mM potassium phosphate (pH 6.5), and 4 mM EGTA. Calpain was activated by the injection of $CaCl_2$ to a final concentration of 5 mM. Cathepsin assays were activated by the injection of the substrate to a final

concentration of 0.5 μM. Varying concentrations of inhibitor, 1-100 μM, were used for each assay. All assays were done at a total well volume of 100 μL in 96-well plate, and each well contained a separate inhibitor concentration. Fluorescence was read in a Berthold Tri-Star fluorimeter. The excitation wavelength was 380 nm and the emission wavelength was 500 nm for NH_2-Glu(Edans)-Pro-Leu-Phe-Ala-Glu-Arg-Lys(Dabcyl)-OH. The excitation wavelength 351 nm and emission wavelength was 430 nm for Z-FR-Amc.

3.4.3 Protease Cleavage Assays:

Protease cleavage assays were performed under the same buffer conditions per enzyme as the protease activity assays. Calpain concentration was 150 nM. Cathepsin B and L concentrations were 54 nM. Quench probe and substrate concentrations were 5 μM. Calpain was activated via $CaCl_2$ injection to a final concentration of 5 mM. Quench probe was added to active cathepsins just before fluorescence readings were taken.

CHAPTER 4: Development of Non-covalent, α-Helical Inhibitors of Cathepsins L, S, and K by Mimicking a Natural Protein-Protein Interaction

4.1 Introduction:

The human genome expresses 11 cathepsins that belong to the papain cysteine protease family (clan CA, family C1).[125] Cathepsins are involved in normal cellular processes such as endosomal/lysosomal protein turnover[125], bone remodeling, immunity[29], apoptosis, and prohormone processing and in various disease states including viral invasion[148,149], tumor growth, cancer tumor invasion[16,150,151], angiogenesis[16,151], rheumatoid arthritis[14], and osteoporosis[18,152].

Due to their involvement in various diseases, cathepsins have become attractive targets for drug development. Previous efforts to develop specific inhibitors of cathepsins have been focused on small molecules, both covalent-irreversible[26] and covalent-reversible[16,153], most of which bind to the unprimed side of the active site. One of the greatest issues with these inhibitors is the difficulty in the development of specificity to differentiate amongst the various closely related cysteine cathepsins. This is mainly due to the high conservation in the unprimed binding pockets of the papain superfamily active site.[125,154,155] Additionally, most of the inhibitors developed to date covalently modify the cysteine residue via an electrophilic warhead group, which in turn also reduces the potential for specificity. Herein we set out to develop a set of specific, non-covalent inhibitors that utilize an α-helix-based scaffold for inhibition of three canonical members of the cathepsin L subfamily: cathepsin L, S, and K.

4.2 Results and Discussion:

Cathepsins are composed of three domains: a signal peptide, prodomain, also known as the propeptide, and the catalytic domain.[3,11,29,156] We were interested in utilizing the prodomain as a scaffold since it acts as potent, reversible inhibitor of its cognate enzyme.[9,157,158] Each prodomain contains three α-helices wherein one α-helix occupies a binding site within the prime side of the active site along with a beta strand that further occludes substrate entry (Figure 4.1). The entire prodomain, including this α-helix, binds to the active site cleft in the reverse direction of a normal peptide substrate to eliminate proteolytic cleavage. Every α-helix has a unique sequence that creates specific interactions with its respective enzyme, suggesting that these α-helices could be used to create specific inhibitors. Additionally, creating inhibitors that bind to the prime side of the protease active site opens up new avenues to explore for therapeutic development.

Previously, an α-helical inhibitor for the cysteine protease calpain was developed using a structure-based design approach.[159] This inhibitor was modeled after an α-helix in calpastatin, the endogenous proteinaceous inhibitor of calpain that binds across several domains within calpain, but makes one specific α-helical interaction within the prime side of the calpain active site. We hypothesized that we could similarly develop α-helix derived specific and potent inhibitors based on the prodomains of cathepsins that inhibit the enzymes via non-covalent binding to the prime side of the protease active site.

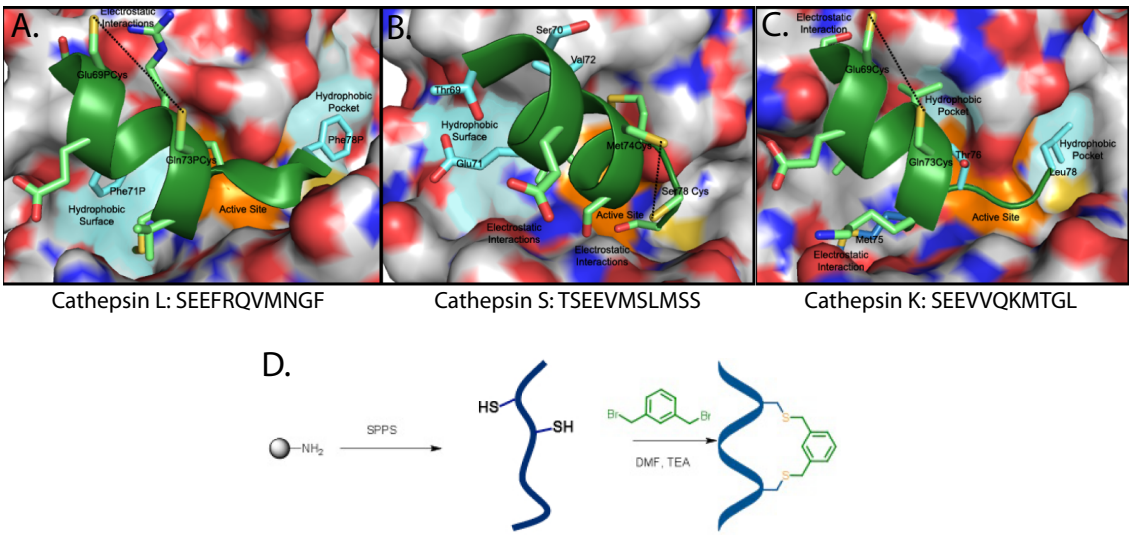

Figure 4.1: A-C) Zymogen crystal structures with the α-helix prodomain highlighted in the prime side of three different Cathepsins.[31] A) Cathepsin L; sequence: SEEFRQVMNGF; pdb: 1CS8[3,156]. B) Cathepsin S; sequence: TSEEVMNSLMSS; pdb: 2C0Y[29]. C) Cathepsin K; sequence: SEEVVQKMTGL; pdb: 1BY8[11]. Colored areas on the enzyme depict areas for enhancing peptide-enzyme interactions. Orange designates active site, blue designates hydrophobic surfaces, pockets, and amino acids, and the dotted line designates helix linker. D) Schematic of α-helix stabilization via attachment of dibromo-*m*-xylene linker to cysteine side chain.[31,159]

Each cathepsin L, S, and K zymogen crystal structure was examined to identify the prime-side prodomain α-helix of interest (Figure 4.1, A-C). The α-helices from these prodomains were synthesized (**7a**, **8a**, and **9a)** using standard solid-phase peptide synthesis and analyzed for inhibitory activity and secondary structure (Tables 4.1-4.3; Figures S4.1-4.3, S4.10, and S4.23 Supporting Information). Peptides **7a**, **8a**, and **9a** showed no inhibition of their cognate enzymes and were primarily random coil in solution,[7,73,159] presumably due to the inability of these short peptides to overcome the free energy barrier needed to form an α-helix. To address this issue, these short peptides were conformationally restricted to enhance α-helicity, using a protocol previously developed by the Greenbaum laboratory (Figure 4.1).[159] This stabilization technique involves reacting the side chains of two cysteine residues in *i*, *i*+4 positions with a

dibromo-*m*-xylene linker. A series of paired cysteines to be used for stabilization were introduced into the peptide scaffold at positions that, from visual inspection of the zymogen crystal structure, would appear not to disrupt key protein-helix interactions. Several stabilized peptides were synthesized and screened for inhibition of cathepsin activity using a standard fluorescence-based protease activity assay (Tables 4.1-4.3, Figures S4.3-S4.35 Supporting Information). The development of a potent and selective inhibitor lead for each target cathepsin is discussed in detail below.

4.2.1 Design of an α-helical Cathepsin L Inhibitor

Starting with the native sequence of the cathepsin L prodomain α-helix (**7a**), peptides **7b** and **7c** were mutated with two cysteines spaced *i*, *i*+4 within the parent sequence. These two cysteines were then crosslinked using a dibromo-*m*-xylene linker. cathepsin L was inhibited by **7b** and **7c** with a K_i of 84.7 μM and 29.4 μM, respectively (Table 4.1, Figures S4.3-S4.5 Supporting Information). Peptide **7b** displayed weak inhibition, possibly due to a steric clash between the linker and the enzyme. In the case of **7c**, the linker seems to be completely solvent exposed and unlikely to interact with the enzyme, resulting in better inhibition. These results indicate that the location of the linker can influence not only the helicity of the peptide, but also the inhibitory properties of the peptides.

	Inhibitor	Cathepsin K (μM)	Cathepsin L (μM)	Cathepsin S (μM)	Calpain-1 (μM)
7a	SEEFRQVMNGF	NT	133.1 ± 1.4	NT	NT
7b	SE**C**FRQ**C**MNGF	NT	83.1 ± 1.2	NT	NT
7c	S**C**EFR**C**VMNGF	NI	29.4 ± 1.1	92.3 ± 1.2	NI
7d	S**C**E*n*R**C**VMNGF	102.2 ± 1.4	6.1 ± 1.0	20.2 ± 1.1	NI
7e	S**C**E*b*R**C**VMNGF	NI	3.4 ± 1.0	43.1 ± 2.0	100.7 ± 31.3
7f	S**C**EFR**C**VMNG*n*	64.3 ± 12.5	6.7 ± 1.0	48.1 ± 1.2	NI
7g	S**C**E*b*R**C**VMNG*n*	32.0 ± 1.2	0.3 ± 1.2	27.4 ± 1.4	19.8 ± 6.3

Linked cysteines are bolded and underlined, mutated residues are italicized; NT=Not Tested; NI= Not Inhibited; *n*= Ala(2-naphthyl); *b*= Ala(4,4'-biphenyl)

Table 4.1: Cathepsin L inhibitor potency and selectivity.

Following optimization of the linker placement (**7c**), a structure-based approach was used to improve the potency and selectivity of the peptides. The prime side of the cathepsin L active site, where the relevant prodomain α-helix primarily binds, has one hydrophobic area: a shallow but wider surface near the canonical S3' binding site (Figure 4.1A).[3] The unprimed side of the cathepsin L active site also has a hydrophobic area: a narrow cleft proximal to the active cysteine around the S2 binding site.[3,158] The hydrophobic residues Leu69, Ala135, and Ala214 line the narrow cleft, while the shallow wider surface is comprised of Phe145, Phe143, Leu144, and Trp189. Based on the zymogen crystal structure the first Phe4 (relative to the N-terminus) in **7c** would be predicted to occupy the narrow cleft, while Phe11 in **7c** most likely is involved in π-π interactions with Trp189 and only partially occupies the hydrophobic surface. Hence, replacement of these residues with non-natural amino acid residues with a larger hydrophobic side chain might create a stronger hydrophobic interaction and in turn greater affinity of the inhibitor for the enzyme.

With this in mind, peptides **7d** and **7e** were synthesized, replacing Phe4 with Ala(2-naphthyl) and Ala(4,4'-biphenyl), respectively. As anticipated, both substitutions demonstrated increased inhibition of cathepsin L: the Ala(2-naphthyl) mutation resulted in a K_i~6 μM while the Ala(4,4'-biphenyl) mutation resulted in a K_i~3 μM (Table 4.1, Figures S4.6 and S4.7 Supporting Information). Interestingly, the biphenyl mutation resulted in a more specific inhibitor than the Ala(2-naphthyl) mutation. It can be postulated that the biphenyl offers an extended hydrophobic surface as well as some flexibility due to possible rotation between the two phenyl rings avoiding unfavorable steric clashes. Phe11 was mutated to Ala(2-naphthyl), **7f**. For the C-terminal modification, Ala(4,4'-biphenyl) was not considered because it would extend the peptide too far into the unprimed side possibly reducing specificity. This C-terminal Ala(2-naphthyl) mutation resulted in a K_i~6.7 μM (Table 4.1, Figure S4.8 Supporting Information). Combining the mutations from **7e** and **7f** resulted in an additive effect with the double mutant peptide **7g** showing a K_i against cathepsin L of ~300 nM that was at least 66 times more specific for cathepsin L over other enzymes (Table 4.1, Figure S4.9 Supporting Information). These results demonstrate that the prime side interactions are sufficiently different to allow us to create potent and highly specific cathepsin L inhibitors.

4.2.2 Design of an α-helical Cathepsin S Inhibitor

The cathepsin S inhibitor was designed similarly to the cathepsin L inhibitor. The putative α-helix scaffold **8a** was mutated to incorporate paired cysteines and then stabilized[159]; **8b** was stabilized closer to the N-terminus and **8c** was stabilized closer to

the C-terminus. Only inhibitor **8c** increased inhibition (Table 4.2, Figures S4.10-S4.12 Supporting Information). One hypothesis for the lack of potency of **8b** is that the *m*-xylene linker that stabilizes the α-helix creates a steric clash between the peptide and the enzyme (Figure 4.1B).

	Inhibitor	Cathepsin K (μM)	Cathepsin L (μM)	Cathepsin S (μM)	Calpain-1 (μM)
8a	TSEEVMSLMSS	NT	NT	101.6 ± 1.5	NT
8b	T**C**EEV**C**SLMSS	NT	NT	184.6 ± 1.1	NT
8c	TSEEV**C**SLM**C**S	NI	16.7 ± 2.6	52.1 ± 1.1	33.4 ± 10.3
8d	*W*SEEV**C**SLM**C**S	NI	76.0 ± 1.2	51.0 ± 1.2	108.4 ± 1.2
8e	T*W*EEV**C**SLM**C**S	67.5 ± 1.2	93.9 ± 1.3	29.7 ± 1.1	NI
8f	TSE*W*V**C**SLM**C**S	NI	57.1 ± 1.2	33.1 ± 1.1	NI
8g	TSEE*W***C**SLM**C**S	NI	>100	80.4 ± 1.2	NI
8h	T*W*E*W*V**C**SLM**C**S	65.7 ± 1.5	33.8 ± 1.2	14.3 ± 1.1	88.4 ± 1.1
8i	T*n*E*n*V**C**SLM**C**S	62.9 ± 1.2	2.4 ± 1.3	12.9 ± 1.1	97.3 ± 1.4
8j	*WW*E*W*V**C**SLM**C**S	19.5 ± 1.2	16.1 ± 1.4	6.7 ± 1.1	85.5 ± 1.3
8k	*WW*E*WW***C**SLM**C**S	37.9 ± 1.4	28.1 ± 1.1	1.1 ± 1.1	66.7 ± 1.2
8l	*FF*E*FF***C**SLM**C**S	NT	NT	13.1 ± 1.1	NT
8m	*WW*E*Wb***C**SLM**C**S	NT	NT	9.7 ± 1.0	NT

Linked cysteines are bolded and underlined, mutated residues are italicized. NT=Not Tested; NI=Not Inhibited; *n*=Ala(2-naphthyl); *b*=Ala(4,4'-biphenyl)

Table 4.2: Cathepsin S inhibitor potency and selectivity data.

Stabilized peptide **8c** inhibited cathepsin S with a modest K_i of ~54 μM (Table 4.2). Interestingly, **8c** was much more potent for cathepsin L over cathepsin S, but did not inhibit cathepsin K (Table 4.2). The cathepsin L activity could be attributed to the similarity in charge and polarity of the amino acid residues at the N-terminus of the stabilized parent peptides of cathepsin L and cathepsin S. Intriguingly, the area of the enzyme in proximity to the polar N-terminus of the α-helix (**8a**) is a large hydrophobic surface lined by residues Tyr117, Phe245, Trp285, and Phe289. Phe245 and Trp285 also comprise part of the S1' subsite where the parent peptide Met binds.[29] Therefore,

introducing hydrophobic residues into the N-terminus of the cathepsin S inhibitor would not only increase binding but also may increase specificity for cathepsin S over cathepsin L and cathepsin K since both these enzymes have a much smaller and more localized hydrophobic surface. Four of the five N-terminal residues were thus mutated to tryptophan beginning with single mutants (Table 4.2, Figures S4.13-S4.16 Supporting Information). The tryptophans in the first and second positions are likely binding to novel prime side sites.[29] The tryptophan residues at the fourth and fifth positions are most likely partially binding to the residues lining the S1' subsite as well as the novel hydrophobic surface. The single mutant studies demonstrated that changing any one of the N-terminal residues to tryptophan generally increased the peptides' affinity for cathepsin S (Table 4.2). The glutamate was not mutated because this residue appears to be involved in hydrogen bonding interactions with the enzyme via bridging water molecules.

Based on these findings, double, triple, or quadruple tryptophan mutants were synthesized using the hypothesis that adding multiple hydrophobic amino acid residues might increase the potency of the inhibitor, due to this presence of the much larger hydrophobic surface near the active site of cathepsin S. Two double mutants were synthesized, a double tryptophan mutant, **8h**, and a double Ala(2-naphthyl) mutant, **8i**. The tryptophan is largely hydrophobic, but it also has the ability to hydrogen bond directly or through water molecules using the indole ring. Both double mutants showed the same potency profile, suggesting that the hydrophobic interactions are the primary mode of binding at the N-terminus (Table 4.2, Figure S4.17 and S4.18 Supporting Information). The specificity profile for the two mutants was different though, with **8h** being more selective for cathepsin S than **8i** (Table 4.2). The tryptophan double mutant

8h, showed a K_i~14μM, and the specificity profile remained the same as **8c** (Table 4.2). The triple mutant **8j** further enhanced the inhibitory activity (K_i~7μM) (Table 4.2, Figure S4.19 Supporting Information). Finally, the quadruple mutant **8k** inhibited cathepsin S with a K_i~1.23μM and was 30-60-fold more selective for cathepsin S over other enzymes (Table 4.2, Figure S.4.20 Supporting Information). A quadruple phenylalanine mutant, **8l**, further emphasized the role of the hydrophobic interactions as phenylalanine has a smaller surface area, and subsequently creates weaker hydrophobic interactions thereby resulting in a less potent inhibitor (Table 4.2, Figure S4.21 Supporting Information).

4.2.3 Design of an α-helical Cathepsin K Inhibitor

Like cathepsin L and S, the unstabilized, native α-helix derived from the prodomain of cathepsin K demonstrated no inhibition of cathepsin K. After visual inspection of the zymogen structure, only one location seemed appropriate for side chain stabilization, peptide **9b** (Figure 4.1C). Unfortunately this inhibitor was not as potent as the other stabilized parent α-helical inhibitors (Table 4.3, Figures S4.23 and S4.24 Supporting Information).

	Peptide	Cathepsin K (μM)	Cathepsin L (μM)	Cathepsin S (μM)	Calpain-1 (μM)
9a	SEEVVQKMTGL	NI	NT	NT	NT
9b	S**C**EVV**C**KMTGL	196.9 ± 1.6	NI	255.3 ± 1.6	NI
9c	S**C**E*S*V**C**KMTGL	3.8 ± 1.1	116.9 ± 2.7	10.8 ± 1.0	217.6 ± 1.8
9d	S**C**E*H*V**C**KMTGL	15.7 ± 1.1	NT	NT	NT
9e	S**C**E*N*V**C**KMTGL	78.8 ± 1.3	NT	NT	NT
9f	S**C**E*L*V**C**KMTGL	19.0 ± 1.1	NT	NT	NT
9g	S**C**EVV**C**K*P*TGL	4.4 + 1.1	48.0 ± 1.20	58.3 ± 1.2	147.9 ± 1.5
9h	S**C**EVV**C**KM*W*GL	2.9 ± 1.0	16.8 ± 1.2	50.0 ± 1.0	37.1 ± 11.6
9i	S**C**EVV**C**KM*F*GL	10.2 ± 1.2	NT	NT	NT
9j	S**C**EVV**C**KMTG*P*	4.9 ± 1.1	53.9 ± 1.2	27.8 ± 1.5	NI
9k	S**C**E*S*V**C**KMTG*P*	20.3 ± 1.2	NT	NT	NT
9l	S**C**EVV**C**K*P*TG*P*	39.8 ± 1.1	NT	NT	NT
9m	S**C**E*S*V**C**K*PW*G*P*	16.0 ± 1.1	143.0 ± 1.4	375.0 ± 1.8	102.3 ± 1.6

Linked cysteines are bolded and underlined, mutated residues are italicized; NT=Not Tested; NI=Not inhibited

Table 4.3: Cathepsin K inhibitor potency and selectivity data.

To optimize electrostatic interactions with Gln242 on the enzyme surface, the Val was mutated to Ser, **9c**, His, **9d**, Asp, **9e**, or Leu, **9f** (Table 4.3 Figures S4.25-4.28 Supporting Information). Peptide **9c** (K_i~3.8 ± 1.1 μM) was by far the most potent peptide out of the mutants suggesting that perhaps there was a hydrogen bond forming at that location (Table 4.3).

In the zymogen crystal structure, the cathepsin K α-helix is terminated at the Met75 in the P2' position followed by a curve around the active site (Figure 4.3). Subsequently, the C-terminus (the last four amino acids) of peptide **9g** is unstructured in solution. It was hypothesized that replacing Met with Pro, a constrained amino acid, would provide some structure to the C-terminus to reduce binding energy as well as terminate the α-helix and enhance the curve around the active site. Inhibitor **9g** resulted

in an inhibitor with a K_i value of 4.4 μM, suggesting that Pro works as a constraint (Table 4.3, Figure S4.29 Supporting Information).

Other single mutations were a Thr to Trp mutation, **9h**, and Thr to Phe mutation, **9i**. Peptides **9h** and **9i** were designed to fit the respective tryptophan or phenylalanine into the S1' subsite.[11] The tryptophan could still form electrostatic interactions with Gln260 while also giving the possibility of forming a π-π interaction with the catalytic histidine. The phenylalanine could possibly only form π-π interaction with histidine. Peptide **9h** had a K_i~2.9 compared to **9i** which had a K_i~10.2 μM suggesting that π-π interactions as well as hydrogen bonding interactions are important (Table 4.3, Figures S4.30 and S4.31 Supporting Information).

It has been suggested that Pro is an optimal amino acid to bind to the S2 pocket of cathepsin K.[11,160] Thus we synthesized an inhibitor with a Leu to Pro mutation at the C-terminus, **9j**. The proline in the P2 position should be specific to cathepsin K, as it has been suggested that cathepsins S and L do not tolerate proline well at this position.[161] Inhibitor **9j** inhibited cathepsin K at a K_i~4 μM (Table 4.3, Figure S4.32 Supporting Information).

Double mutants **9k** and **9l** and quadruple mutant **9m** were synthesized to explore the effects of combining the single mutations. Unlike the inhibitors of the other enzymes the multiple mutants reduced the effectiveness of the inhibitor (Table 4.3, Figures S4.33-S4.35 Supporting Information). These results could stem from each single mutation slightly adjusting how the inhibitor fits into the prime side of the active site thereby changing the effect of the other mutation.

Each single mutant had a substantial inhibitory effect on cathepsin K. Peptide **9h** was the most potent inhibitor, while **9g** was almost as potent but about 10 fold more specific for cathepsin K over the all other enzymes. Thus, we were again able to create potent and specific leads for inhibitor development using rational structure-based design.

4.2.4 Peptide Characterization and Kinetics

After testing the inhibitory activity of the inhibitors, the peptides' helical character and the mode of inhibition were determined. First, circular dichroism analysis (CD) was used to characterize α-helicity. As expected, the parent peptides **7a**, **8a**, and **9a** showed some helical character but were primarily random coil as evidenced by a minimum closer to 200 nm rather than at 208 and 222 nm.[117] CD analysis of the linked peptides **7c**, **8c**, and **9b** showed an increased helical character upon stabilization (Figures S4.1 and S4.2 Supporting Information) as a decrease in the minimum at 222 nm and a shift in minimum to 208 nm from 200 nm. Thus the more helical the peptide, the more potent inhibitor, which supports the theory that the free energy needed for secondary structure formation is a substantial barrier to inhibitory activity of small, unstabilized peptides. Beyond the increase of helical character, it was clear that hydrophobic and π-π stacking interactions could further optimize inhibitor potency and specificity. Finally, standard Michaelis-Menten kinetics confirmed that all inhibitors acted in a competitive manner (Figure S4.36, Tables S4.2-S4.4 Supporting Information).

4.3 Conclusion:

We have used a structure-guided approach to develop competitive, non-covalent, α-helical inhibitors for cathepsins L, S, and K by mimicking their prodomain active site α-helices. We were able to generate inhibitor leads for each class of enzymes with good selectivity and moderate potency using only a small set of compounds. This proof-of-concept study provides the basis for the future optimization of more potent and specific inhibitors of cathepsins.

4.4 Materials and Methods:

4.4.1 Crosslinking with the unpurified peptide:

The lyophilized crude peptide was dissolved in DMF with 2% triethylamine. The alkylating agent (app. 3 eq) was added to the solution and shaken for the 2 h. The crude mixture was purified by HPLC.

4.4.2 Protease Activity Assays:

Peptides were evaluated for ability to bind and subsequently inhibit the cysteine proteases using standard proteolytic fluorescence activity assays. Inhibition was assayed using a standard donor quencher strategy using a previously published peptide substrates[62,140,141].

CHAPTER 5: Future Directions

Structure-based design has allowed us to create potent and specific inhibitors for papain family cysteine proteases. We have further used our knowledge of structure, endogenous inhibitor binding, and substrate specificity to increase the potency and specificity of each inhibitor. These inhibitors have thus become the basis for activity based probe and quench activity based probe development.

5.1 Incorporation of Cell Penetrating Peptides to Increase Cell Permeability

One of the issues faced during the development of these α-helical inhibitors and probes is the lack of cell penetrability. Cell permeability can be improved through the addition of cell penetrating peptides or CPPs. Cell penetrating peptides are generally derivatives of proteins that translocate cargo through the cellular membrane.[162,163] The parent proteins are often found in viruses or antimicrobial peptides.[162,163] CPPs can be amphipathic or polypositive. Amphipathic CPPs are generally α-helical with a positively charged face and a hydrophobic face. Polypositive CPPs are usually unstructured peptides with multiple arginines and/or lysines.[162,163] Cell penetrating peptides have been suggested to enter the cell via either endocytsosis, the method of entry of many of the virus derived CPPs, or via direct permeation, the suggested method of entry for polyarginine CPPs and amphipathic CPPs.[164]

CPPs have been successfully added to a calpastatin derivative, a 27 amino acid calpain inhibitor, to enhance cell permeability. One such CPP is penetratin.[62] Penetratin is a 7 or 16 amino acid derivative of the antennapedia homeodomain from Drosophila.[62,165] Penetrating was attached to the calpastatin derivative via a disulfide bond. The calpastatin

based inhibitor was then able to translocate through the cell membrane, localize to the cytoplasm, resulting in the inhibition of calpain-1.[62]

To increase cell penetration by the quench probes we propose the addition of 9-arginines, the 7 amino acid penetratin, or the CPP low molecular weight protamine or LMWP (a 14 amino acid derivative of protamine, a protein that binds DNA).[162,166] These peptides were chosen for their presumed ability to transport cargo to the cytoplasm rather than the lysosome or nucleus. For polyarginine CPPs it has been suggested that there is a threshold above which direct permeation is the predominate mode of entry as opposed to endocytsosis.[164] Amphipathic CPPs were avoided because they tend to have α-helical secondary structures and an additional α-helix may disrupt binding of the inhibitor to the enzyme.

For calpain inhibitors and probes the cell penetrating peptides would be added to the N-terminus of the quench probe In the crystal structure the portion of the calpastatin that binds to calpain domain-3 appears to mostly form backbone interactions with the enzyme rather than side chain interactions.[30,69] Furthermore, this portion of calpastatin also does not have many conserved residues (among the four calpastatin domains) making the sequence amenable to amino acid changes.[30,69] Furthermore, Betts et al. demonstrated that changing these residues to β-alanine did not affect the potency of the 27-mer calpastatin suggesting again that this region can be easily mutated with few adverse effects on potency.[123]

The cell penetrating ability of the probes can be tested in both a canonical HeLa cell line as well as a mouse embryo fibroblast (mEF) line that has both a wild type (WT) and calpain small subunit (CAPNS1-/-) constitutive knockout lines. The CAPNS1-/- line

allows for an additional negative control regarding the inhibitors/probes binding to active calpains. Enzymes can be manually activated using calcium ionophore. These cell studies will give us an idea as to how useful the inhibitors/probes will be in actual disease models.

5.2 Development of Cathepsin Probes

The small peptidic α-helical inhibitor of calpain was turned into an activity based probe through the addition of a warhead or substrate sequence and a tag, a fluorophore or biotin. The small α-helical prodomain based inhibitors developed for each individual cathepsin can also be models for activity based probe development. Similarly to calpastatin, these inhibitors will only bind to active enzymes because the prodomain in the inactive enzyme would sterically prevent the inhibitor/probe from binding to the enzyme.

The cathepsin inhibitor sits in the reverse direction of the substrate meaning that the C-terminus faces the unprimed side of the enzyme while the N-terminus faces the prime side. Based on the crystal structure models the N-terminus of these inhibitors is solvent exposed and not interacting with the enzyme. Thus the tag can be added via a peptide bond to the N-terminus of the inhibitor. Adding the tag to the N-terminus eliminates the necessity of having an alloc protected lysine or the cost of buying an amino acid with a biotin or fluorophore already attached. The development of these probes would help isolate the individual protease is involved in each respective disease.

5.3 α-helical Inhibitors for Other Classes of Proteases

We have primarily focused on designing α-helical inhibitors and probes for cysteine proteases, however we believe this inhibitory motif can be expanded to include other classes of proteases.

Thrombin is an enzyme involved in the clotting of blood, subsequently it is of great pharmaceutical interest as specific inhibitors of thrombin could be good anticoagulants.[167] When the insect the mosquito takes a blood meal it injects an enzyme called anophelin into the site of the blood draw to prevent clotting.[168] Interestingly, based on the crystal structure, it appears that anophelin binds to thrombin in the same way calpastatin binds to calpain. Anophelin is unstructured in solution and has a slow tight binding mechanism in which the inhibitor binds to the enzyme in the same N to C orientation as the substrate.[168] Anophelin also forms an α-helix at the active site just like calpain.[168,169]

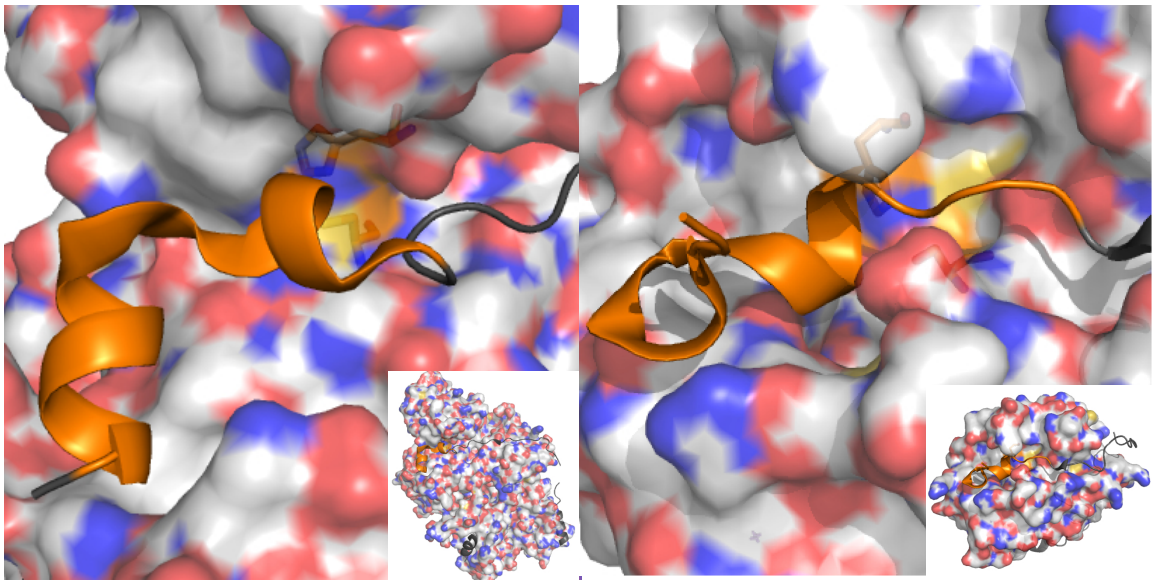

Figure 5.1: Active site α-helices of the calpain bound calpastatin (left) and the thrombin bound anophelin (right). Insets show the enzymes in their entirety. (Calpain: 3BOW; Thrombin: 4E06).[30,31,168]

Rather than appearing as a classical two-turn α-helix like in calpastatin, it appears that anophelin has a single α-helical turn followed by a β-turn. However, it is possible that either the single α-helical turn or the β-turn could be stabilized by the linker. Furthermore, from the information gathered during the calpain inhibitor stabilization studies it appears that a single proline near the stabilization site can result in a stable loop which could be a useful mutation in this inhibitor to stabilize the β-turn.

Development of inhibitors such as this could be quite useful as a scaffold for the development of new anticlotting therapeutics.

5.4 Concerns

Stabilized α-helices as inhibitors have previously successful as inhibitors of protein-protein interactions.[44] The advantage of these α-helical peptide inhibitors has been their increased specificity and potency due to the large number of inhibitor-protein contacts and the ability to interact with a large surface area. Furthermore, the stabilization of these peptides has reduced the entropic penalty of binding to the enzyme and in many cases also increased the cell permeability and proteolytic stability. Thus the inhibitors and probes that we have developed have the potential to begin a completely new class of tools for investigation into protease role in cell processes and disease.

The use of stabilized α-helices as protease inhibitors does have some drawbacks, though. We are targeting proteases, so we are deliberately sending the peptides to areas of high protease activity thereby increasing the potential for degradation. Furthermore, the protease inhibitors we have designed are stabilized in an *i*, *i*+4 conformation leaving the unstabilized portion of the inhibitor open to proteolysis. With these weaknesses in mind, cytoplasmic or extracellular proteases such as calpain-1 are probably the best targets for

the α-helical peptidic inhibitors as proteases in these locations are generally tightly regulated which reduces the likelihood of proteolysis. However, the work we have done on the cathepsin inhibitors is not in waste as we can use the knowledge we gained to synthesize non-peptidic inhibitors that exploit the same enzymatic binding sites as the α-helical inhibitors.

Another concern with the α-helical protease inhibitors was the lack of cell permeability of these peptides. This problem can be addressed through the use of other stabilization methods, like those discussed in the introduction (Chapter 1.5) which have been shown to possibly increase cell permeability, or through the use of cell penetrating peptides (Chapter 5.1).[170]

Finally, α-helical protease inhibitors and probes are likely most useful in the laboratory setting for the investigation of the role these cysteine proteases play in cell processes and disease models. However, the knowledge gained through the development and use of these probes may be helpful for creating small molecule inhibitors or therapeutics in the future.

APPENDIX

Abbreviations

ABP	activity based probe
β	Ala(4,4'-biphenyl)
βA	β-alanine
βP	β-proline
CAPNS1-/-	calpain-1 small subunit knockout
CD	circular dichroism
CPP	cell penetrating peptide
DCM	dichloromethane
DIPEA	diisopropylethylamine
DMF	α,α'-dimethylformamide
DMSO	dimethyl sulfoxide
DTT	dithiothreitol
EDT	1,2-ethanedithiol
EGTA	ethylene glycol tetraacetic acid
ESI	electrospray ionization
FITC	fluorescein isothiocyanate
HBTU	O-(benzotriazol-1-yl)-N,N,N',N'-tetramethyluronium hexafluorophosphate
HCl	hydrochloric acid
HCTU	O-(*1H*-6-chlorobenzotriazol-1-yl)-N,N,N',N'-tetramethyluronium hexafluorophosphate
HPLC	high pressure liquid chromatography

HRP	horseradish peroxidase
IC_{50}	concentration at which 50% of the enzyme is inhibited
INFIT	inverse Fourier transformation of in-phase multiplets
K_i	inhibition constant
K_m	Michaelis constant
MALDI-TOF	matrix-assisted laser desorption/ionization-time of flight
mEF	mouse embryo fibroblast
Mmt	methoxytrityl
MS	mass spectrometer
N	Ala(2-naphthyl)
NMP	N-methylpyrrolidone
NMR	nuclear magnetic resonance
PDB	protein database
pfF	pentafluorophenylalanine
PVDF	polyvinyl difluoride
RCM	ring closing metathesis
RFU	relative fluorescence units
SDS-PAGE	sodium dodecyl sulfate polyacrylamide gel electrophoresis
TCEP	*tris*(2-carboxyethyl)phosphine
TFA	trifluoroacetic acid
TFE	trifluoroethanol
TIPS	triisopropylsilane
Trt	trityl
WT	wild type

Chapter 2 Supporting Information

General Information

Amino acids were purchased from Advanced ChemTech(Louisville, KY) or Chem-Impex (Wood Dale, IL). Biotinylated lysine was purchased from Anaspec (Freemont, CA). All crosslinkers and the enzyme papain were purchased from Sigma-Aldrich® (St. Louis, MO). Chemicals were purchased from Fisher Scientific (Pittsburgh, PA). Calpain-1 and cathepsin B were purchased from BioVision (Milpitas, CA). Cathepsin L was purchased from EMD Millipore (Billerica, MA). Substrates were purchased from Peptides International (Louisville, KY). Single fritted reservoirs for peptide synthesis were purchase from Biotage (Redwood City, CA). Film for imaging blots was purchased from Kodak (Rochester, NY). Bis-Tris NuPAGE® gels and a Novex® Colloidal Blue Staining Kit were purchased from Life Technologies (Grand Island, NY). A Vectastain® Elite® ABC kit for biotin blotting was purchased from Vector Laboratories (Burlingame, CA). A Bio-Rad Silver Stain Plus Kit was purchased from Bio-Rad (Hercules, CA). Peptides were synthesized on an Argonaut Quest™ 210 (Argonaut Technologies, Inc. now owned by Biotage, Redwood City, CA) or on a Symphony automated peptide synthesizer (Protein Technologies, Inc., Tuscon, AZ). Peptides were purified on an Agilent 1100 Series LC/MS or an Agilent 1200 Series LC/MS (Agilent Technologies, Inc., Santa Clara, CA) Hewlett Packard ChemStation software using a Vydac® C8 column (Grace, Deerfield) or a Zorbax XDB-C18 column (Agilent Technologies, Inc., Santa Clara, CA). Matrix assisted laser desorption/ionization time of flight (MALDI-TOF) mass spectra were obtained using a Bruker Ultraflex III

mass spectrometer (Billerica, MA). Electrospray ionization (ESI) mass spectra were obtained with a QTRAP® 3200 (AB SCIEX, Framingham, MA). Circular dichroism (CD) spectra were obtained with a JASCO J-810 spectropolarimeter (JASCO, Inc., Easton, MD) equipped with a Peltier temperature control unit. NMR spectra were obtained using a Bruker Avance III 500 MHz spectrometer equipped with a cryogenic probe (Billerica, MA). UV-Vis absorbance spectra were obtained using a NanoDrop 1000 spectrophotometer (Thermo Scientific, Wilmington, DE). Fluorescence spectra were collected with a Berthold Tri-Star multimode microplate reader (Berthold Technologies, GmbH & Co. KG, Bad Wildbad, Germany). Gels were visualized with a Typhoon Fluorescent Imager (GE Healthcare Biosciences, Pittsburgh, PA). Graphing was performed using GraphPad Prism (GraphPad Software, La Jolla, CA).

Synthetic procedure

General peptide synthesis: All peptides were synthesized at 0.1 or 0.2 mmol scales using Chemmatrix Rinkamide Resin (substitution: 0.52 mmol/g) or CLEAR^{TM} Amide resin (substitution: 0.46 mmol/g). Fmoc-protected amino acids (5-fold excess) were activated with 0.95 equivalents (relative to the amino acid) of HBTU in the presence of 10 equivalents of diisopropyethanolamine (DIPEA). Amino acids were coupled for 5 min at 65 ^{o}C in DMF (Quest synthesis) or 25 min at room temperature in DMF (Symphony synthesis). Fmoc deprotection was performed using 20% 4-methyl piperidine in DMF for 5 min at 65 ^{o}C (Quest Synthesis) or 2.5 min (x 2) at room temperature (Symphony Synthesis). Side chain deprotection and the simultaneous cleavage from the resin were carried out using a mixture of TFA/thioanisole/ethanedithiol/anisole (90:5:3:2, v/v) at room temperature, for 2.5 hours. The crude peptide was precipitated using cold diethyl ether and purified via reverse-phase chromatography with a C8 preparative column using buffer A (0.1% TFA in Millipore water) and buffer B' (0.1% TFA in 60% iso-propanol/30% acetonitrile /10% Millipore water). Initial HPLC conditions were 5% B'/95% A. Initial conditions were run for 5 min, followed by an increase of solution B' to 100% at 25 min (5%/min.) at a flow rate of 5 ml/min unless otherwise indicated. The mass of all peptides was verified by MALDI-TOF or ESI-MS and purity (greater than 95%) was checked by analytical HPLC.

	Sequence	Calcd m/z	Obsvd m/z	HPLC-Gradient	Retention Time (min)
Model Peptide	Ac-YGGEAAREACARECAARE-NH_2[171]	1954.4	1954.1	0-100%	13.3

(C4 Vydac column over a gradient 0% to 100% of acetonitrile in water (0.1% TFA) over 40 minutes)

Table S2.1. Calculated and observed model peptide masses.

Crosslinker Screening Procedure

Preparation of stock solution: A peptide solution (0.114 mM) in NH_4HCO_3 buffer (12mL, 50 mM, pH=8.0) was treated with TCEP (1M solution in the same NH_4HCO_3 buffer, 1.1 eq.) at room temperature for 1 h.[42,105,172] The concentration of the peptide solution was measured by A_{280}= 1280 $M^{-1}cm^{-1}$ or by a weight based method (molecular weight was adjusted by adding one TFA salt per basic residue and by adding 10% (of the calculated molecular weight) to account for hydration after lyophilization).

Crosslinking procedure in 96-well plate: 90 μL of the stock solution was added to each well of a black round-bottomed 96-well plate (polypropylene). 10 μL of the freshly prepared alkylating agent solution (1.5 mM in anhydrous DMF, 1.5 eq.) was added to each well at room temperature and stirred for 2 h while protected from light. MALDI analysis was done to see the reaction progress and more alkylating agent was added if needed. Addition of 5% HCl to each well neutralized and subsequently quenched the reaction. 100 μL of diethyl ether was added to the organic layer to remove excess alkylating agent. The ether layer was removed by pipetting and MALDI-TOF spectra were taken of the sample in the remaining aqueous solution mixture.

High concentration of Reactants (for "selection of the fittest" reaction)

Preparation of stock solution: A peptide solution (1.2 mM) in Tris-HCl buffer (100 mM, pH=8.0) was treated with TCEP (1M solution in the Tris-HCl buffer, 1.1 eq.) at room temperature for 1 h. The concentration of the peptide solution was measured by A_{280}= 1280 $M^{-1}cm^{-1}$ or by a weight based method (molecular weight was adjusted by adding one TFA salt per basic residue and by adding 10% (of the calculated molecular weight) to account for hydration after lyophilization).

Crosslinking procedure in 1.5 mL centrifuge tube: This procedure is slightly modified from the procedure in Materials and Methods. 450 μL of the stock solution of peptide was added to a 1.5 mL polypropylene microcentrifuge tube. 50 μL of the freshly prepared alkylating agent solution (225 mM in anhydrous DMSO, app. 20 eq.) was added to each well at room temperature and the turbid mixture was shaken for 2 h under protection from light. The reaction was quenched by neutralization through the addition of 0.6 N HCl (10 μL) into each well. Each tube was centrifuged to remove the insoluble material and the supernatant was either purified by HPLC analysis or lyophilized.

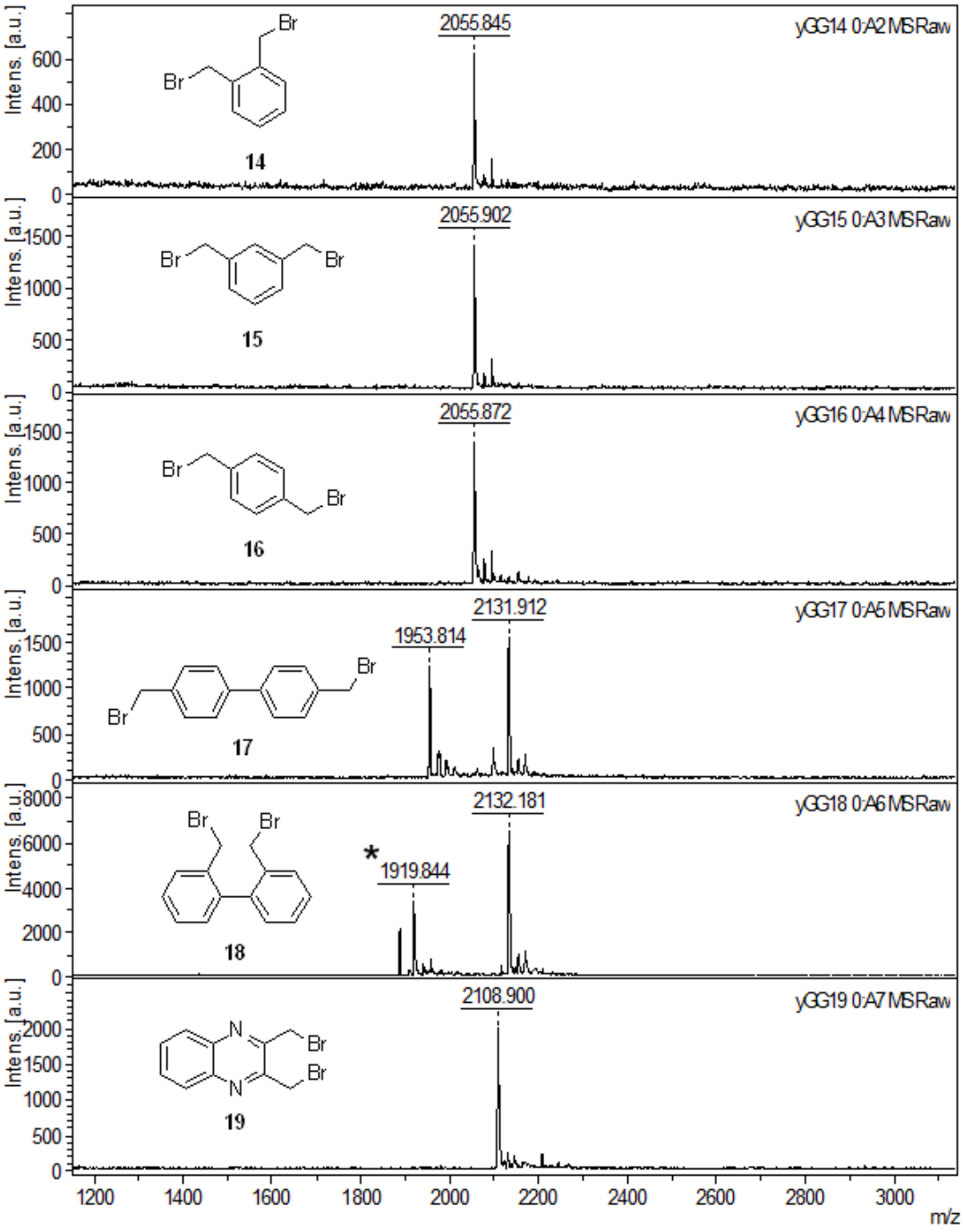
Intens. [a.u.]
2055.845
yGG14 0:A2 MSRaw
Br
Br
14
2055.902
yGG15 0:A3 MSRaw
Br
Br
15
2055.872
yGG16 0:A4 MSRaw
Br
Br
16
2131.912
1953.814
yGG17 0:A5 MSRaw
Br
Br
17
2132.181
yGG18 0:A6 MSRaw
*
1919.844
Br
Br
18
2108.900
yGG19 0:A7 MSRaw
N
N
Br
Br
19
1200
1400
1600
1800
2000
2200
2400
2600
2800
3000
m/z

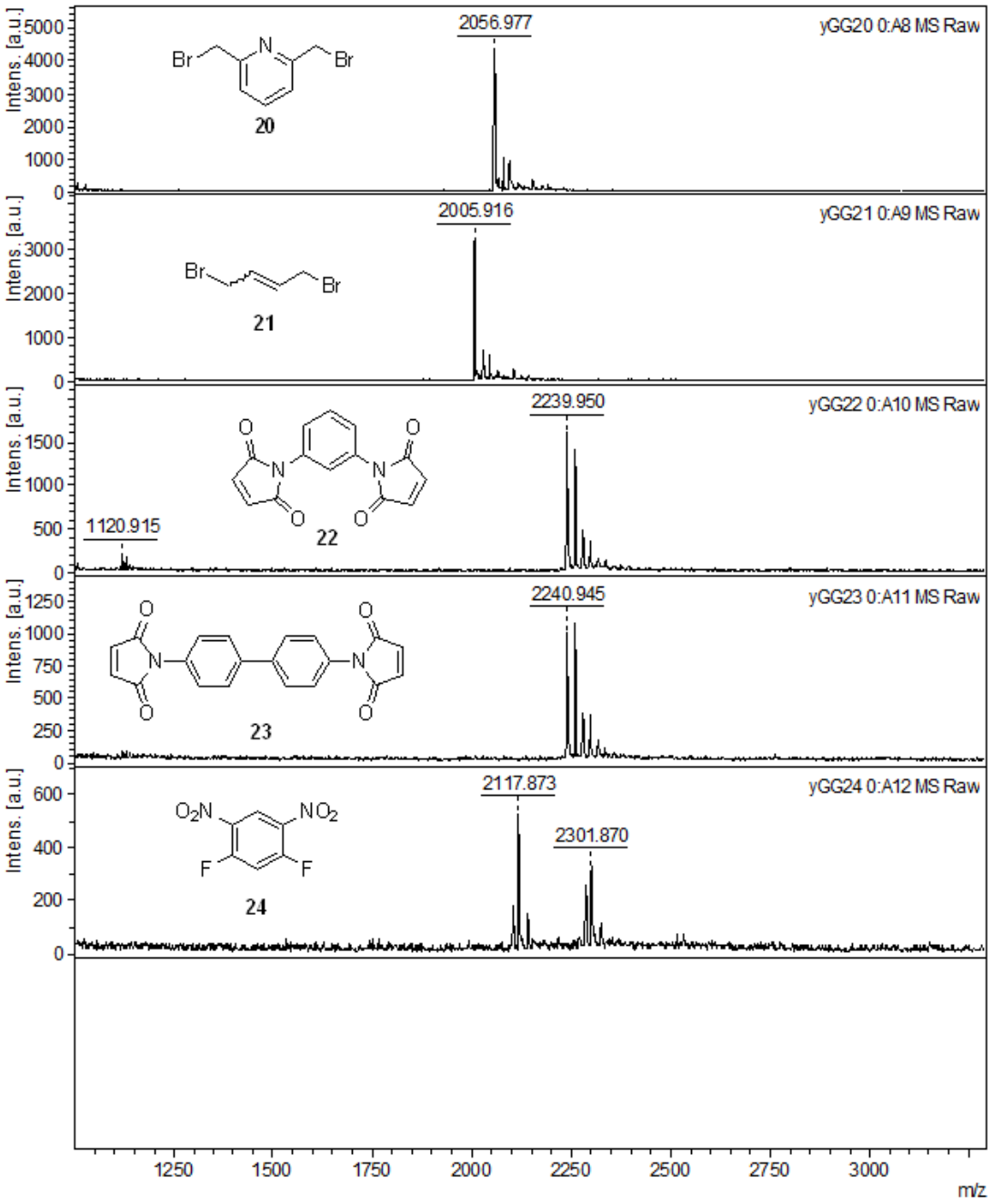

* 1919.84 appeared to be elimination of thiol from the cysteine.

Figure S2.1. MALDI spectra of low concentration linker with the model peptide.

Without Crosslinker

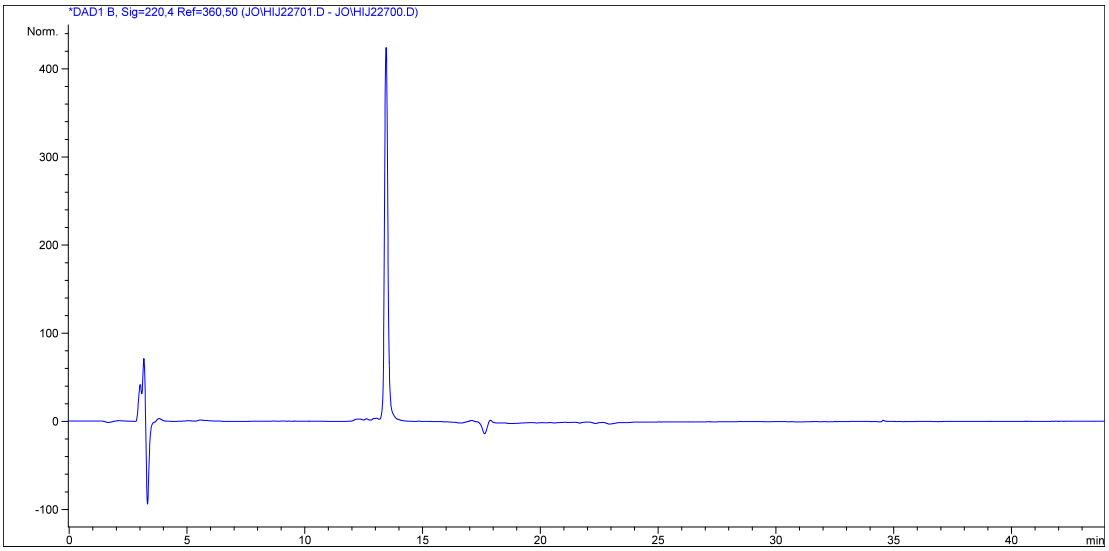

Reaction with crosslinker **c14**

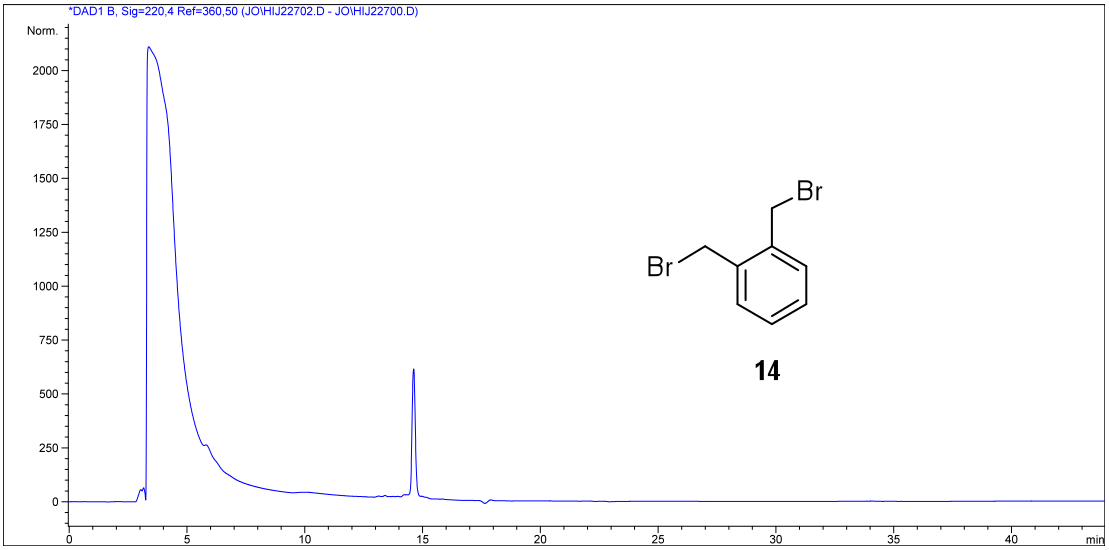

14

Reaction with crosslinker **c15**

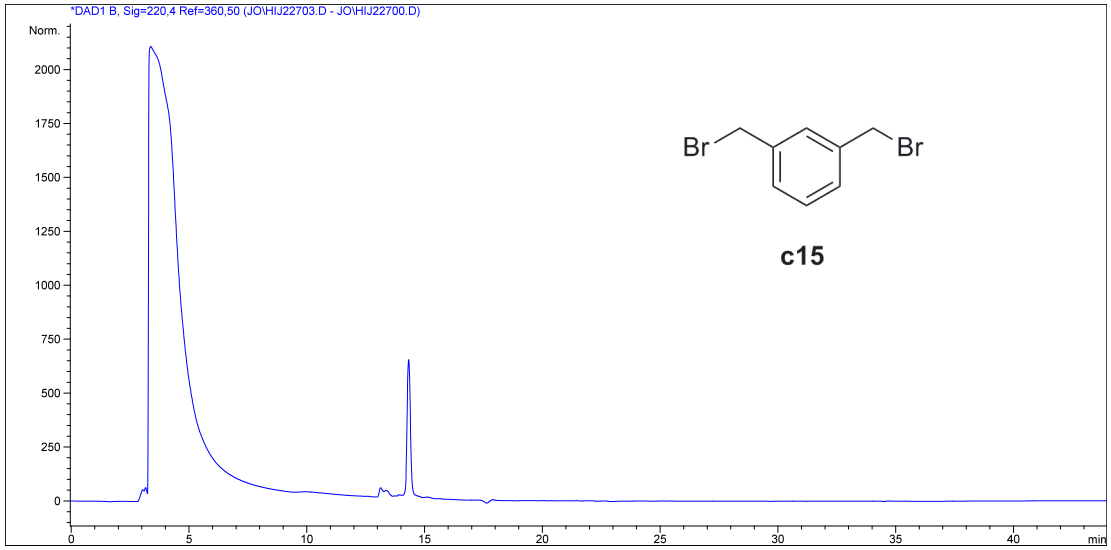

Reaction with crosslinker **c16**

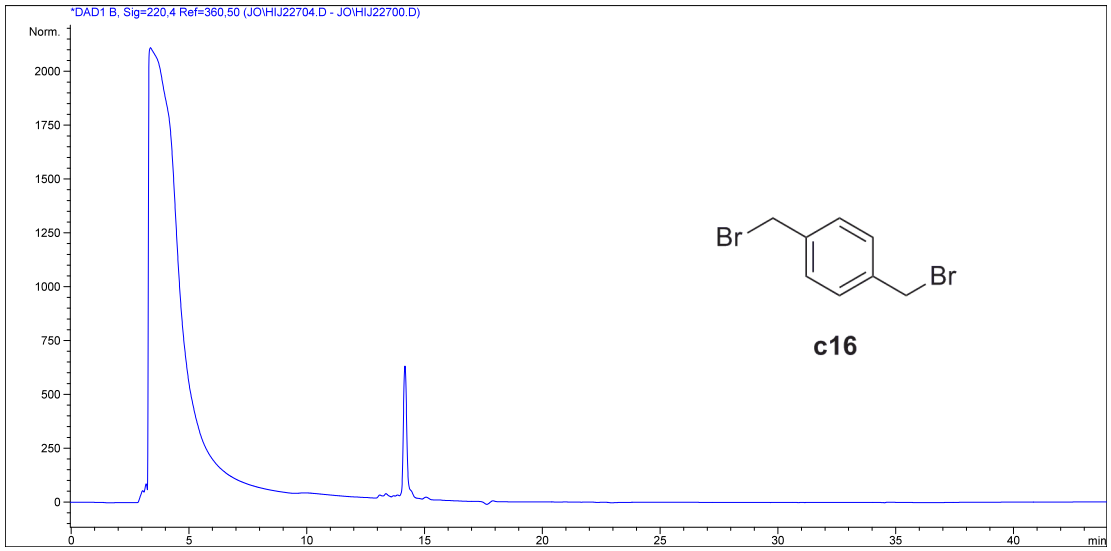

Reaction with crosslinker **c17**

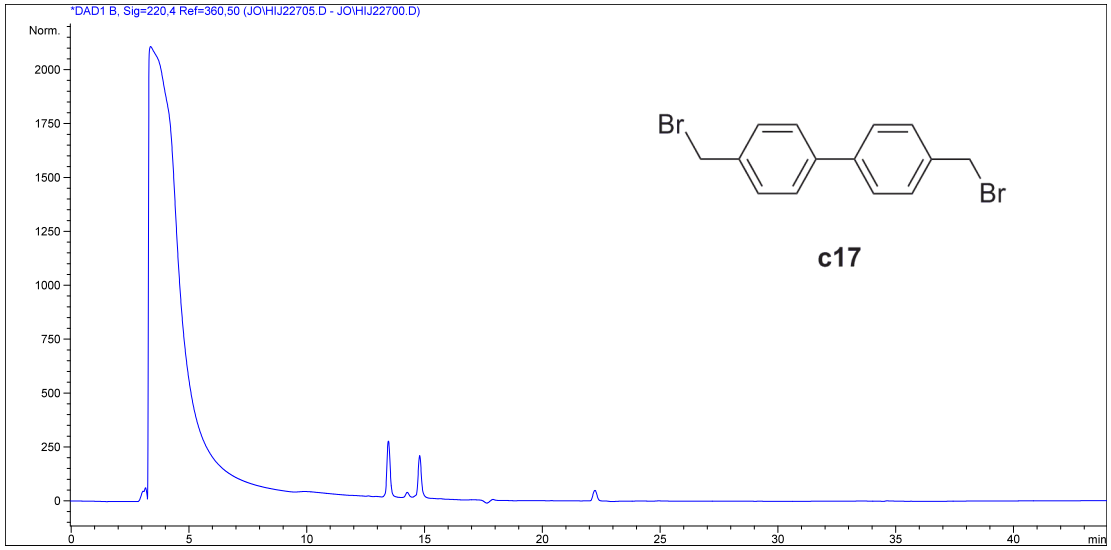

Reaction with crosslinker **c18**

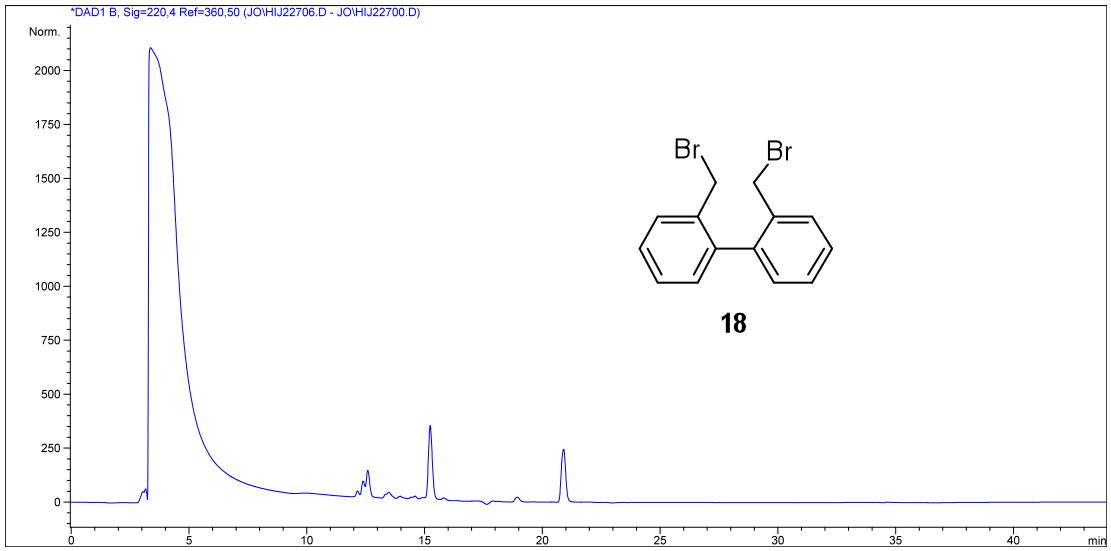

Reaction with crosslinker **c19**

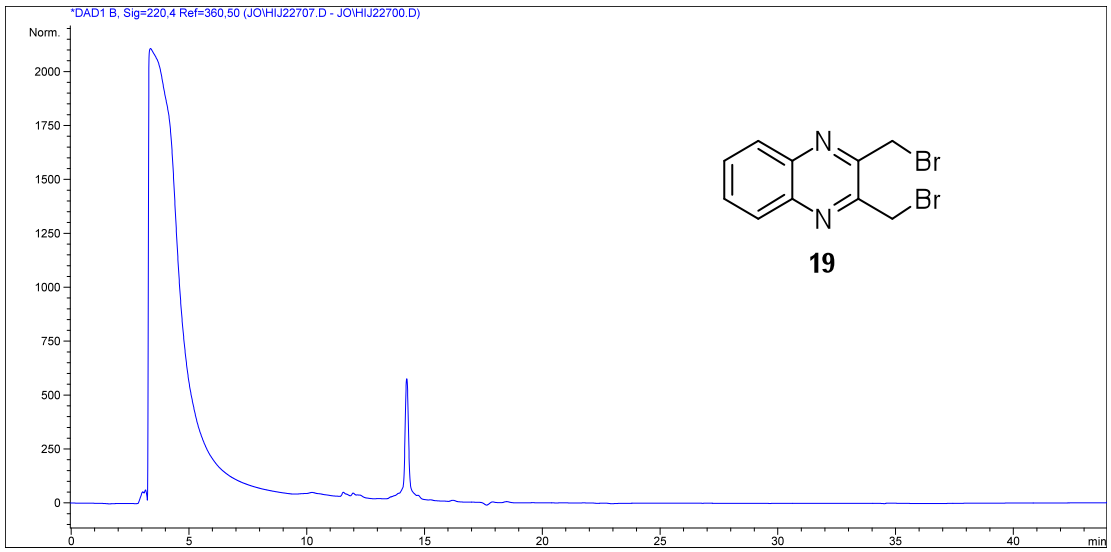

Reaction with crosslinker **c20**

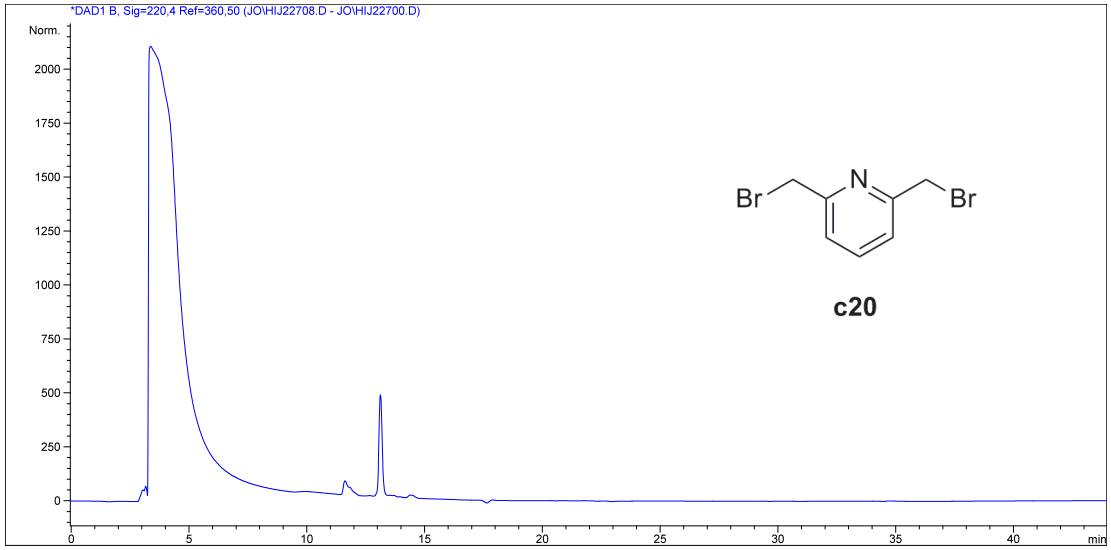

Reaction with crosslinker **c21**

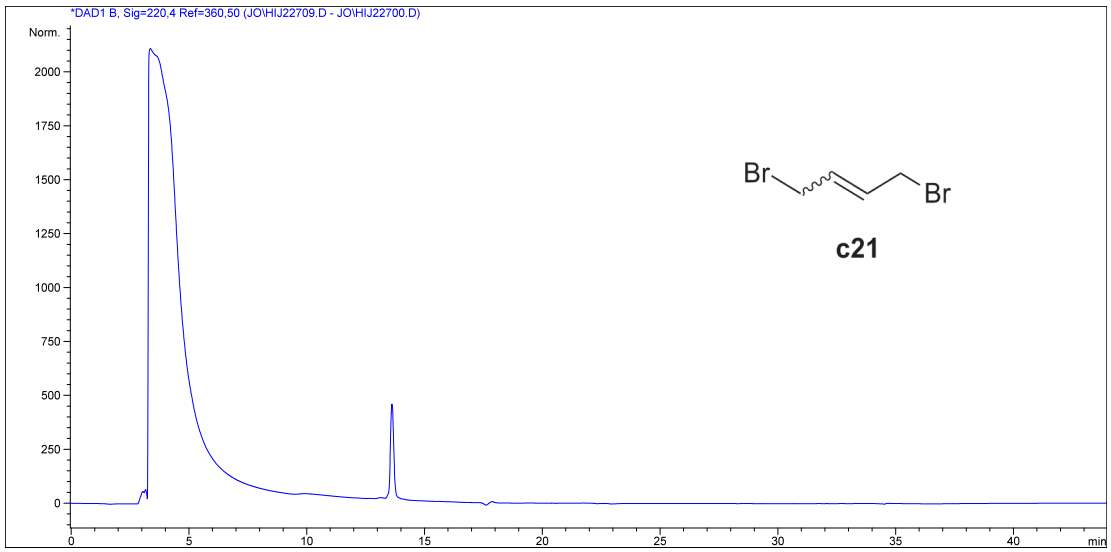

Reaction with crosslinker **c22**

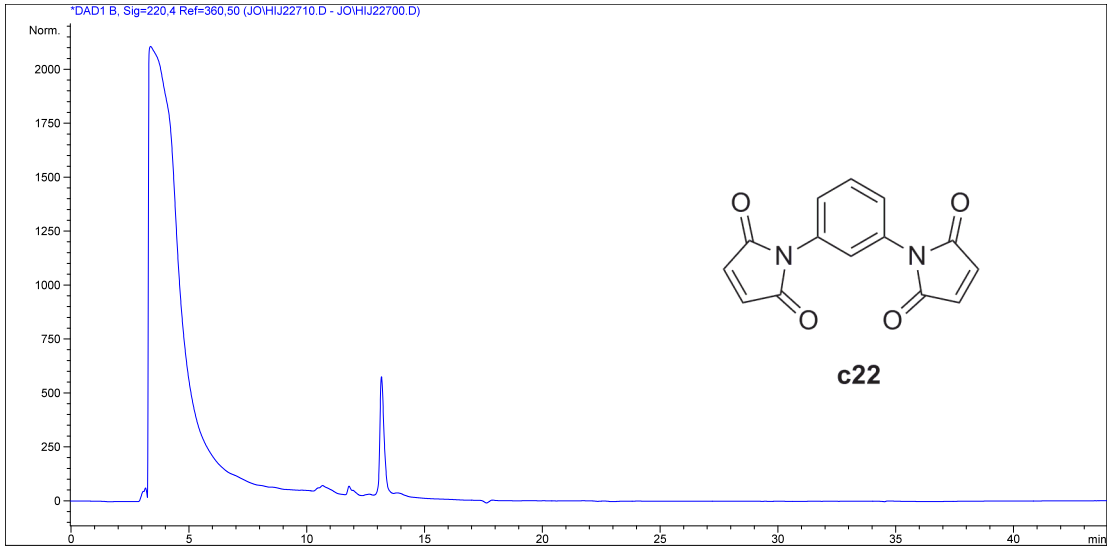

Reaction with crosslinker **c23**

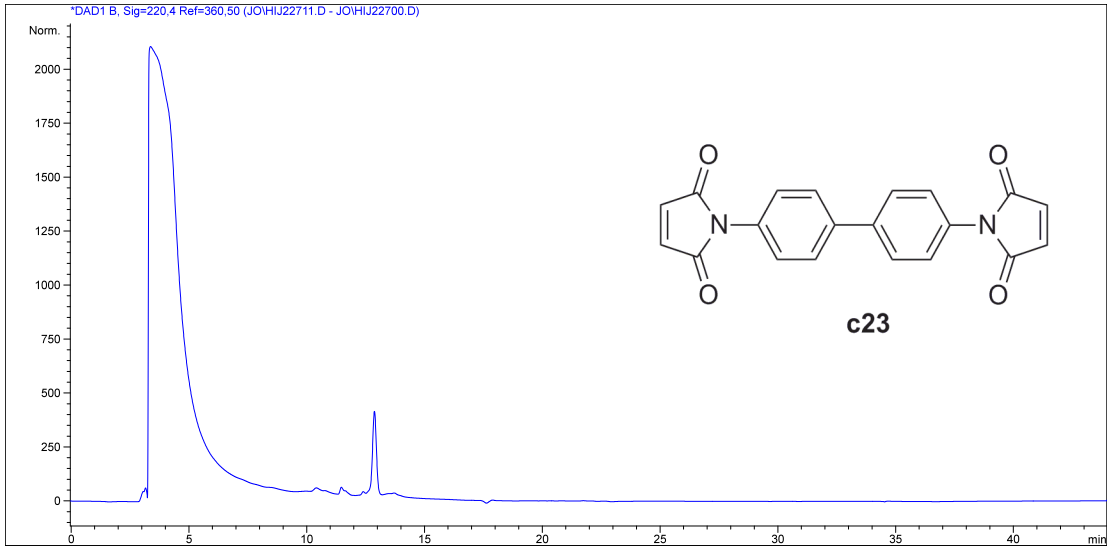

Reaction with crosslinker **c24**

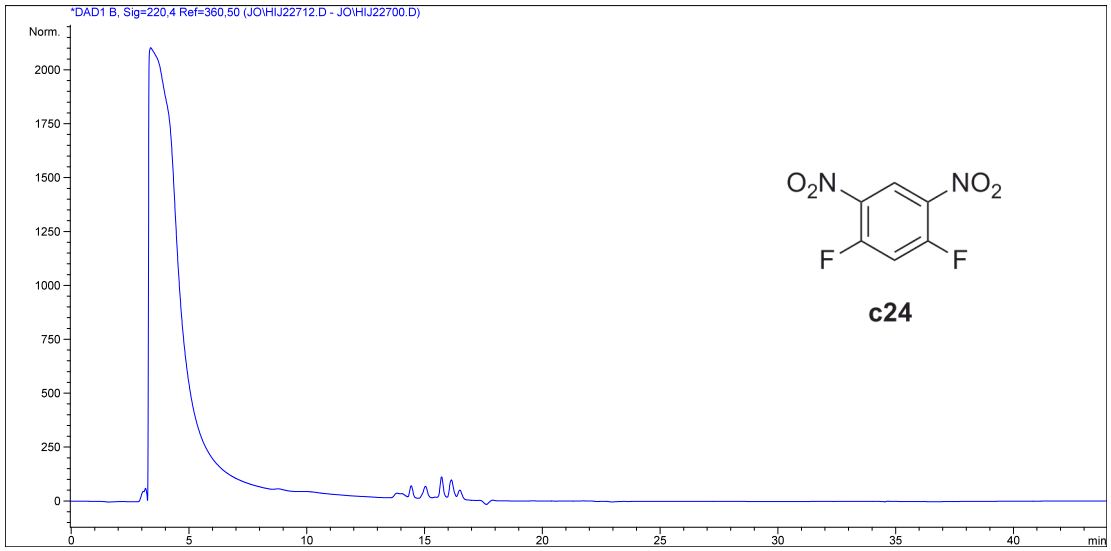

Figure S2.2 Crude HPLC profile (Low Concentration Reaction with the model peptide).

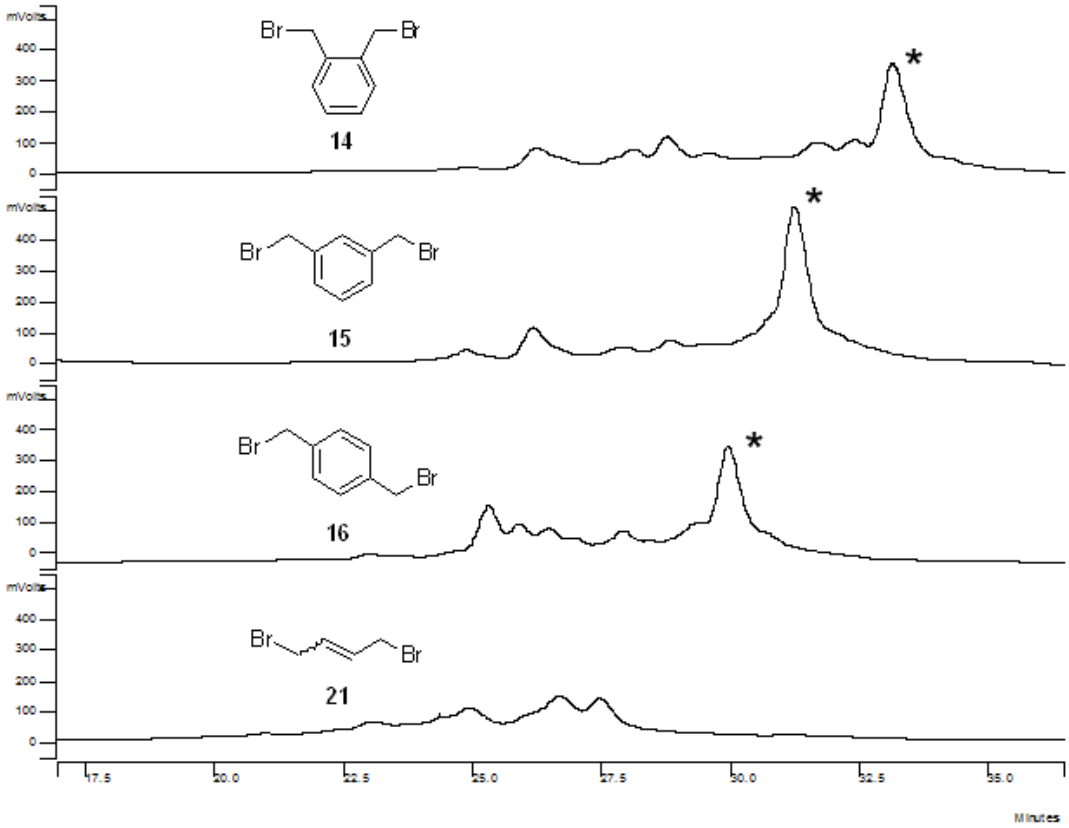

* denotes the major monocyclization product

Figure S2.3. Crude HPLC profile – "selection of the fittest" reaction

NMR spectroscopy

The peptide sample was prepared using peptide concentrations of 2 mM in 0.6 mL of a 9:1 v/v water/D_2O mixture in 50mM sodium phosphate, pH 5.5. All spectra were recorded at 10 ^oC on a Bruker Avance III 500 MHz spectrometer equipped with a cryogenic probe.

All 2D homonuclear spectra were recorded with standard pulse sequences[173]. 2D NOESY experiments were carried out with mixing times of 150 ms and 250 ms, respectively, 5483 Hz on both t_1 and t_2 dimensions with $t_{1,max}$ = 93 ms and $t_{2,max}$ = 183 ms, 32 scans. 2D TOCSY experiments were carried out with a mixing time of 75 ms, 5000 Hz on both t_1 and t_2 dimensions with $t_{1,max}$ = 93 ms and $t_{2,max}$ = 205 ms. 2D DQF-COSY experiments were carried out with 5000 Hz on both t_1 and t_2 dimensions with $t_{1,max}$ = 120 ms and $t_{2,max}$ = 205 ms. The ^1H carrier frequency was always set to the water peak and chemical shifts were referenced with respect to the residual water peak at 4.90 ppm.

Spectra were processed and analyzed using the programs nmrPipe[174] and XEASY[175], respectively. Time domain data were multiplied by sine square bell window functions shifted by 60^o and zero-filled once.

Using DQF-COSY, TOCSY, and NOESY sequence specific assignments were obtained following standard procedures[173].

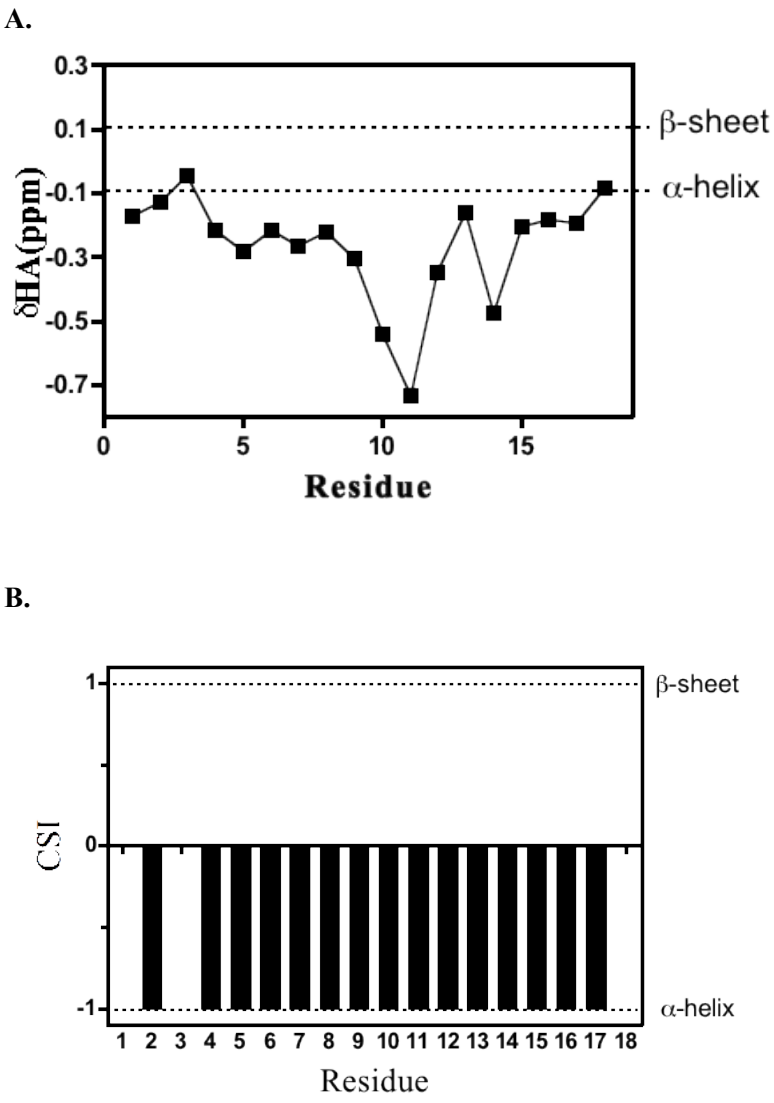

Figure S2.4. Characterization of helix formation in the peptide by NMR spectroscopy. **A) Secondary chemical shifts of α-H as a function of residue. B) Chemical shift index (CSI) output as a function of residue. Both strongly demonstrate helix formation even in the fraying terminus.**

α-H chemical shifts have a strong relationship to protein secondary structures[176]. Secondary chemical shifts are calculated by subtracting the experimental values from the intrinsic values. Secondary chemical shifts indicate that all 18 residues show helix formation in the peptide. Output from Chemical Shift Index (CSI) [176,177] clearly shows that 83% (15 out of 18) residues form helical structures. Two of the three non-helical residues are terminal residues. The third non-helical residue is the helix breaker glycine.

Alanine Scanning Mutagenesis

To identify the hot spot residues that are important to the protein-peptide interaction, the molecular modeling software package Rosetta[178] was used to calculate the binding free energy changes upon alanine mutation of each residue. The hot spots are defined as the residues that have changes in the binding free energy more than 1 kcal/mol when mutating to alanine (ΔΔG value).[179] Modeling was begun with the 3BOW.pdb crystal structure. The target sequence was threaded into the backbone, namely E622K(204), H625E(207) and D628A(210), and then the whole peptide was repacked as the starting structure. Alanine scanning was performed for each residue sequentially and the ΔΔG value was calculated as show in table S2.2.

Residue	Chain ID	Mutation	ΔΔG (kcal/mol)
207	C	E→A	-0.1
206	C	R→A	0.0
210	C	A→A	0.0
211	C	N→A	0.1
201	C	I→A	0.3
204	C	K→A	0.4
203	C	P→A	0.5
202	C	P→A	1.1
205	C	Y→A	1.5
209	C	L→A	1.7
208	C	L→A	1.9

Table S2.2. Alanine Scanning Mutagenesis,

Synthesis of calpain inhibitors

Calpain inhibitors were synthesized via solid phase peptide synthesis in the same manner as the model peptide. Helical calpain inhibitors were stabilized using the α,α'-dibromo-*m*-xylene crosslinker c15 and the "low concentration" linking protocol.

Peptide No.	Sequence	Calcd (m/z)	Obsvd (m/z)	HPLC-Gradient	Retention Time (min)
Parent	Ac-IPPKYRELLA-NH_2	1240.5	1240.5	0-100%	6.91
3a	Ac-IPCKYRCLLA-NH_2	1220.6	1220.5	0-100%	6.85
3b	Ac-IPPCYRECLA-NH_2	1205.5	1205.3	0-100%	7.60
3c	Ac-IPPKYCELLC-NH_2	1219.6	1219.4	0-100%	8.30
3a	Ac-IPCKYRCLLA-NH_2	1322.6	1322.6	0-100%	7.99
3b	Ac-IPPCYRECLA-NH_2	1307.5	1307.5	0-100%	8.60
3c	Ac-IPPKYCELLC-NH_2	1321.6	1321.5	0-100%	9.83

Table S2.3. Uncrosslinked and crosslinked calpastatin fragment peptides. 3a-c are all *m*-xylyl crosslinked. Peptides were run on an Agilent LC-MS with an Eclipse XDB-C18 column over a gradient of acetonitrile in water (0.1% HCOOH) over 20 minutes.

CD Spectra of Calpain Inhibitors without TFE

Peptide solutions were prepared at ~100 μM in 50 mM Tris-HCl (pH 7.5) without TFE. Concentrations were determined by measuring tyrosine absorbance at 276 nm with an extinction coefficient of 1400 M^{-1} cm^{-1}. Scans were conducted from 260 nm to 200 nm.[113,117,180] Measurements were conducted at 20°C in 1 nm step mode with a response time of 4 seconds in a 1 mm path length quartz cuvette.

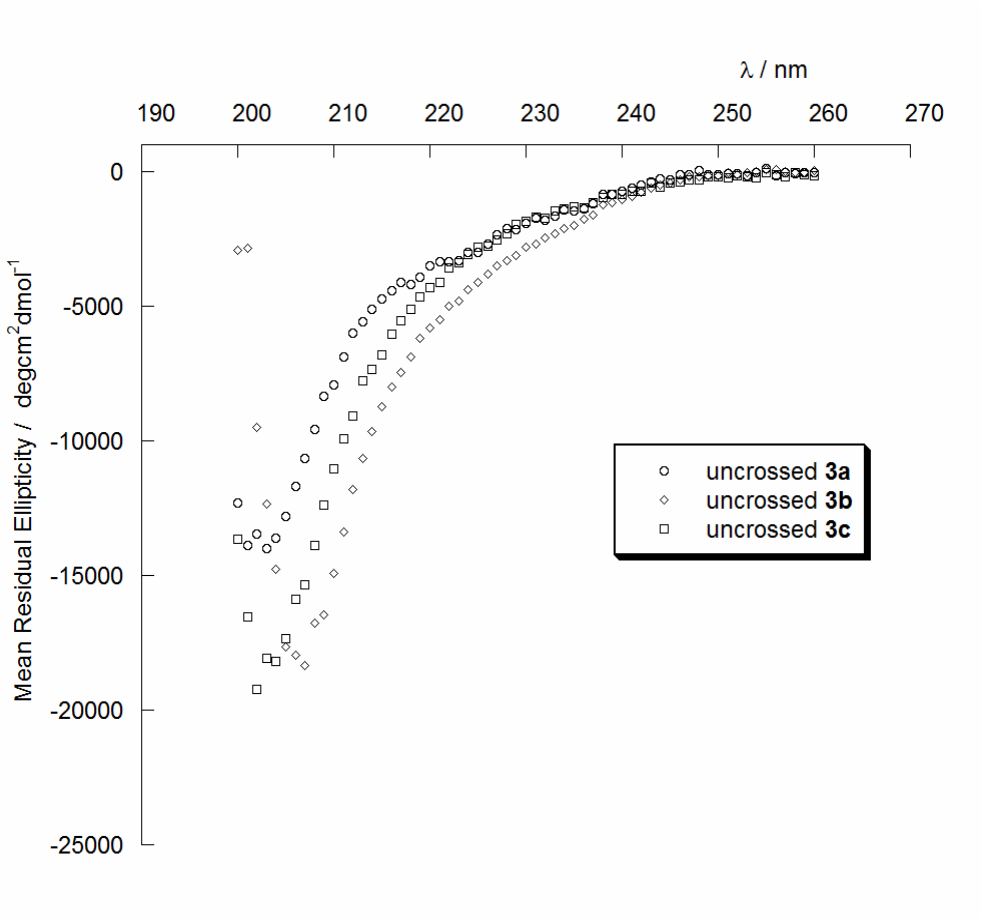

Figure S2.5. CD spectrum of uncrosslinked peptide 3a-c in Tris buffer (50mM, pH=7.5).

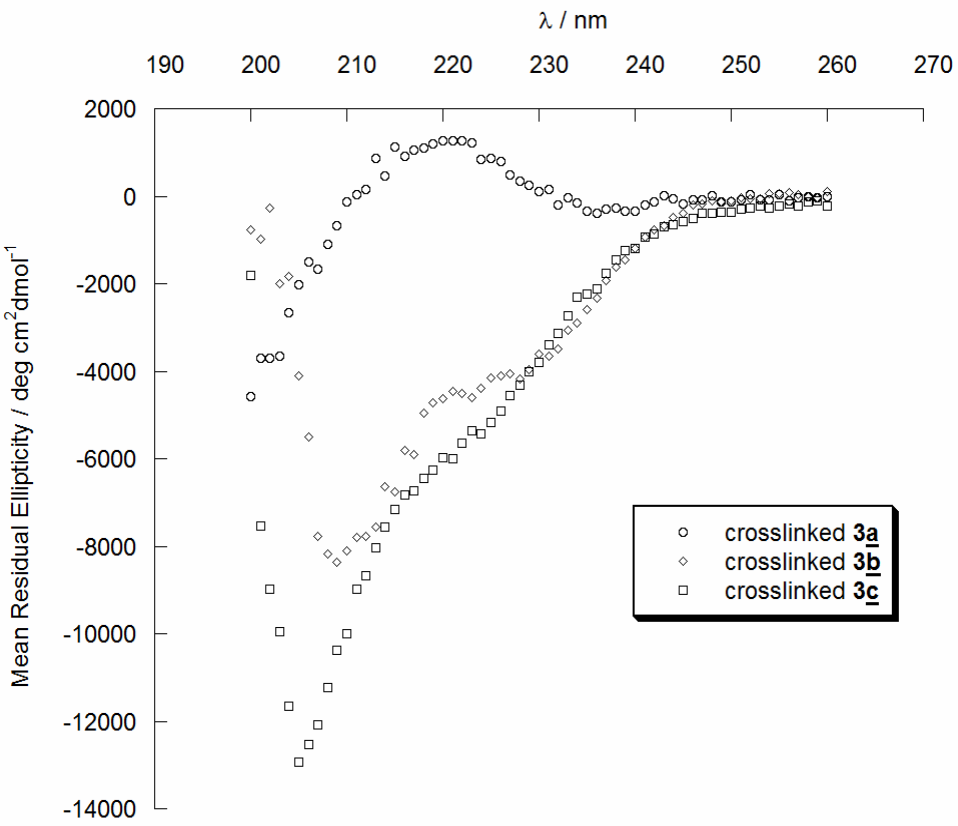

Figure S2.6. CD spectrum of crosslinked peptide 3a-c in Tris buffer (50mM, pH=7.5).

Protease Activity Assays

All peptides were evaluated for ability to bind and subsequently inhibit the cysteine protease calpain using standard proteolytic fluorescence activity assays. Inhibition was assayed using a standard donor-quencher strategy using a previously published calpain peptide substrate.[62,140,141]

Calpain Assay: Enzyme concentration for calpain-1 was 25 nM. The buffer contained 10 mM dithiothreitol (DTT), 100 mM KCl, 2 mM EGTA, 50 mM Tris-HCl (pH 7.5), and 0.015% Brij-35. Substrate concentration was 0.25 μM H-Glu(Edans)-Pro-Leu-Phe-Ala-Glu-Arg-Lys(Dabcyl)-OH.[62,140,141] Varying concentrations of inhibitor, 0, 0.5, 1, 2, 5, 7, 10, 15, 25, 50, and 100 μM, were used for each assay. Positive controls contained no inhibitor and negative controls contained no calcium. Enzyme, buffer, substrate, and inhibitor (or DMSO in controls) were combined. Calpain was activated by the injection of $CaCl_2$ to a final concentration of 5 mM. All assays were done in triplicate at a total well volume of 100 μL in 96-well plate, and each well contained a separate inhibitor concentration. Fluorescence readings were taken every 13 seconds for one hour in a fluorescent plate reader. Excitation wavelength was 380 nm and the emission wavelength was 500 nm.

Papain Assay: Enzyme concentration for papain was 25 nM. The buffer contained 10 mM dithiothreitol (DTT), 100 mM KCl, 2 mM DGTA, 50 mM Tris-HCl (pH 7.5), 0.015% Brij-35. Substrate concentration was 10 μM H-Glu(Edans)-Pro-Leu-Phe-Ala-Glu-Arg-Lys(Dabcyl)-OH.[62,140,141] Varying concentrations of inhibitor, 0, 0.5, 1, 2, 5, 7, 10, 15, 25, 50, and 100 μM, were used for each assay. Buffer, papain, and

inhibitor were all combined first. The assay was initiated by the addition of substrate via a multichannel pipette. All assays were done at a total well volume of 100 µL in 96-well plate, and each well contained a separate inhibitor concentration. Fluorescence readings were taken every 13 seconds for one hour in fluorescent plate reader. The excitation wavelength was 380 nm and the emission wavelength was 500 nm.

Cathepsin Assay: Enzyme concentration for cathepsin B and cathepsin L was 3 nM. The buffer contained 10 mM DTT, 500 mM sodium acetate (pH 5.5), and 4 mM EGTA, and 0.015% Brij-35.[62,140,141] Substrate concentration for both enzymes was 0.25 µM Z-FR-Amc. 0, 0.5, 1, 2, 5, 7, 10, 15, 25, 50, and 100 µM, were used for each assay. Buffer, enzyme, and inhibitor were combined. Cathepsin assays were activated by the addition of substrate via a multichannel pipette. All assays were done at a total well volume of 100 µL in 96-well plate, and each well contained a separate inhibitor concentration. Fluorescence readings were taken every 13 seconds for one hour in fluorescent plate reader. The excitation wavelength was 351 nm and emission wavelength was 430 nm.

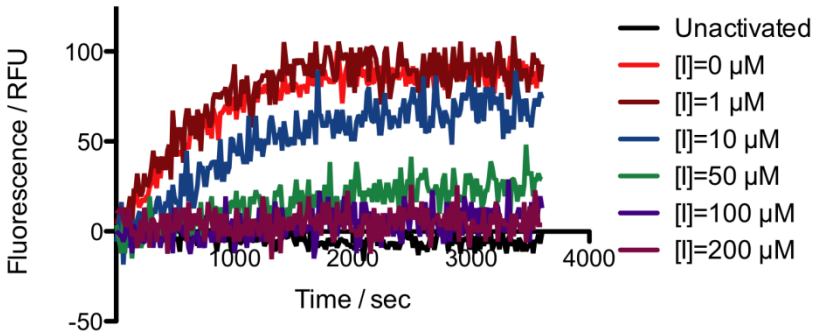

Figure S2.7. Representative calpain activity assay progress curve. Progress curves were truncated at ~500 seconds. After 500 seconds the progress curve loses linearity due autoproteolysis of the enzyme.[181] Data collected after curvature began was not used in any calculations.

K_m Determination for calpain substrate

We calculated the K_m for the NH_2-Glu(Edans)-Pro-Leu-Phe-Ala-Glu-Arg-Lys(Dabcyl)-OH substrate when cleaved by calpain using standard Michaelis-Menten kinetics.[142] We identified the initial velocity of calpain at substrate concentrations, 1, 3, 5, 10, 20, and 30 μM. Velocities were determined in RFU/sec then converted to μM/sec using the conversion factor 1386 RFU/μM. The conversion factor was obtained by the total hydrolysis of the substrate NH_2-Glu(Edans)-Pro-Leu-Phe-Ala-Glu-Arg-Lys(Dabcyl)-OH in a known concentration by papain. We then plotted velocity vs. substrate concentration and used GraphPad Prism program Michaelis-Menten (under kinetics) to determine the K_m. At high concentrations, >10 μM, of substrate the inner filter effect, whereby free quencher absorbed the fluorescence emission of the cleaved fluorophore, became evident. To take this quenching into consideration, the velocity at each substrate concentration was multiplied by the corresponding correction factor: Corr%=f_{EDANS} (at each substrate concentration)/f_{EDANS} (in the absence of substrate).[182]

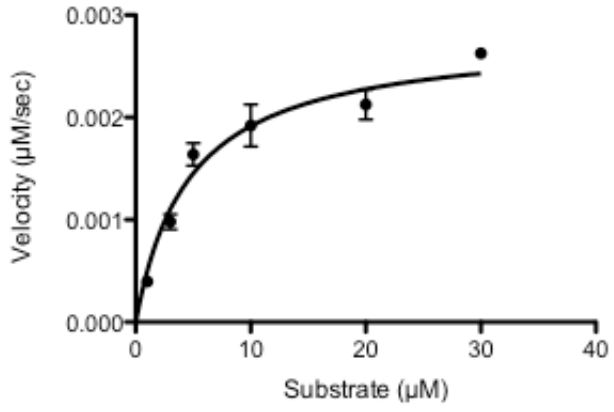

Figure S2.8. Michaelis-Menten curve for determining K_m of calpain substrate.

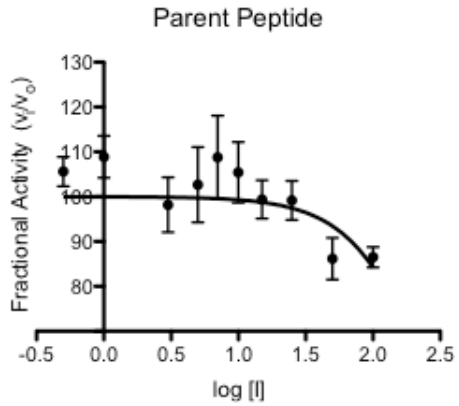
Parent Peptide
Fractional Activity (v_i/v_o)
130
120
110
100
90
80
-0.5
0.0
0.5
1.0
1.5
2.0
2.5
log [I]

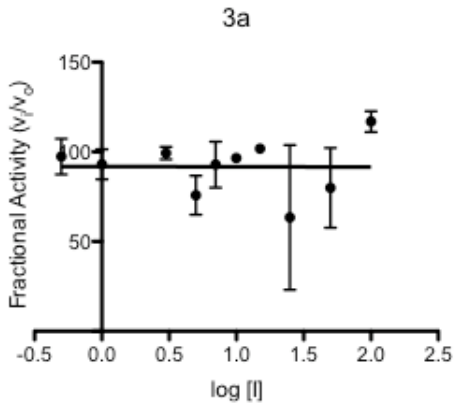
3a
Fractional Activity (v_i/v_o)
150
100
50
-0.5
0.0
0.5
1.0
1.5
2.0
2.5
log [I]

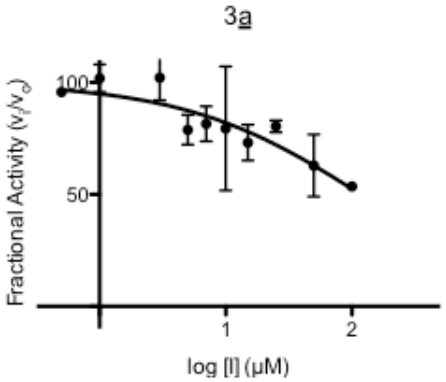
3a
Fractional Activity (v_i/v_o)
100
50
1
2
log [I] (μM)

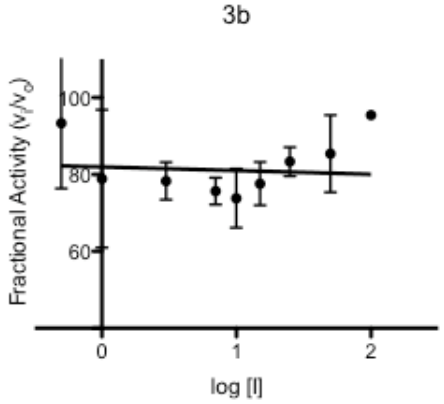
3b
Fractional Activity (v_i/v_o)
100
80
60
0
1
2
log [I]

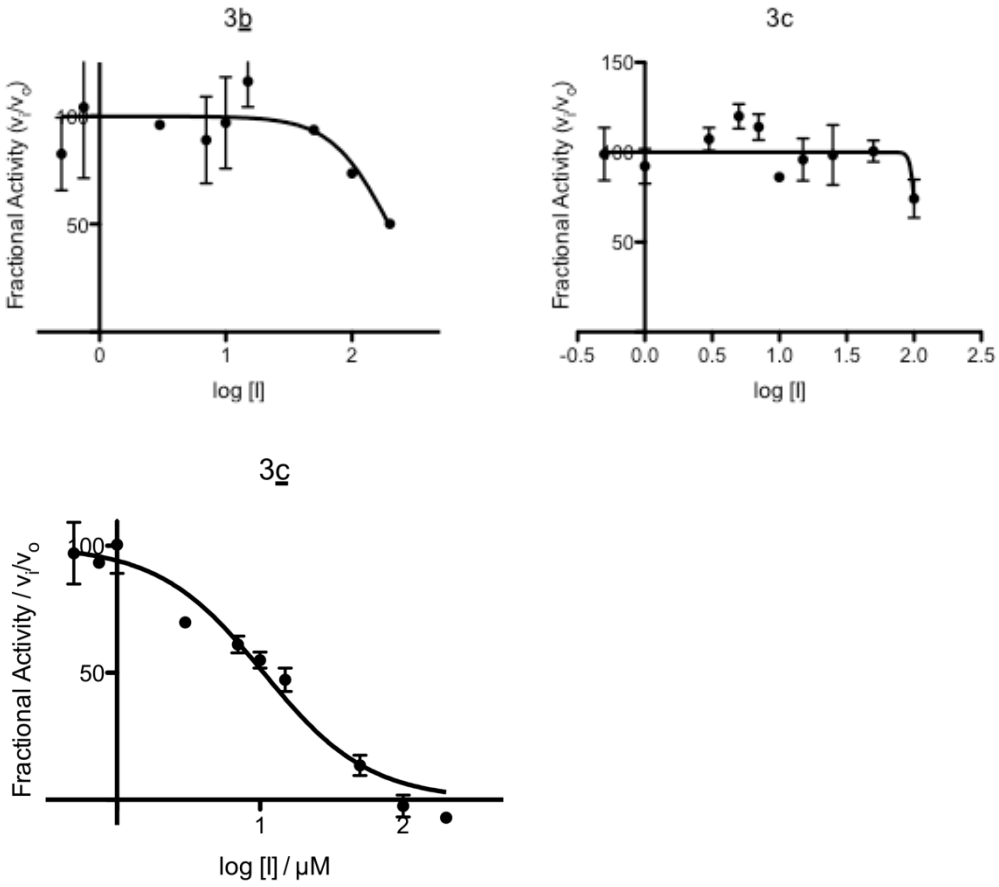

Figure S2.9. IC_{50} Curves for enzyme assays. K_i was calculated from IC_{50} using the equation: $K_i = \frac{IC_{50}}{1 + \frac{[S]}{K_m}}$ **.[124,142] The inhibitor was tested against purified human calpain-1. The K_m used for the calpain K_i determination was 4.66 µM.**

Kinetic analysis of Calpain-1 by 3c

To identify inhibition type we used standard Michaelis-Menten treatment. Initial velocities were calculated from the linear segment of the progress curves then plotted against their substrate concentration.[142] Due to the linearity of the first segment of the progress curve we believe that autoproteolysis during the first 500 seconds was not substantial enough to prevent the use of simple Michaelis-Menten kinetics, i.e. loss of enzyme did not change the velocity enough to cause it to deviate from linearity and incorporation of this additional complex would severely complicate the kinetics. Velocities were determined in RFU/sec then converted to µM/sec using the conversion factor 1386 RFU/µM. The conversion factor was obtained by the total hydrolysis of the substrate NH_2-Glu(Edans)-Pro-Leu-Phe-Ala-Glu-Arg-Lys(Dabcyl)-OH in a known concentration by papain.

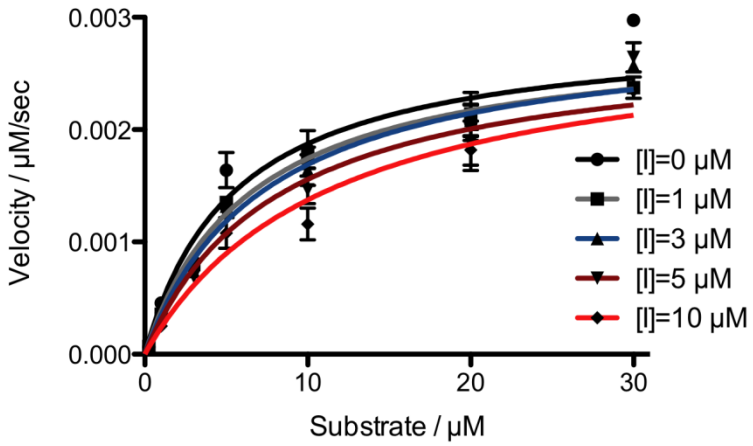

Figure S2.10. Michaelis-Menten plot of initial velocities at different substrate and inhibitor concentrations.

[3c] (μM)	V_{max}^{app} (μM/sec)	K_m^{app}
0	0.0029 ± 0.0003	4.66 ± 1.08
1	0.0029 ± 0.0002	6.47 ± 0.95
3	0.0029 ± 0.0003	7.40 ± 1.63
5	0.0028 ± 0.0003	8.11 ± 1.96
10	0.0030 ± 0.0004	11.35 ± 3.76

Table S2.4. V_{max}^{app} and K_m^{app} values obtained from the above Michaelis-Menten plot.

V_{max}^{app} is the same at all inhibitor concentrations while K_m^{app} increases with increasing inhibitor concentration. These results are indicative of competitive inhibition. To avoid weighting errors we used the values of K_m^{app} and V_{max}^{app} determined directly from the non-linear least-squares best fits of the untransformed data and put these values into the reciprocal equation:

$$\frac{1}{v} = (\frac{K_m}{V_{max}} \times \frac{1}{[S]}) + \frac{1}{V_{max}} .^{142}$$

We then plotted the resulting reciprocal velocities against the respective reciprocal substrate concentrations.

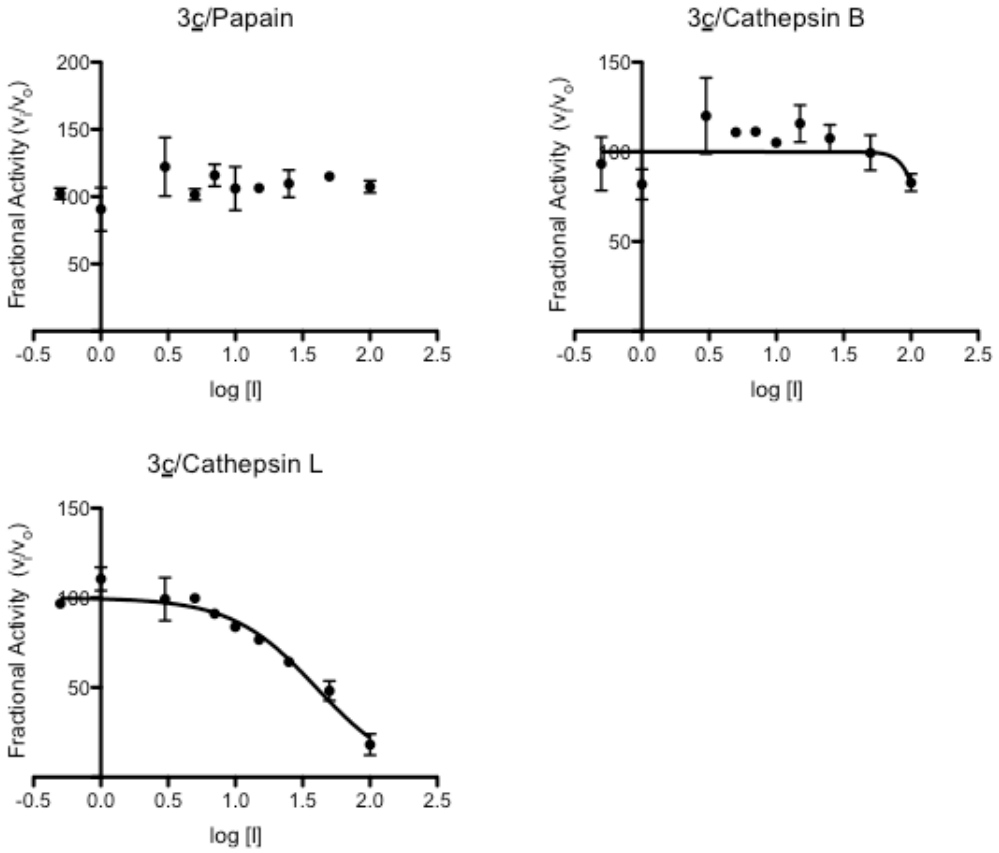

Figure S11. IC_{50} Curves for enzyme assays using inhibitor 3c. K_i was calculated from IC_{50} using the equation: $K_i = \frac{IC_{50}}{1 + \frac{[S]}{K_m}}$.[124,142,183]

Calpain Activity Based Probe Synthesis

All probes were synthesized by standard solid phase synthesis techniques using single fritted reservoir on Rink Amide resin (0.59 mmol/g substitution). Activation of Fmoc-amino acids (5-fold excess) was achieved with O-(1*H*-6-chlorobenzotriazol-1-yl)-N,N,N′,N′-tetramethyluronium hexafluorophosphate (HCTU) in the presence of DIPEA. The reaction solvent contains 100% N,N-dimethylforamide (DMF) (HPLC grade, Fisher). The epoxysuccinic acid was synthesized according to a procedure reported in the literature.[184] The epoxysuccinic acid was added using the same coupling procedure as the amino acids.

Biotin tag addition was done using biotinylated lysine in the peptide synthesis process. Fluorescein isothiocyantate (FITC) tag was added post cleavage to the crude peptides. FITC addition was performed post-cleavage by adding 1 eq. fluorescein isothiocyanate and 10 eq. DIPEA to the peptide dissolved in DMF and stirred under argon for 1 hr. For FITC labeled probe an allyloxycarbonyl (alloc) protected lysine was used for the non-tagged lysine. The alloc was removed using 1 eq. tetrakis(triphenyl phosphine)palladium(0) with 10 eq. 5,5-dimethyl-1,3-cyclohexane dione stirred for 2 hr.

Deprotection of side chains and cleavage of peptides from amide resin: Side chain deprotection and simultaneous cleavage from the resin were carried out using a mixture of trifluoroacetic acid (TFA)/triisopropylsilane (TIPS)/water (90:5:5, v/v) at room temperature, for 3 hours. Crude peptide was obtained by ether precipitation and purified by reverse-phase chromatography. The mass of all peptides was verified by ESI-MS.

	Sequence	Calcd (m/z)	Obsvd (m/z)	HPLC-Gradient	Retention Time (min)
NM-01-biotin	Epoxide-AAIPPKY**C**ELL**C**K-biotin	1890.29	1890.1	0-100%	9.864
NM-02-biotin	Epoxide-βAAIPPKY**C**ELL**C**K-biotin	1890.29	1890.1	0-100%	10.085
NM-03-biotin	Epoxide-AβPIPPKY**C**ELL**C**K-biotin	1928.92	1928.2	0-100%	10.137
NM-02-FITC	Epoxide-βAAIPPKY**C**ELL**C**K-FITC	2033.84 1016.92 (M/2)	1016.5 (M/2)	0-100%	8.655

Table S2.5. Calculated and Observed Masses for Calpain Activity Based Probes.

Enzyme Labeling Experiments

For enzyme labeling experiments a greater concentration of enzyme was used than for the kinetic experiments for visualization of the enzyme of gel stains.

Calpain Probe Linker Experiments

Experimental conditions included 10 mM dithiothreitol (DTT), 1.5 µg Calpain, 100 mM KCl, 2 mM EGTA, 50 mM Tris-HCl (pH 7.5), 0.015% Brij-35, and either 1 µM or 10 µM of biotinylated probe (DCG-04 (positive control), NM-01, NM-02, NM-03).[62,140,141] Calpain was activated by the addition of calcium (3.33 µM of 50 mM $CaCl_2$) to a final concentration of 8.3 mM. The negative control contained water instead of $CaCl_2$, in a calpain solution with 10 µM probe. Probes were allowed to bind to the calpain for 20 minutes at room temperature. The reaction was stopped by the addition of 10 µL NuPage® LDS Running Buffer. 10 µL of each labeling experiment was loaded on a 10% Bis-Tris NuPAGE® gel for 1.5 hrs, 140 V. The bands were then transferred to a PVDF membrane at 30 V for 70 min. The membrane was blocked with casein and blotted for biotin. Film was exposed for 1 hr. and developed.

Calpain Labeling experiments

Experimental conditions were 10 μM dithioreitol (DTT), 1.5 μg Calpain-1 or 6 μM Calpain-2 (the calpain-2 was not as active), 100 mM KCl, 2 mM EGTA, 50 mM Tris-HCl (pH 7.5), 0.015% Brij-35, and 1, 2.5, 5, 10, or 20 μM of FITC-labeled NM-02, or 2 μM DCG-04.[62,140,141] Calpain was activated by the addition of calcium (3.33 μM of 50 mM $CaCl_2$) to a final concentration of 8.3 mM. The negative control was unactivated calpain tube containing 10 μM probe where water was added instead of calcium. Probes were allowed to bind to the calpain for 20 minutes at room temperature. The reaction was stopped by the addition of 10 μL NuPage® LDS Running Buffer. 10 μL of each condition was loaded on a 10% Bis-Tris NuPAGE® gel for 1.5 hrs at 140 V. The gel was visualized on a Typhoon Fluorescent Imager. Following scanning the gel was stained with a Novex® Colloidal Blue Staining Kit.

Papain Labeling experiments

Experimental conditions were 10 μM dithioreitol (DTT), 1.5 μg Papain, 100 mM KCl, 2 mM EGTA, 50 mM Tris-HCl (pH 7.5), 0.015% Brij-35, and 1, 2.5, 5, or 10 μM of FITC-labeled NM-02, or 2 mM DCG-04.[62,140,141] Probes were allowed to bind to the papain for 20 minutes at room temperature. The reaction was stopped by the addition of 10 μL NuPage® LDS Running Buffer. 10 μL of each condition was loaded on a 10% Bis-Tris NuPAGE® gel for 1.5 hrs at 140 V. The gel was evaluated on a Typhoon Fluorescent Imager. Following scanning the gel was stained to verify loading with a Bio-Rad Silver Stain Plus Kit.

Cathepsin Labeling experiments

Experimental conditions were 10 μM dithioreitol (DTT), 1.5 μg Cathepsin B or Cathepsin L, 500 mM sodium acetate, 4 mM EGTA, (pH 5.5), and 1, 2.5, 5, or 10 μM of FITC-labeled NM-02, or 2 mM DCG-04.[62,140,141] Probes were allowed to bind to the enzymes for 20 minutes at room temperature. The reaction was stopped by the addition of 10 μL NuPage® LDS Running Buffer. 10 μL of each condition was loaded on a 12% Bis-Tris NuPAGE® gel for 1.5 hrs., 140 V. The gel was evaluated on a Typhoon Fluorescent Imager. Following scanning the gel was stained to verify loading with a Bio-Rad Silver Stain Plus Kit.

Chapter 3 Supporting Information

Alanine Scanning Mutagenesis

Alanine scanning is a technique in which each respective residue in a peptide is sequentially mutated to alanine to identify how important that residue is for inhibition.

Peptide No.	Sequence	Calcd m/z	Obsvd m/z	HPLC-Gradient	Retention Time (min)
3c	IPPKY**C**ELL**C**	1320.6	1321.6	1-100%	9.67
3d	APPKY**C**ELL**C**	1278.6	1279.6	1-100%	8.20
3e	IAPKY**C**ELL**C**	1294.6	1296.5	1-100%	9.25
3f	IPAKY**C**ELL**C**	1293.6	1294.2	1-100%	6.13
3g	IPPAY**C**ELL**C**	1263.5	1264.5	1-100%	12.48
3h	IPPKA**C**ELL**C**	1228.6	1229.4	1-100%	9.07
3i	IPPKY**C**ALL**C**	1262.6	1263.4	1-100%	8.83
3j	IPPKY**C**EAL**C**	1278.6	1279.4	1-100%	8.98
3k	IPPKY**C**ELA**C**	1278.6	1279.3	1-100%	8.89

(Peptides were run on an Agilent LC-MS with an Eclipse XDB-C18 column over a gradient of acetonitrile in water (0.1% HCOOH over 20 minutes.) Cysteines that are bold and underlined are linked residues.

Table S3.1. Calculated and observed masses of crosslinked inhibitors with alanine mutations.

	Inhibitor	Calpain-1 (μM)	Cathepsin L (μM)	Cathepsin S (μM)
3c	IPPKY**C**ELL**C**	10.2 ± 2.9	39.9 ± 1.1	50.2 ± 1.2
3d	APPKY**C**ELL**C**	65.6 ± 20.5	12.5 ± 1.2	26.1 ± 1.3
3e	IAPKY**C**ELL**C**	13.7 ± 4.4	0.6 ± 1.4	13.1 ± 1.11
3f	IPAKY**C**ELL**C**	27.4 ± 8.6	NT	NT
3g	IPPAY**C**ELL**C**	17.7 ± 5.6	24.6 ± 1.2	20.7 ± 1.2
3h	IPPKA**C**ELL**C**	>100	8.1 ± 1.2	16.8 ± 1.1
3i	IPPKY**C**ALL**C**	28.9 ± 9.1	12.5 ± 1.1	15.6 ± 1.6
3j	IPPKY**C**EAL**C**	30.9 ± 9.2	21.4 ± 1.2	13.9 ± 1.0
3k	IPPKY**C**ELA**C**	25.2 ± 7.9	19.7 ± 1.1	15.2 ± 1.1

Cysteines that are bold and underlined are linked residues.

Table S3.2. K_i determination of alanine mutated crosslinked inhibitors against cysteine proteases.

APPKY**C**ELL**C**/Calpain

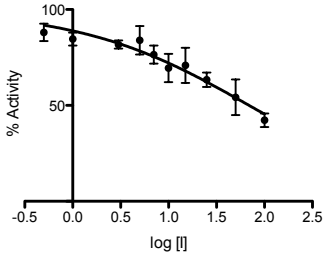

APPKY**C**ELL**C**/Cat L

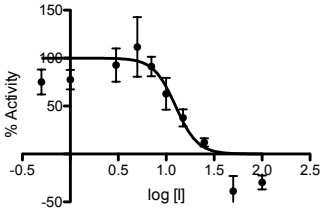

APPKY**C**ELL**C**/Cat S

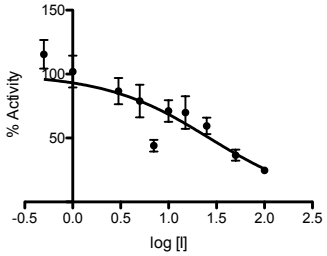

IAPPKY**C**ELL**C**/Calpain

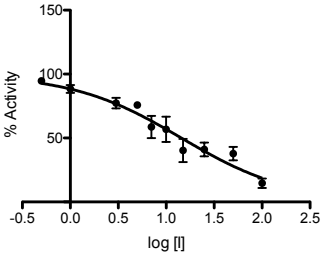

IAPPKY**C**ELL**C**/Cat L

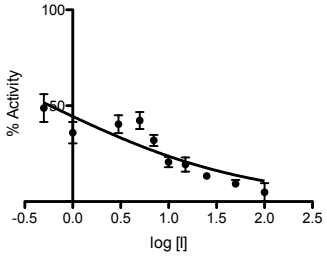

IAPPKY**C**ELL**C**/Cat S

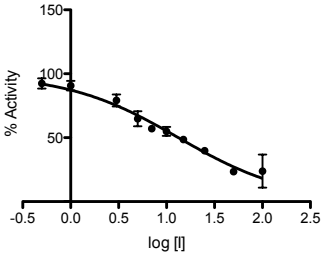

IPAKY**C**ELL**C**/Calpain

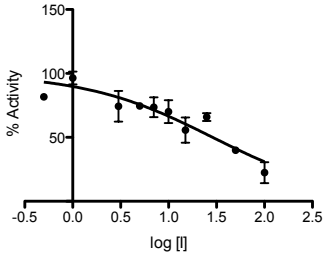

IPPAY**C**ELL**C**/Calpain

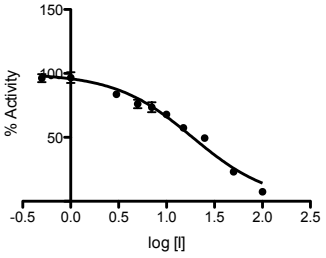

IPPAY**C**ELL**C**/Cat L

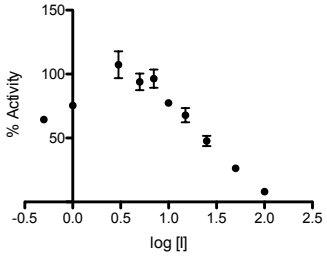

IPPAY**C**ELL**C**/Cat S

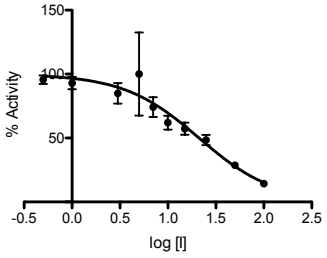

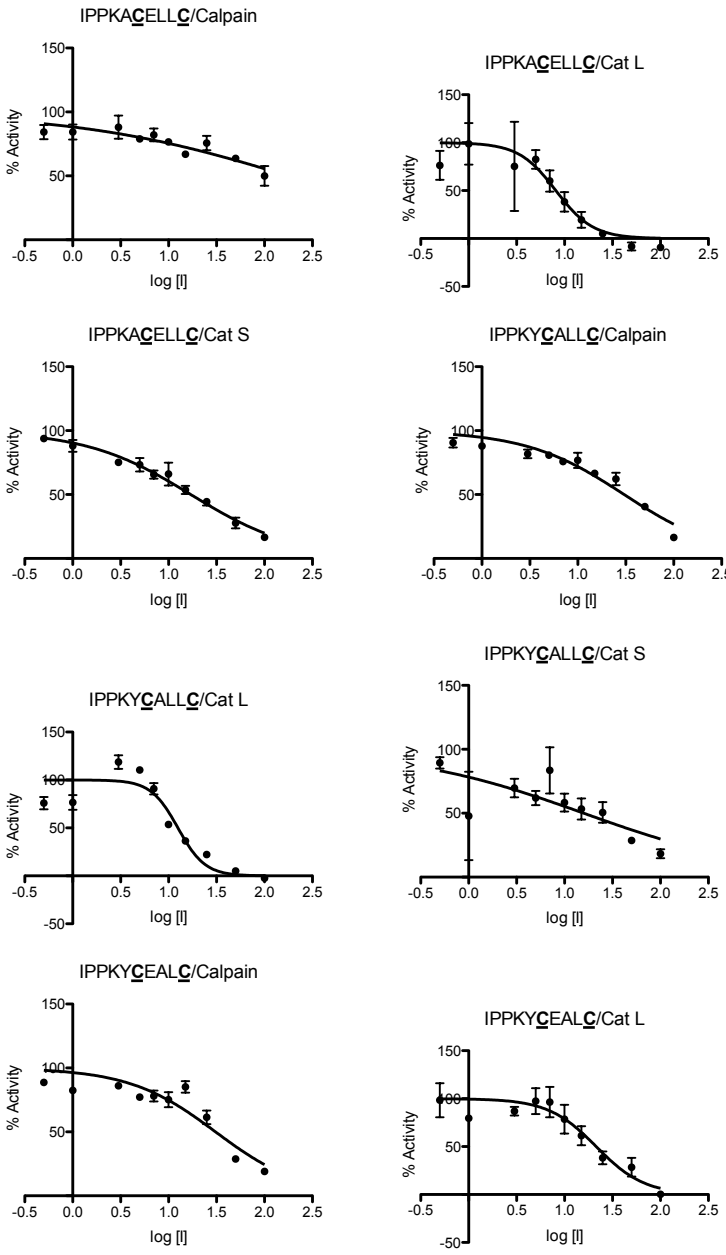
IPPKACELLC/Calpain
IPPKACELLC/Cat L
IPPKACELLC/Cat S
IPPKYCALLC/Calpain
IPPKYCALLC/Cat S
IPPKYCALLC/Cat L
IPPKYCEALC/Calpain
IPPKYCEALC/Cat L
% Activity
log [I]

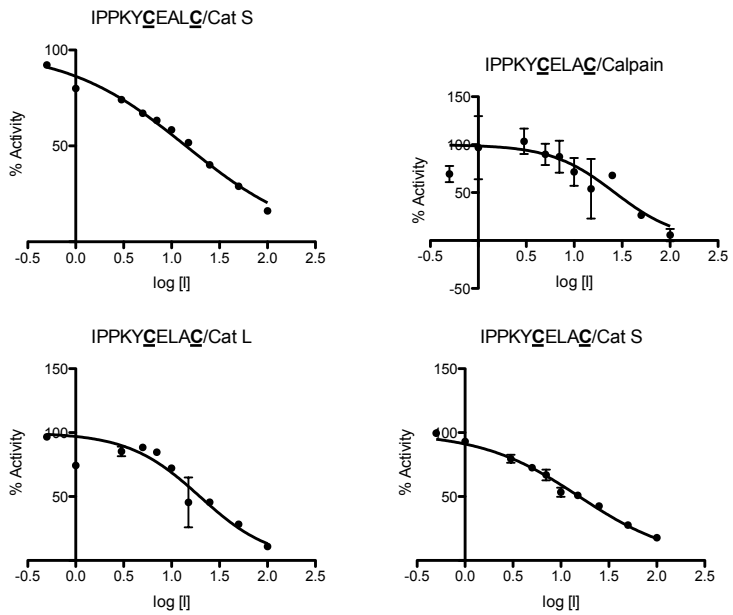

Figure S3.1. IC_{50} curves of alanine mutants against cysteine proteases.

Calpain Inhibitor Mutants

Isoleucine and tyrosine were mutated to other polar, nonpolar, and extended side chain amino acids to investigate the role the specific side chain played in inhibition.

Peptide No.	Sequence	Calcd m/z	Obsvd m/z	HPLC-Gradient	Retention Time (min)
3m	*L*PPKY**C**ELL**C**	1320.6	1321.5	1-100%	8.92
3n	*Q*PPKY**C**ELL**C**	1335.6	1336.6	1-100%	8.66
3o	IPPK*b***C**ELL**C**	1381.5	1382.5	1-100%	11.57
3p	IPPK*bzlY***C**ELL**C**	1410.5	1411.6	1-100%	11.98

(Peptides were run on an Agilent LC-MS with an Eclipse XDB-C18 column over a gradient of acetonitrile in water (0.1% HCOOH over 20 minutes.). Cysteines that are bold and underlined are linked residues. *b*=Ala(4,4'-biphenyl); *bzlY*=*O*-benzyl tyrosine

Table S3.3. Calculated and observed masses of calpain-1 inhibitor mutants.

	Inhibitor	Calpain-1 (μM)	Cathepsin L (μM)	Cathepsin S (μM)
3m	*L*PPKY**C**ELL**C**	10.96 ± 3.6	38.1 ± 1.2	46.3 ± 1.2
3n	*Q*PPKY**C**ELL**C**	35.02 ± 10.4	NT	NT
3o	IPPK*b***C**ELL**C**	9.65 ± 3.2	1.9 ± 1.1	1.4 ± 1.1
3p	IPPK*bzlY***C**ELL**C**	21.26 ± 6.7	16.7 ± 1.3	3.3 ± 1.2

Cysteines that are bold and underlined are linked residues. *b*=Ala(4,4'-biphenyl); *bzlY*=*O*-benzyl tyrosine

Table S3.4. K_i of calpain-1 mutant inhibitors. Isoleucine was mutated to various polar and nonpolar residues. Tyrosine was mutated to various resides to determine if extending the side chain would enhance calpain binding.

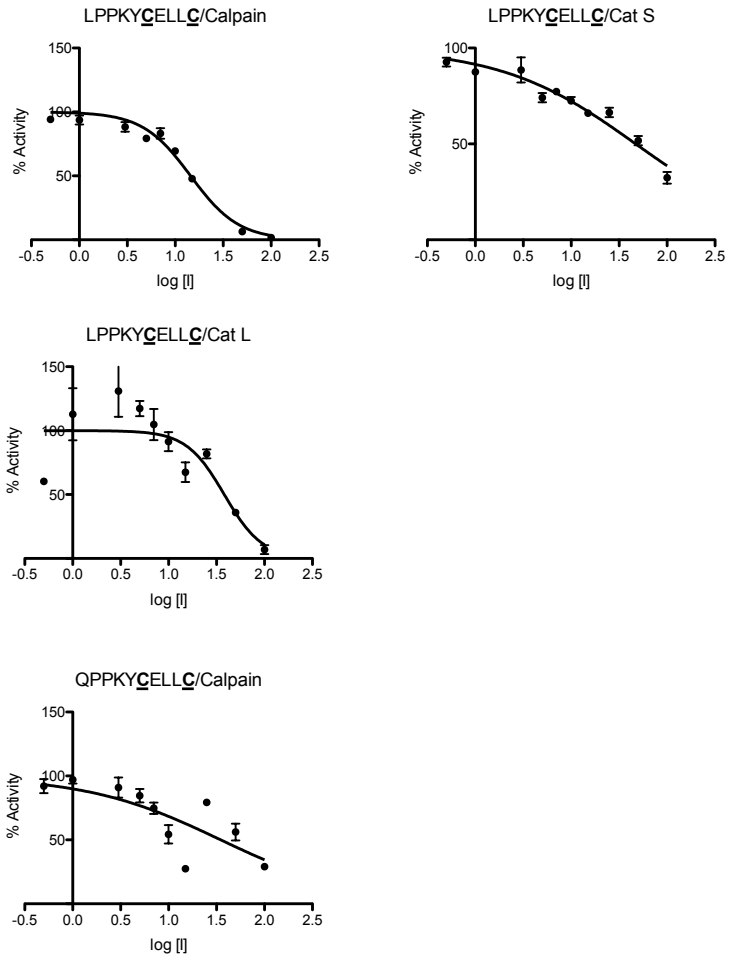

Figure S3.2. IC_{50} curves of calpain-1 inhibitors with isoleucine mutated to various polar and nonpolar residues.

Single and Double Mutants Determined by Alanine Scanning Mutagenesis and Structure Based Design

Alanine scanning mutagenesis identified two residues in the ten amino acid calpain-1 inhibitor that were not essential for inhibition, and subsequently were amenable to mutation. Structure based design was then used to pick amino acids that would enhance proposed binding interactions. Each individual single mutant resulted in increased inhibition, however the double mutant had reduced inhibition.

Peptide No.	Sequence	Calcd m/z	Obsvd m/z	HPLC-Gradient	Retention Time (min)
4a	I*pf*FPKY**C**ELL**C**	1410.6	1411.8	1-100%	13.10
4b	IPP*R*Y**C**ELL**C**	1348.6	1349.6	1-100%	9.50
4c	I*pf*FP*R*Y**C**ELL**C**	1488.6	1489.4	1-100%	10.77

(Peptides were run on an Agilent LC-MS with an Eclipse XDB-C18 column over a gradient of acetonitrile in water (0.1% HCOOH over 20 minutes.). Cysteines that are bold and underlined are linked residues. *b*=Ala(4,4'-biphenyl); *bzlY*=*O*-benzyl tyrosine

Table S3.5. Calculated and observed masses for single and double mutant calpain-1 inhibitors.

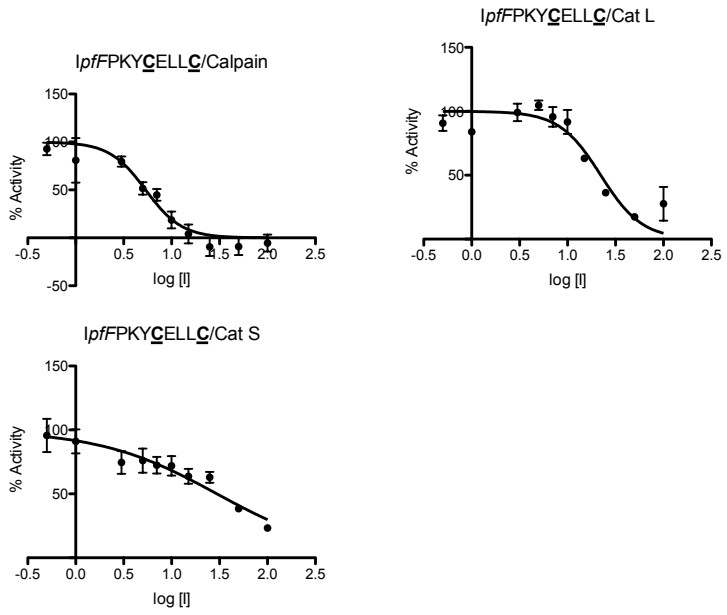

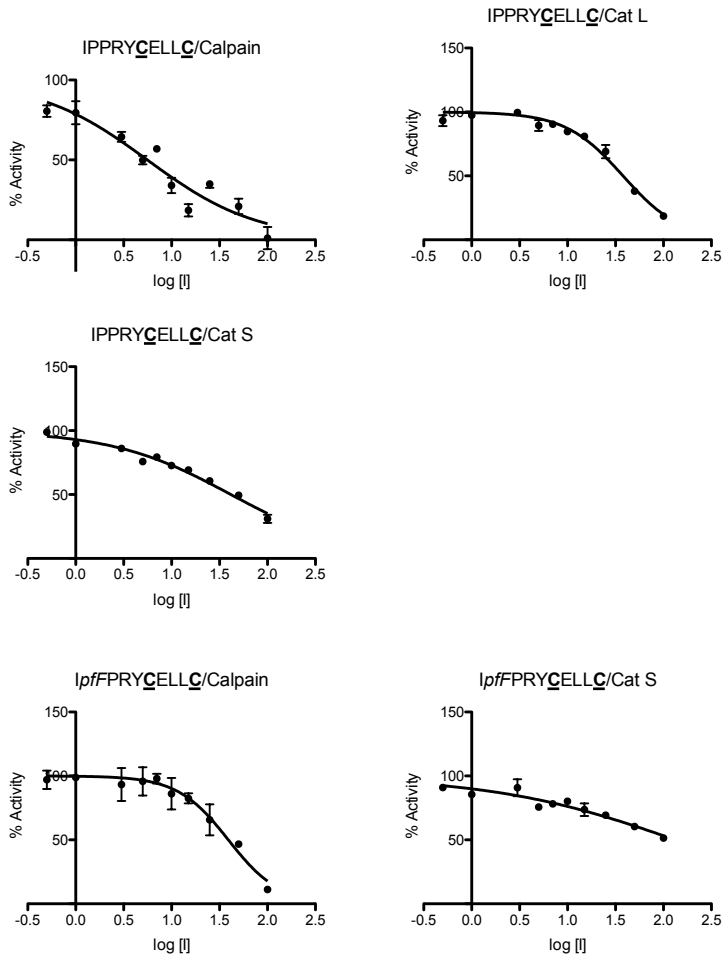

Figure S3.3. IC_{50} curves of single and double mutants of the mutable residues of the calpain-1 inhibitor.

Lengthened Peptide Inhibitors

Calpain-1 inhibitors were extended using the activity based probe sequence and the endogenous calpastatin sequence to investigate how additional amino acids affected inhibitory activity.

Peptide No.	Sequence	Calcd m/z	Obsvd m/z	HPLC-Gradient	Retention Time (min)
5a	βAAIPPKY**C**ELL**C**	1462.7	1463.7	1-100%	9.02
5b	EVTIPPKY**C**ELL**C**	1649.8	1650.7	1-100%	8.07
5c	LGKREVTIPPKY**C**ELL**C**	2104.1 1052.1 (M/2)	1053.5	1-100%	7.88
5d	LFKREVTIPPKY**C**ELL**C**	2192.1 1096.1 (M/2)	1097.6	1-100%	8.51
5e	EVTIPPKYCELLC	1547.8	1548.3	1-100%	9.38

(Peptides were run on an Agilent LC-MS with an Eclipse XDB-C18 column over a gradient of acetonitrile in water (0.1% HCOOH over 20 minutes.). Cysteines that are bold and underlined are linked residues.

Table S3.6. Calculated and observed masses for calpain-1 inhibitors of increasing length.

	Inhibitor	Calpain-1 (μM)	Cathepsin L (μM)	Cathepsin S (μM)
5e	EVTIPPKYCELLC	80.4 ± 25.0	NT	NT

Cysteines that are bold and underlined are linked residues. NT=not tested

Table S3.7. K_i of the unstabilized 13 amino acid calpain-1 inhibitor.

bAAIPPKY**C**ELL**C**/Calpain

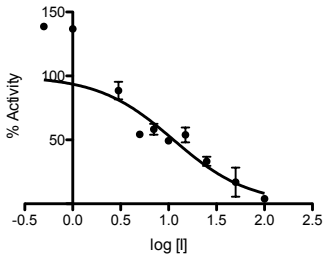

bAAIPPKY**C**ELL**C**/Cat L

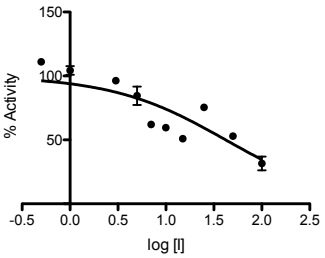

bAAIPPKY**C**ELL**C**/Cat S

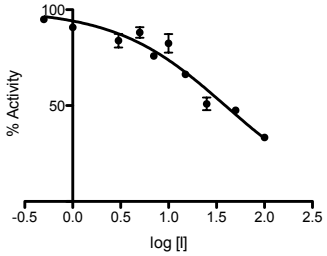

EVTIPPKY**C**ELL**C**/Calpain

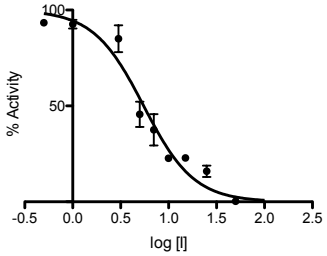

EVTIPPKY**C**ELL**C**/Cat L

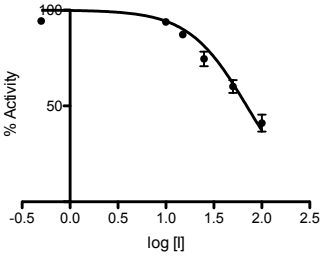

EVTIPPKY**C**ELL**C**/Cat S

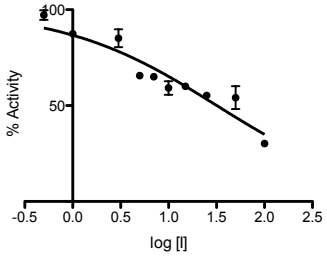

LGKREVTIPPKY**C**ELL**C**/Calpain

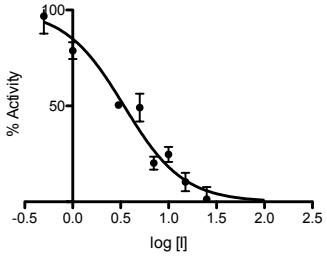

LGKREVTIPPKY**C**ELL**C**/Cat L

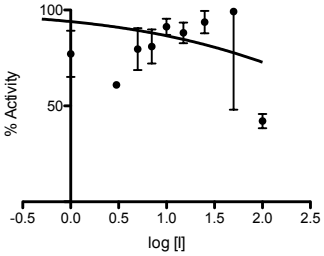

LGKREVTIPPKY**C**ELL**C**/Cat S

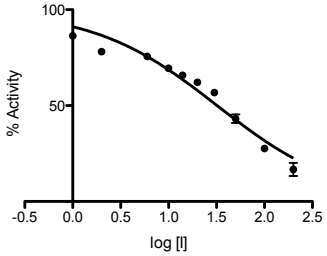

LFKREVTIPPKY**C**ELL**C**/Cat L

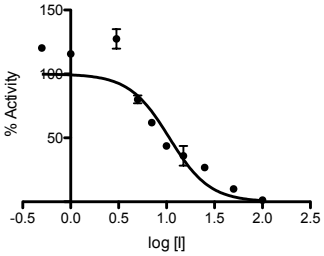

LFKREVTIPPKY**C**ELL**C**/Calpain

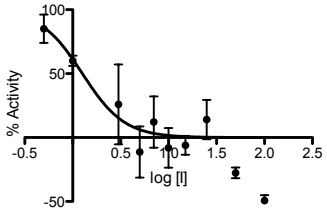

LFKREVTIPPKY**C**ELL**C**/Cat S

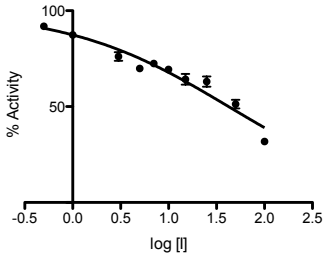

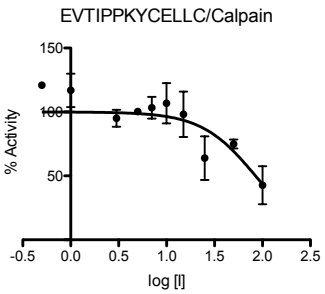

Figure S3.4.IC_{50} curves of lengthened calpain-1 inhibitors.

Quench Probe Development

For the development of the quenched activity based probe numerous peptides were synthesized to address possible locations for the donor and quencher and identify the potency of inhibitors without the fluorophores.

Peptide No.	Sequence	Calcd m/z	Obsvd m/z	HPLC-Gradient	Retention Time (min)
6a	PLFAARIPPKY**C**ELL**C**K	2103.1 1051.6.0 (M/2)	1052.6	1-100%	16.51
6b	IPPKY**C**ELL**C**R	1476.7	1477.4	1-100%	8.50

(Peptides were run on an Agilent LC-MS with an Eclipse XDB-C18 column over a gradient of acetonitrile in water (0.1% HCOOH over 20 minutes.). Cysteines that are bold and underlined are linked residues.

Table S3.8. Calculated and observed masses for calpain-1 inhibitors with positive amino acid at C-terminus.

	Inhibitor	Calpain-1 (μM)	Cathepsin L (μM)	Cathepsin S (μM)
6a	PLFAARIPPKY**C**ELL**C**K	16.3 ± 5.2	5.2 ± 1.2	NT
6b	IPPKY**C**ELL**C**R	47.6 ± 14.9	NT	NT

NT=not tested

Table S3.9. K_i of calpain-1 inhibitor and probe that have a charged residue at the C-terminus for either fluorophore addition or cell permeability enhancement.

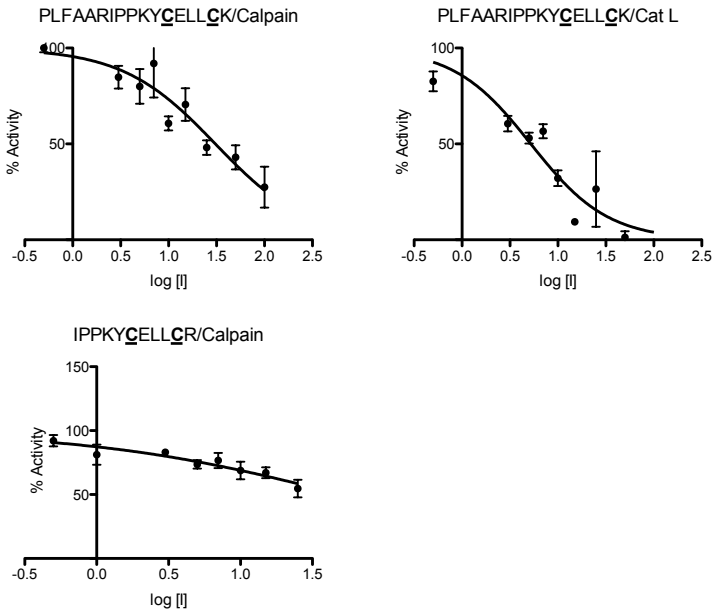

Figure S3.5. IC_{50} curves for calpain-1 inhibitors with C-terminal positively charged amino acids.

Peptide No.	Sequence	Calcd m/z	Obsvd m/z	HPLC Gradient	Retention Time (min)
6c	K(Dabcyl)PLFAARE(Edans)IPPKY**C**ELL**C**	2730.7 1365.4 (M/2)	1366.5	1-100%	13.00
6d	K(Dabcyl)PLFAE(Edans)RIPPKY**C**ELL**C**	2659.7 1329.9 (M/2)	1331.0	1-100%	13.56
6e	K(Dabcyl)PLFAE(Edans)RIpfFPY**C**ELL**C**	2699.7 1349.8 (M/2)	1349.9	1-100%	14.42
6f	K(Dabcyl)PLFAE(Edans)RIPPRY**C**ELL**C**	2687.7 1343.8 (M/2)	1344.9	1-100%	13.57
6g	PLFAERIPPKY**C**ELL**C**	2031.99 1015.99 (M/2)	1017.2	1-100%	10.84
6h	PLFAERIpfFPKY**C**ELL**C**	2072.0 1036.0 (M/2)	1036.6	1-100%	11.37
6i	PLFAERIPPRY**C**ELL**C**	2061.3 1030.7 (M/2)	1031.7	1-100%	10.47

(Peptides were run on an Agilent LC-MS with an Eclipse XDB-C18 column over a gradient of acetonitrile in water (0.1% HCOOH over 20 minutes.). Cysteines that are bold and underlined are linked residues.

Table S3.10. Observed and calculated masses of quench probes and their respective inhibitors without the fluorophores.

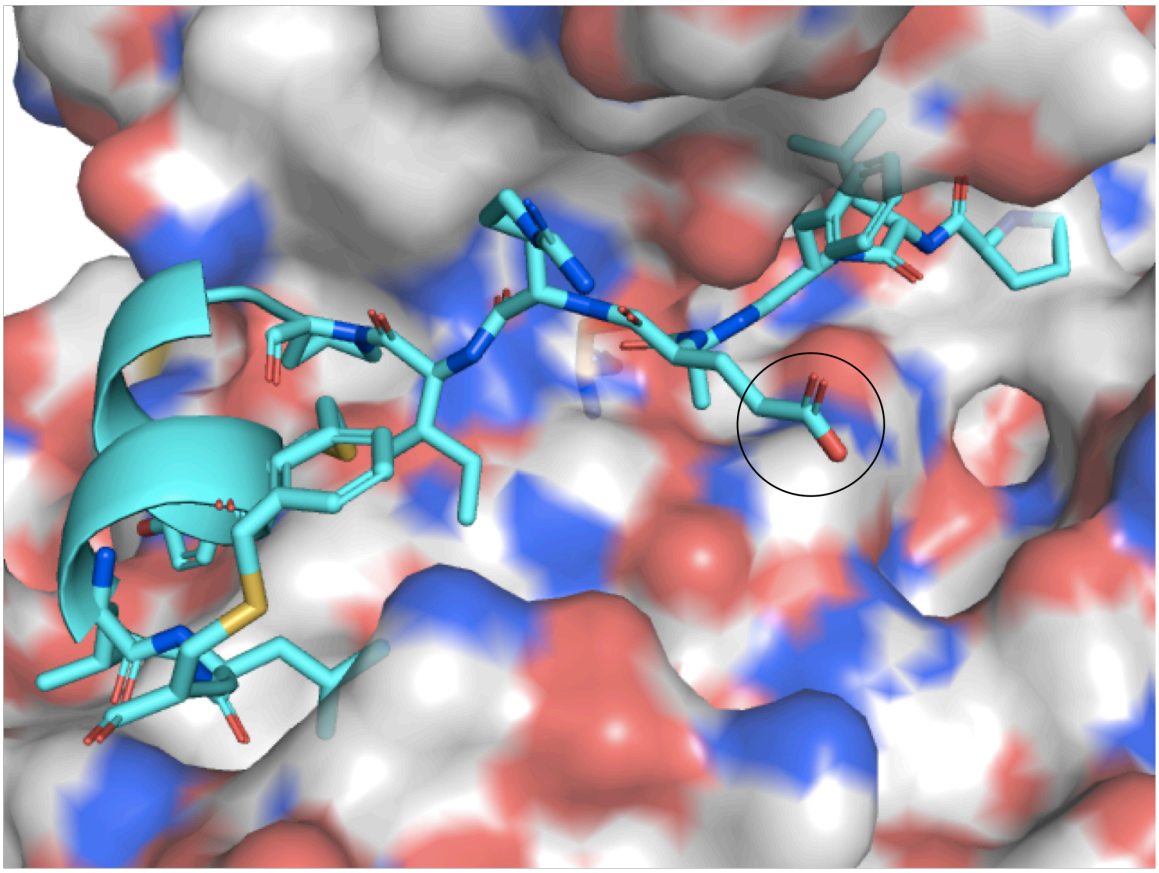

Figure S3.6. Model of stabilized α-helical quench probe with the substrate sequence Pro-Leu-Phe-Ala-Glu-Arg. The glutamate (circled in black) appears to be facing the solution making it a good candidate for fluorophore attachment.[31]

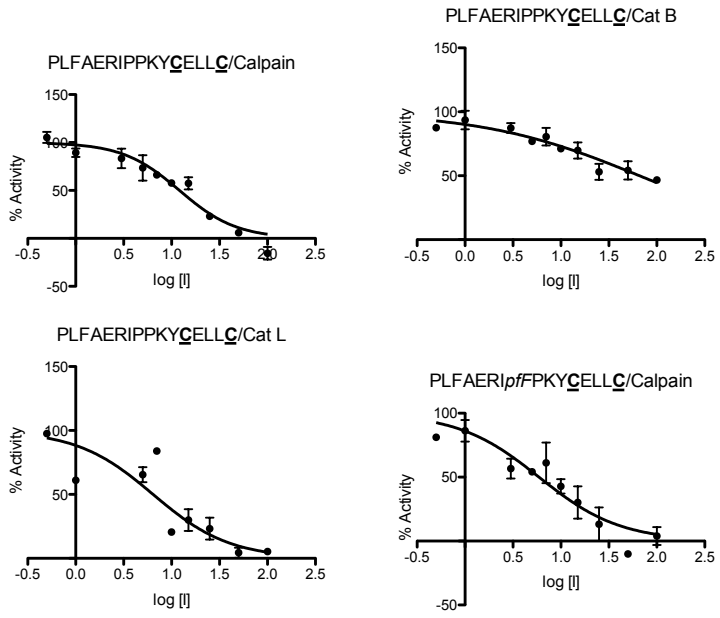

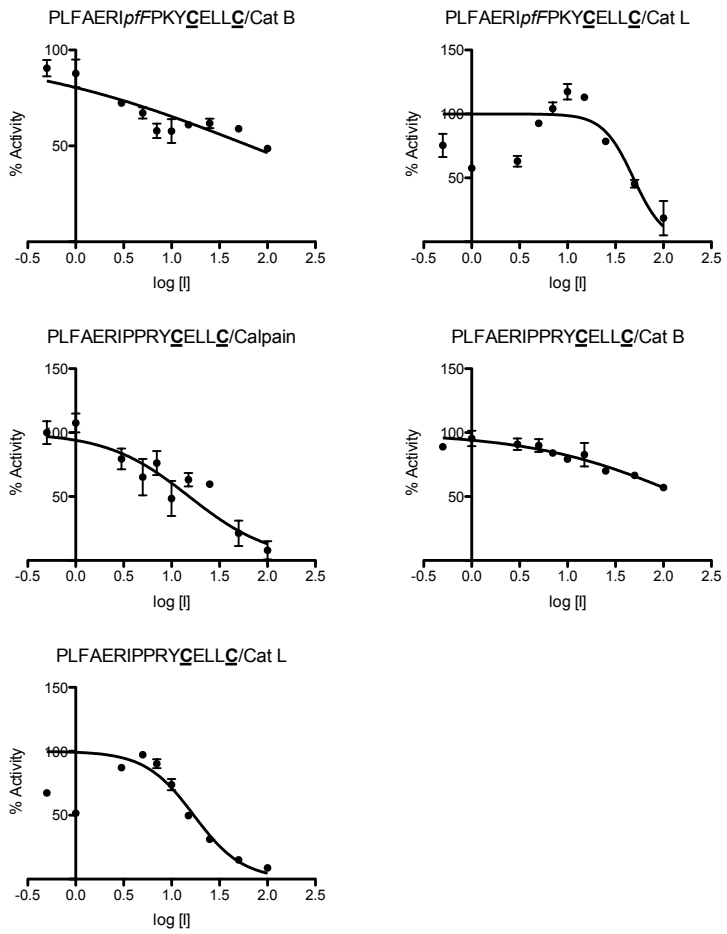

Figure S3.6. IC50 curves for quench probe inhibitors without fluorophores.

Chapter 4 Supporting Information

General Information

Amino acids were purchased from Advanced ChemTech (Louisville, KY) or Chem-Impex (Wood Dale, IL). Chemicals were purchased from Fisher Scientific (Pittsburgh, PA). Calpain-1 was purchased from BioVision (Milpitas, CA). Cathepsin L was purchased from EMD Millipore (Billerica, MA). Cathepsin K and cathepsin S were purchased from Enzo Life Sciences (Farmingdale, NY). Substrate Z-FR-Amc was purchased from Peptides International (Louisville, KY), and substrate Z-VVR-Amc was purchase from Enzo Life Sciences (Farmingdale, NY). Single fritted reservoirs for peptide synthesis were purchase from Biotage (Redwood City, CA).

Peptides were purified on an Agilent 1100 Series LC/MS or an Agilent 1200 Series LC/MS (Agilent Technologies, Inc., Santa Clara, CA) Hewlett Packard ChemStation software using a Zorbax XDB-C18 column (Agilent Technologies, Inc., Santa Clara, CA). Matrix assisted laser desorption/ionization time of flight (MALDI-TOF) mass spectra were obtained using a Bruker Ultraflex III mass spectrometer (Billerica, MA).

Circular dichroism (CD) spectra were obtained with an AVIV spectropolarimeter (AVIV biomedical, Inc., Lakewood, MD) equipped with a temperature control unit. UV-Vis absorbance spectra were obtained using a NanoDrop 1000 spectrophotometer (Thermo Scientific, Wilmington, DE). Fluorescence spectra were collected with a Berthold Tri-Star multimode microplate reader (Berthold Technologies, GmbH & Co.

KG, Bad Wildbad, Germany). Graphing was performed using GraphPad Prism (GraphPad Software, La Jolla, CA).

General peptide synthesis

All peptides were synthesized at a scale of 0.1 mmol using Rink amide Resin (Chemimpex) (substitution: 0.52 mmol/g). Fmoc-protected amino acids (5-fold excess) were activated with 0.95 equivalents (relative to the amino acid) of HCTU in the presence of 5 equivalents of diisopropyethanolamine (DIPEA). Amino acids were coupled for 1 hr at room temperature. Fmoc deprotection was performed using 20% 4-methyl piperidine in DMF for 30 min at room temperature. Side chain deprotection and the simultaneous cleavage from the resin were carried out using a mixture of TFA/triisopropylsilane (TIPS)/water (95:2.5:2.5, v/v) at room temperature, for 2.5 hours. The crude peptide was precipitated using cold diethyl ether. The ether was evaporated and then the crude peptide was dissolved in 50% water/50% acetonitrile and lyophilized.

Crosslinker Addition

The lyophilized crude peptide was dissolved in DMF and to it 1.5 eq. of alkylating agent, α,α'-dibromo-*m*-xylene was added. To the resulting solution 1.5 eq of triethylamine was added to initiate the reaction. The reaction mixture was allowed to react for 1 h under constant shaking.[42,105,159,172] Reaction was monitored for completion by HPLC.

Purification of Peptides

The linked peptide was purified via reverse-phase chromatography with a C18 semi-preparative column using buffer A (0.1% TFA in 95% Millipore water/5% acetonitrile) and buffer B (0.1% TFA in 100% acetonitrile). Initial HPLC conditions were 100% A. Initial conditions were run for 5 min, followed by an increase of solution B to 100% at 30 min (4%/min.) at a flow rate of 4.18 ml/min. The mass of all peptides was verified by ESI-MS and purity (greater than 95%) was checked by analytical HPLC (0 to 100% solution B over 20 min. at 1 mL/min.).

Peptide No.	Sequence	Calcd m/z	Obsvd m/z M+1	HPLC Gradient (analytical)	Retention Time (min)
1a	SEEFRQVMNGF	1383.6	1384.5	0-100%	8.90
1b	SE**C**FRQ**C**MNGF	1463.5	1464.1	0-100%	8.95
1c	S**C**EFR**C**VMNGF	1434.5	1435.7	0-100%	10.21
1d	S**C**E*n*R**C**VMNGF	1484.6	1485.5	0-100%	10.27
1e	S**C**E*b*R**C**VMNGF	1510.6	1511.4	0-100%	10.66
1f	S**C**EFR**C**VMNG*n*	1484.6	1485.5	0-100%	10.20
1g	S**C**E*b*R**C**VMNG*n*	1560.6	1561.4	0-100%	10.55
2a	TSEEVMSLMSS	1240.4	1241.3	0-100%	7.80
2b	T**C**EEV**C**SLMSS	1330.5	1331.6	0-100%	7.41
2c	TSEEV**C**SLM**C**S	1330.5	1331.4	0-100%	9.53
2d	*W*SEEV**C**SLM**C**S	1415.5	1416.3	0-100%	11.13
2e	T*W*EEV**C**SLM**C**S	1429.5	1430.5	0-100%	9.75
2f	TSE*W*V**C**SLM**C**S	1387.5	1488.2	0-100%	10.97
2g	TSEE*W***C**SLM**C**S	1417.5	1418.2	0-100%	9.92
2h	T*W*E*W*V**C**SLM**C**S	1486.6	1487.4	0-100%	14.38
2i	T*n*E*n*V**C**SLM**C**S	1508.6	1509.3	0-100%	17.01
2j	*WW*E*W*V**C**SLM**C**S	1571.6	1572.3	0-100%	15.18
2k	*WW*E*WW***C**SLM**C**S	1658.6	1659.7	0-100%	14.92
2l	*FF*E*FF***C**SLM**C**S	1502.6	1503.5	0-100%	10.36
2m	*WW*E*Wb***C**SLM**C**S	1695.7	1696.5	0-100%	13.66

3a	SEEVVQKMTGL	1261.6	1262.5	0-100%	7.42
3b	S**C**EVV**C**KMTGL	1311.6	1312.5	0-100%	9.04
3c	S**C**E*S*V**C**KMTGL	1299.4	1300.3	0-100%	8.06
3d	S**C**E*H*V**C**KMTGL	1349.5	1350.5	0-100%	7.47
3e	S**C**E*N*V**C**KMTGL	1326.5	1327.2	0-100%	7.80
3f	S**C**E*L*V**C**KMTGL	1325.6	1326.5	0-100%	9.58
3g	S**C**EVV**C**K*P*TGL	1277.6	1278.3	0-100%	7.73
3h	S**C**EVV**C**KM*W*GL	1396.6	1397.4	0-100%	10.24
3i	S**C**EVV**C**KM*F*GL	1357.6	1358.3	0-100%	20.99
3j	S**C**EVV**C**KMTG*P*	1295.5	1296.4	0-100%	7.89
3k	S**C**E*S*V**C**KMTG*P*	1283.5	1284.3	0-100%	7.28
3l	S**C**EVV**C**K*P*TG*P*	1261.5	1262.2	0-100%	8.42
3m	S**C**E*S*V**C**K*PW*G*P*	1334.5	1335.5	0-100%	7.88

Table S4.1: Calculated and observed inhibitor masses of parent peptides and prodomain fragment peptides. Prodomain fragment peptides 1b-1g, 2b-2m, and 3b-3m are all crosslinked with α,α'-*m*-dibromoxylyl crosslinker. Peptides were run on an Agilent LC-MS with an Eclipse XDB-C18 column over a gradient of acetonitrile in water (0.1% HCOOH) over 20 min. *n*=Ala(2-naphthyl); *b*=Ala(4,4'-biphenyl)

Circular Dichroism Spectra of Inhibitors

We analyzed the unstabilized parent peptide and stabilized inhibitor peptides via circular dichroism (CD) data for in buffer without 40% trifluoroethanol (TFE).[117,180] CD traces demonstrate that the unstabilized peptides are primarily random coil with an increase in helicity, to varying degrees, upon stabilization. In buffer the peptide 1g appears to be a loop in solution but likely helix formation occurs upon binding to the enzyme. Peptide 3g is mostly random coil in buffer likely due to the double proline, helix breaker, addition.

Peptide solutions were prepared at ~50 μM in 100 mM potassium phosphate buffer (cathepsin L and K: pH=5.5, cathepsin S: pH=6.5). Concentrations were determined either by measuring aromatic absorbance at 280 nm or 254 nm or by mass. Scans were conducted from 260 nm to 200 nm.[117,180,185] Measurements were conducted at 25 ˚C in 1 nm step mode with a response time of 5 seconds in a 1 mm path length cuvette.

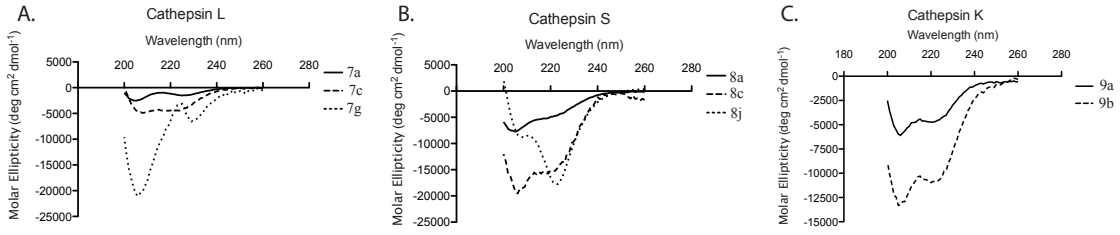

Figure S4.1: A-C) Circular dichroism spectra of parent unstructured peptides and stabilized inhibitors of Cathepsin L (A), Cathepsin S (B), and Cathepsin K (C) in buffer with 40% TFE (100 mM potassium phosphate buffer, Cathepsin L and K: pH 5.5, Cathepsin S: pH=6.5).

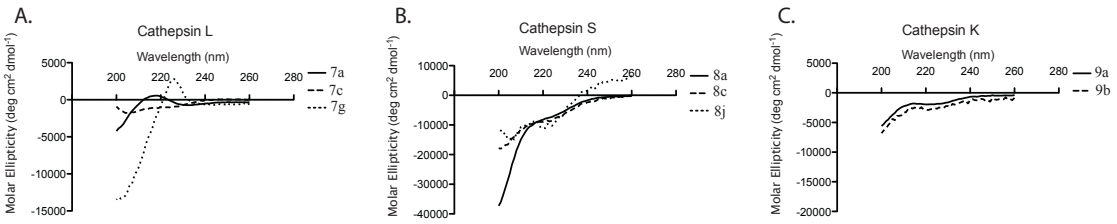

Figure S4.2: Circular dichroism data of parent unstructured peptides and stabilized inhibitors of Cathepsin L (A), Cathepsin S (B), Cathepsin K (C) in buffer without TFE (100 mM potassium phosphate buffer, cathepsin L and K: pH=5.5, cathepsin S: pH=6.5).

Protease Activity Assays

All peptides were evaluated for ability to inhibit the cysteine protease calpain using standard proteolytic fluorescence activity assays. Inhibition was assayed using a standard donor/quencher strategy with standard peptide substrates.

Enzyme concentration for cathepsin L was 4 nM. Enzyme concentrations for cathepsins S and K are 5 nM. Enzyme concentration for Calpain-1 was 25 nM. Cathepsin K and L buffer contained 10 mM DTT, 200 mM sodium acetate (pH 5.5), 2 mM EGTA, and 0.01% Triton X-100 or 10 mM DTT, 500 mM sodium acetate (pH 5.5), and 4 mM EGTA.[62,140,141,186,187] Cathepsin S buffer contained 10 mM DTT, 100 mM potassium phosphate, and 4 mM EGTA. Calpain buffer contained 10 mM dithiothreitol (DTT), 100 mM KCl, 2 mM EGTA, 50 mM Tris-HCl (pH 7.5), and 0.015% Brij-35. Substrate concentration for calpain was 0.5 μM NH_2-Glu(Edans)-Pro-Leu-Phe-Ala-Glu-Arg-Lys(Dabcyl)-OH (Ex=380 nm, Em=500 nm).[62,140,141] Substrate concentration for the cathepsins K and L was 0.5 μM Z-FR-Amc and for cathepsin S was 0.5 μM Z-VVR-Amc (Ex=351 nm, Em=430 nm).[186-188] Inhibitor concentrations of 0, 0.5, 1, 2, 5, 7, 10, 15, 25, 50, and 100 μM, in triplicate, were used for each assay. Buffer, enzyme, and inhibitor were combined. Cathepsin assays were activated by the injection of substrate. Calpain assays were activated by the injection of $CaCl_2$ to a final concentration of 5 mM. All assays were done at a total well volume of 100 μL in 96-well plate, and each well contained a separate inhibitor concentration. Fluorescence was read in a Fluorescence readings were taken every 13 seconds for one hour by a Berthold Tri-Star plate reader.

Velocities were determined by taking only the linear portion of the curve into account (roughly 200-400 sec.). IC_{50} was determined by plotting the fractional activity vs. the log [I]. Fractional activity was calculated by dividing the velocity of the inhibited enzyme by the velocity of the uninhibited enzyme and multiplying by 100 to obtain a percentage. The initial rate was then plotted against the log of the inhibitor concentration, and IC_{50} was calculated by GraphPad Prism. K_i was calculated from the IC_{50} using the equation $K_i = \frac{IC_{50}}{1 + \frac{[S]}{K_m}}$.[142] Inhibitors were tested against purified enzyme. Bolded and underlined residues denote where the linker, α,α'-dibromo-*m*-xylene is attached.

Cathepsin L Inhibitor Assays

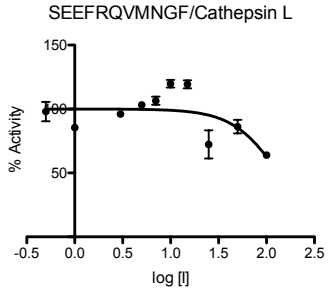

Figure S4.3: IC_{50} curve for SEEFRQVMNGF, 7a.

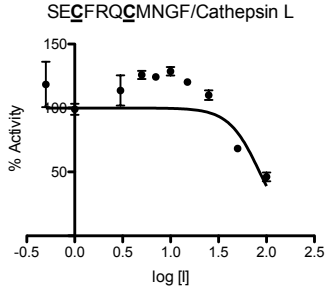

Figure S4.4: IC_{50} curve for SECFRQCMNGF, 7b.

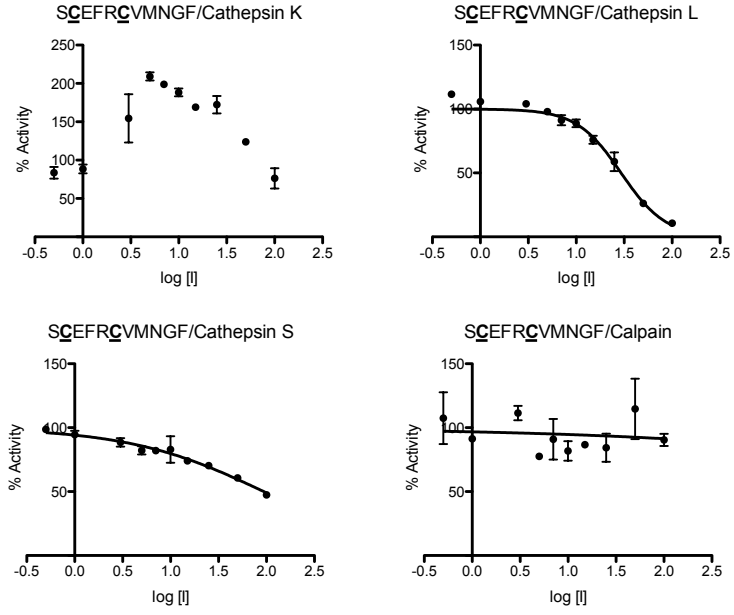

Figure S4.5: IC_{50} curve for SCEFRCVMNGF, 7c.

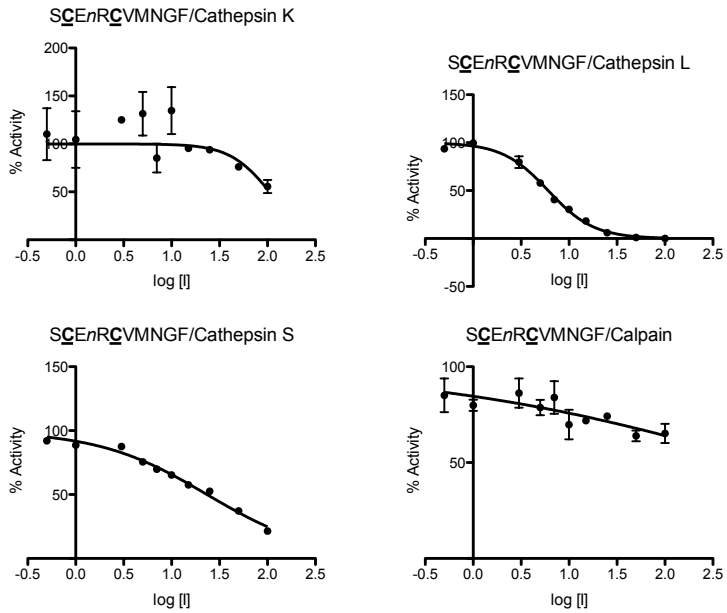

Figure S4.6: IC_{50} curves for S<u>C</u>E*n*R<u>C</u>VMNGF, 7d.

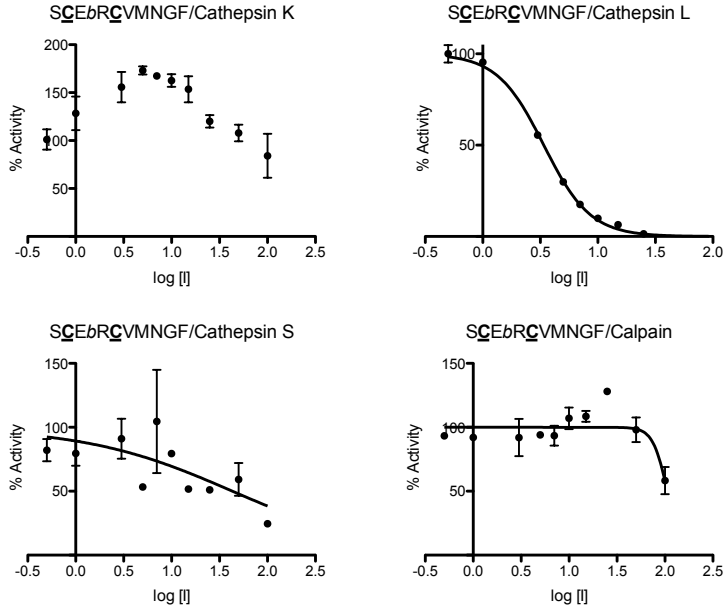

Figure S4.7: IC_{50} curves for S<u>C</u>E*b*R<u>C</u>VMNGF, 7e.

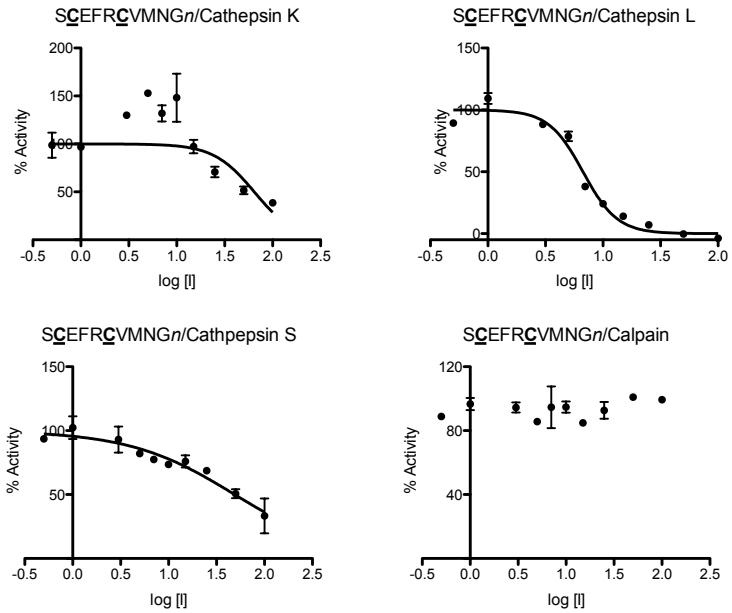

Figure S4.8: IC_{50} curves for S<u>C</u>EFR<u>C</u>VMNG*n*, 7f.

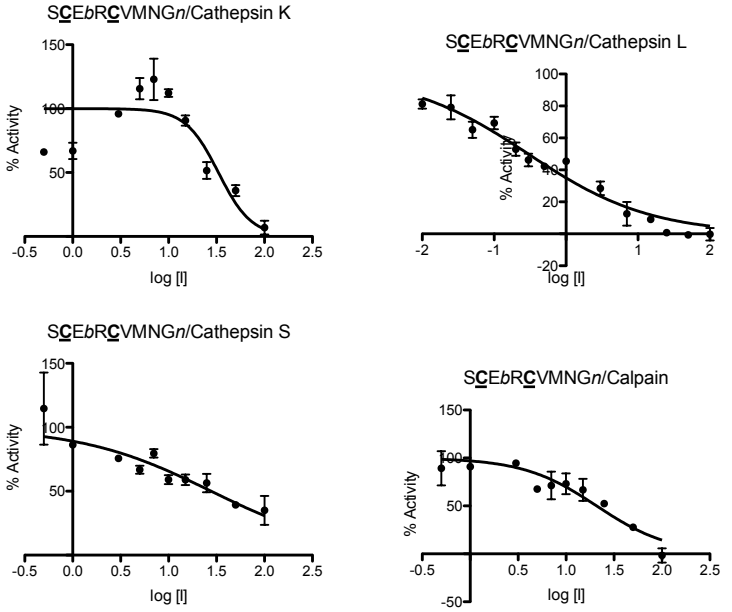

Figure S4.9: IC_{50} curves for S<u>C</u>E*b*R<u>C</u>VMNG*n*, 7g.

Cathepsin S Inhibitor Assays

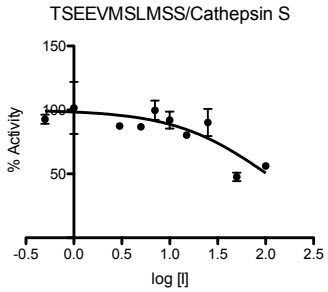

Figure S4.10: IC_{50} curve for TSEEVMSLMSS, 8a.

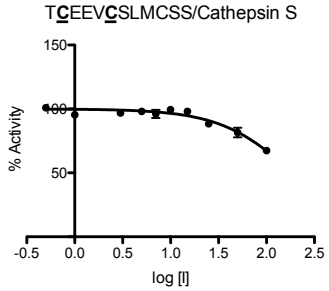

Figure S4.11: IC_{50} curve for TCEEVCSLMSS, 8b.

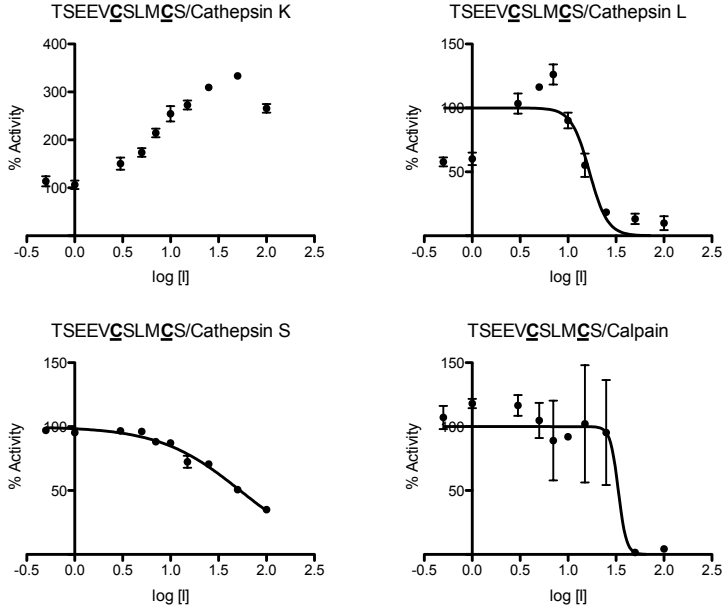

Figure S4.12: IC_{50} curve for TSEEVCSLMCS, 2c.

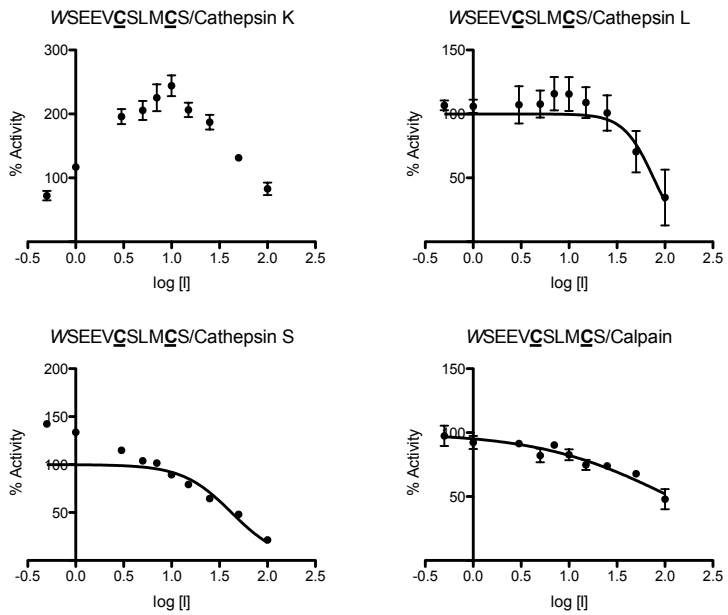

Figure S4.13: IC_{50} curves for *W*SEEV<u>C</u>SLM<u>C</u>S, 8d.

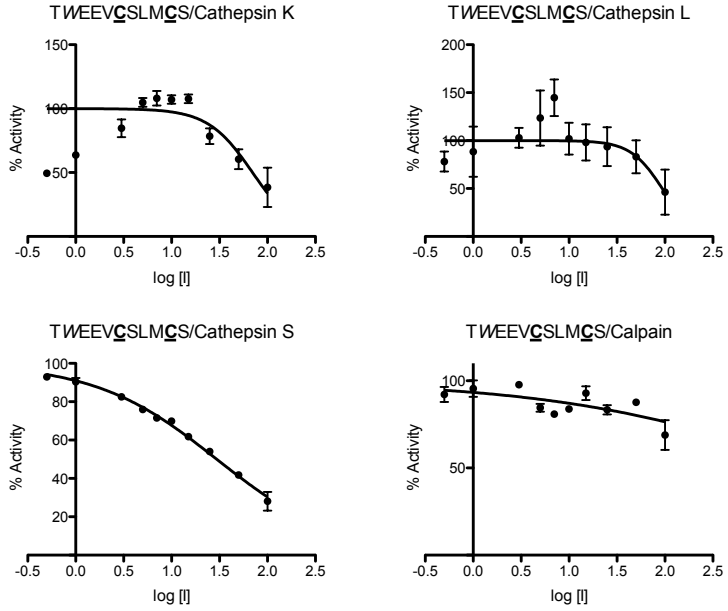

Figure S4.14: IC_{50} curves for T*W*EEV<u>C</u>SLM<u>C</u>S, 8e.

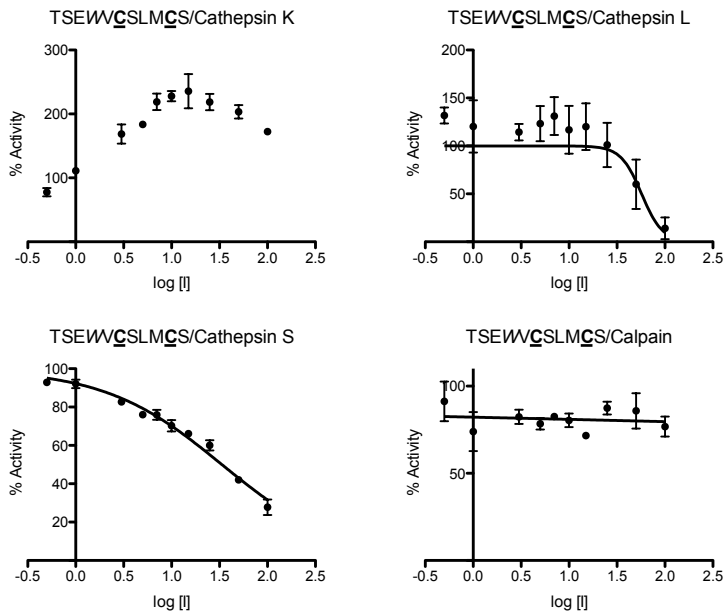

Figure S4.15: IC_{50} curves for TSE*W*VCSLMCS, 8f.

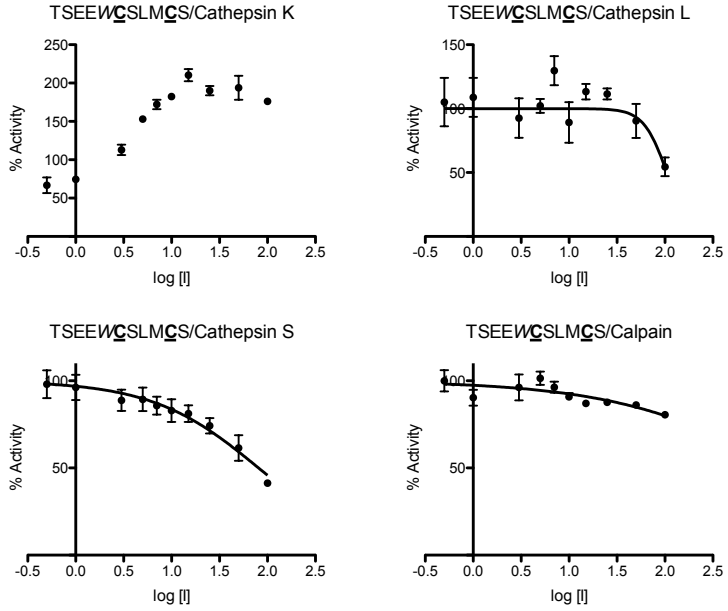

Figure S4.16: IC_{50} curves for TSEE*W*CSLMCS, 8g.

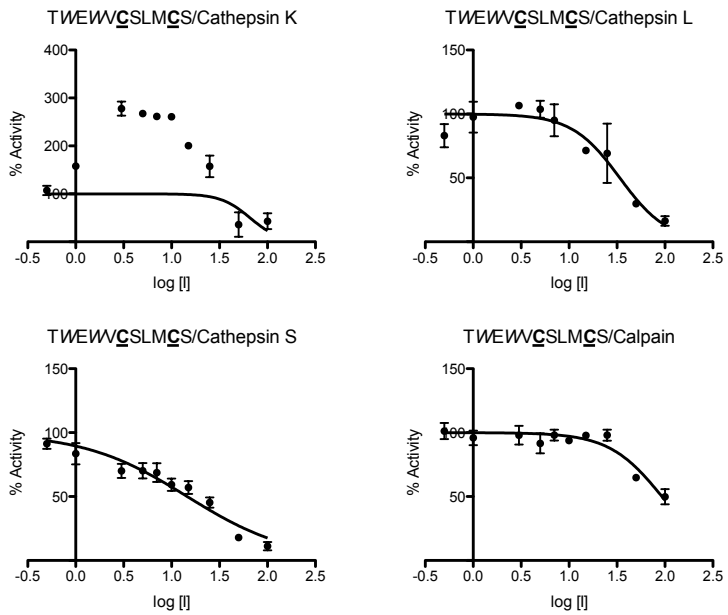

Figure S4.17: IC_{50} curves for T*W*E*W*V<u>C</u>SLM<u>C</u>S, 8h.

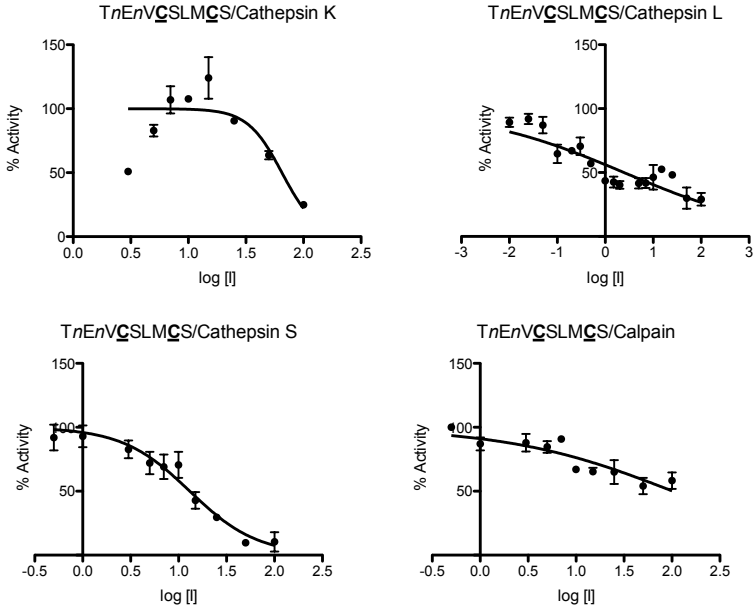

Figure S4.18: IC_{50} curves for T*n*E*n*V<u>C</u>SLM<u>C</u>S, 8i.

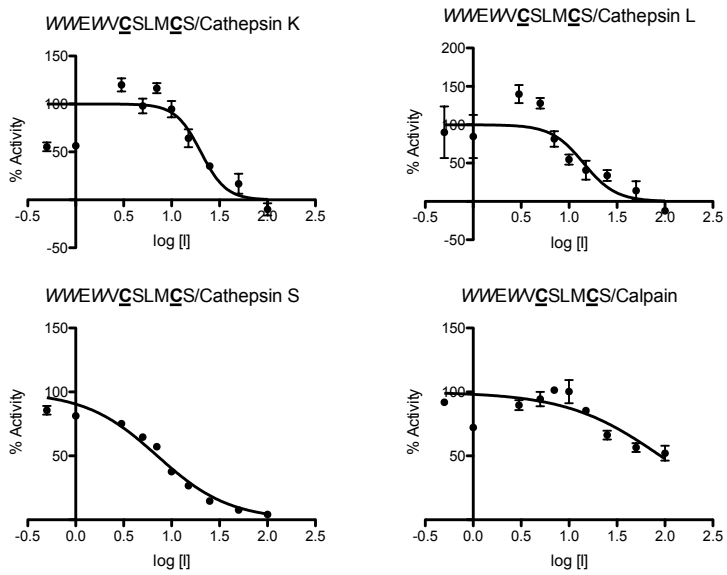

Figure S4.19: IC_{50} curves for *WWEW*V<u>C</u>SLM<u>C</u>S, 8j.

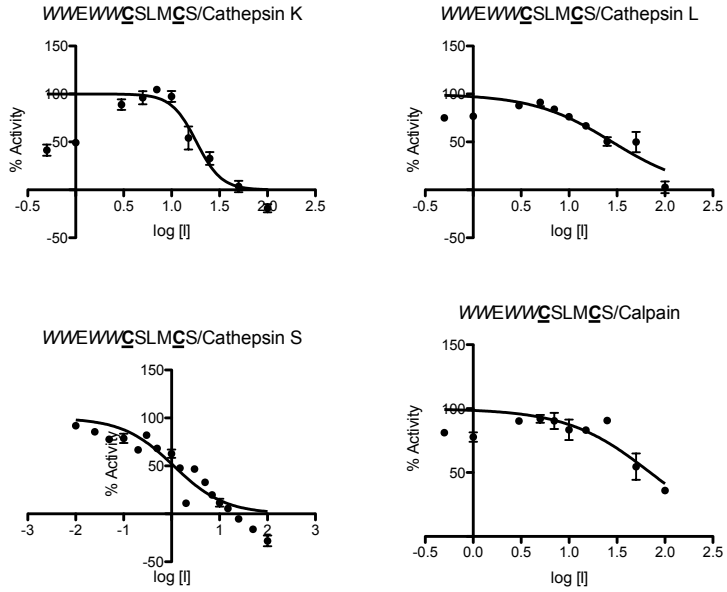

Figure S4.20: IC_{50} curves for *WWEWW*<u>C</u>SLM<u>C</u>S, 8k.

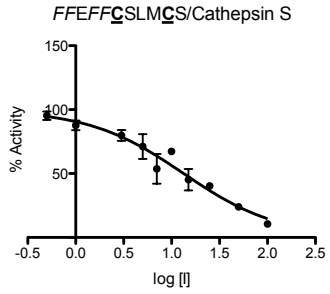

Figure S4.21: IC_{50} curves for *FF*E*FF*<u>C</u>SLM<u>C</u>S, 8l.

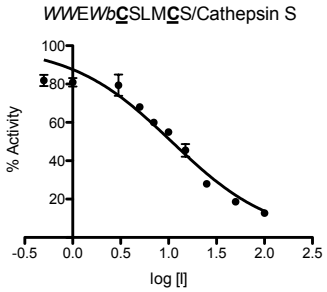

Figure S4.22: IC_{50} curves for *WW*E*Wb*<u>C</u>SLM<u>C</u>S, 8m.

Cathepsin K Inhibitor Assays

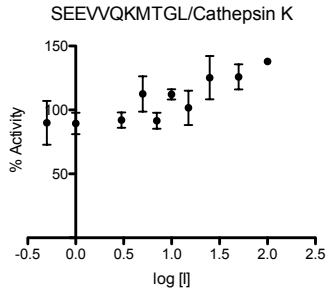

Figure S4.23: IC_{50} curve for SEEVVQKMTGL, 9a.

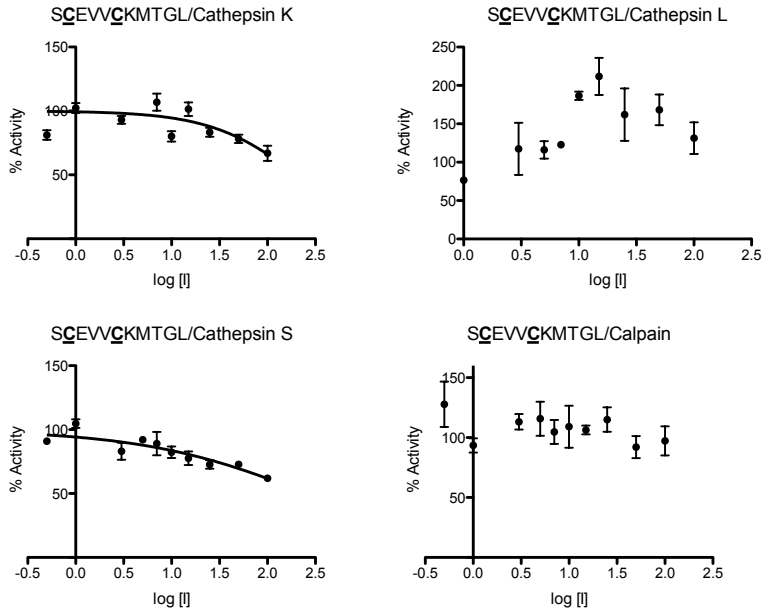

Figure S4.24: IC_{50} curves for SCEVVCKMTGL, 9b.

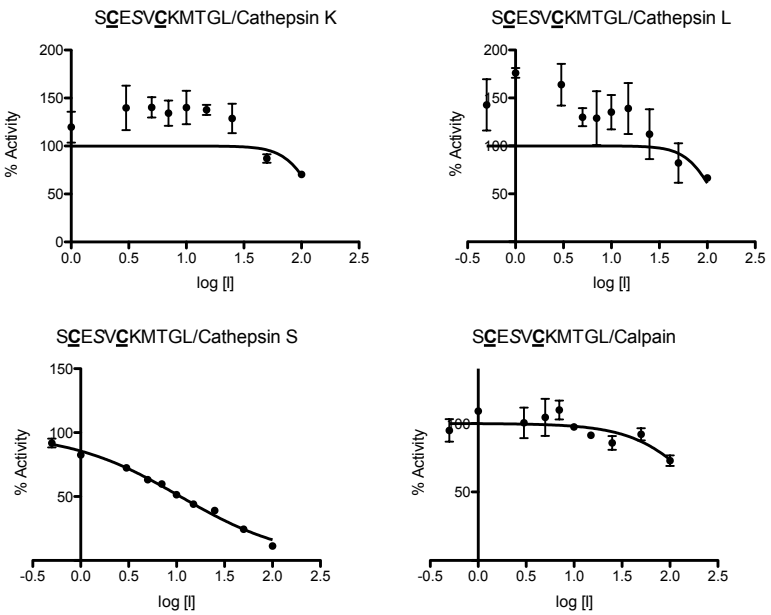

Figure S4.25: IC_{50} curves for S<u>C</u>E*S*V<u>C</u>KMTGL, 9c.

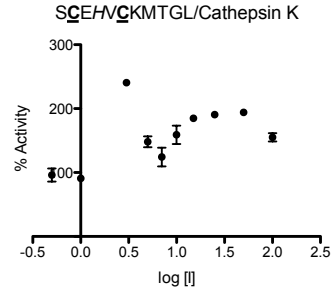

Figure S4.26: IC_{50} curves for S<u>C</u>E*H*V<u>C</u>KMTGL, 9d.

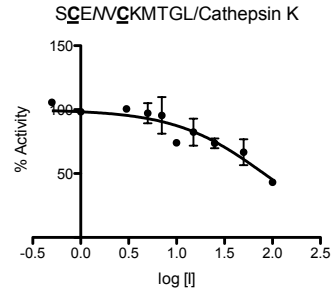

Figure S4.27: IC_{50} curves for S<u>C</u>E*N*V<u>C</u>KMTGL, 9e.

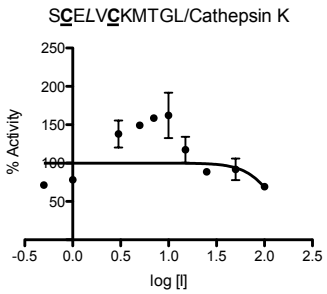

Figure S4.28: IC_{50} curves for SCE*L*VCKMTGL, 9f.

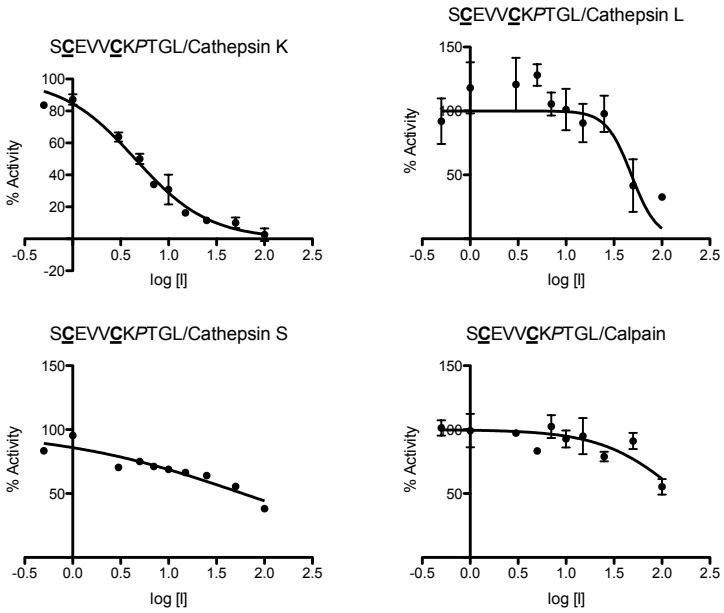

Figure S4.29: IC_{50} curves for SCEVVCK*P*TGL, 9g.

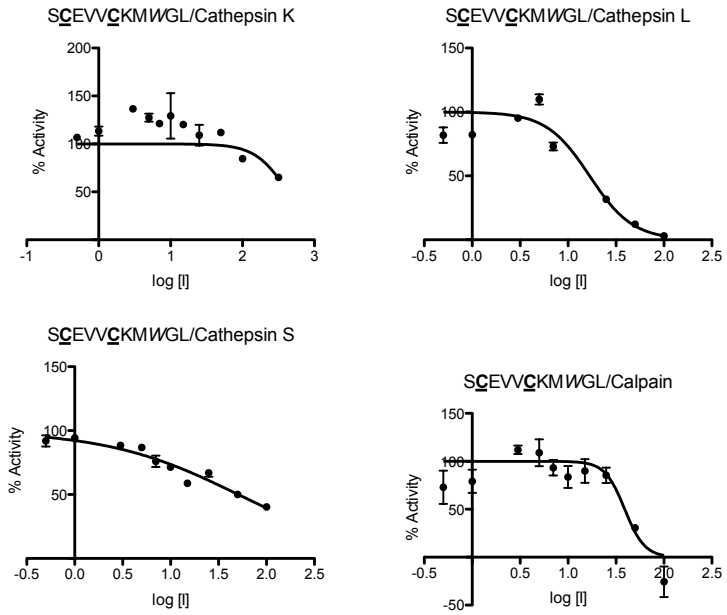

Figure S4.30: IC_{50} curves for S<u>C</u>EVV<u>C</u>KM*W*GL, 9h.

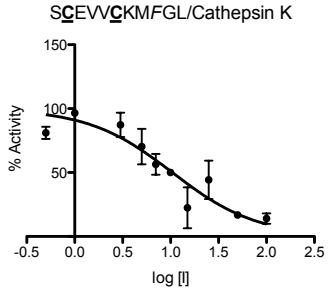

Figure S4.31: IC_{50} curves for S<u>C</u>EVV<u>C</u>KM*F*GL, 9i.

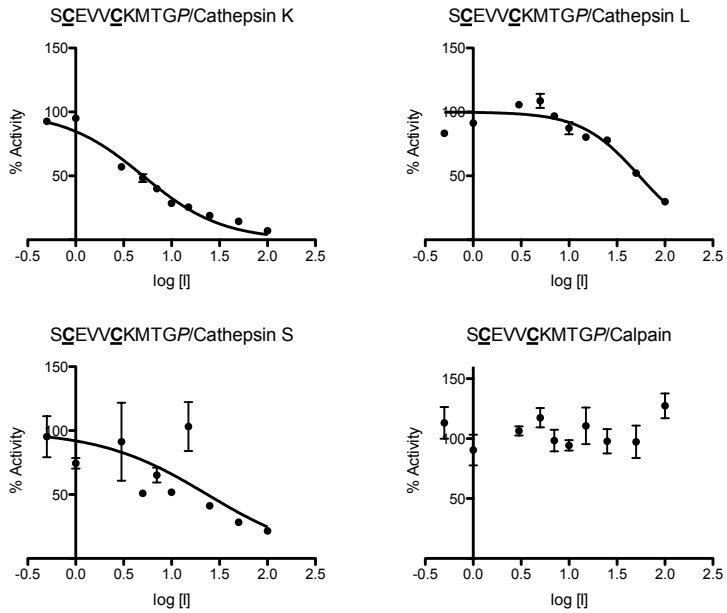

Figure S4.32: IC_{50} curves for S<u>C</u>EVV<u>C</u>KMTG*P*, 9j.

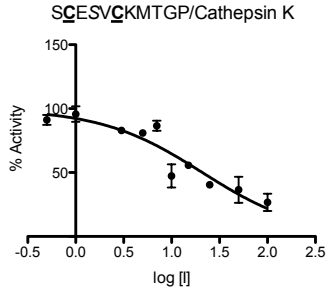

Figure S4.33: IC_{50} curves for S<u>C</u>E*S*V<u>C</u>KMTG*P*, 9k.

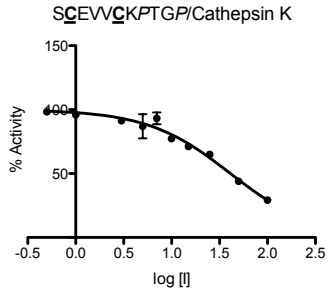

Figure S4.34: IC_{50} curves for S<u>C</u>EVV<u>C</u>K*P*TG*P*, 9l.

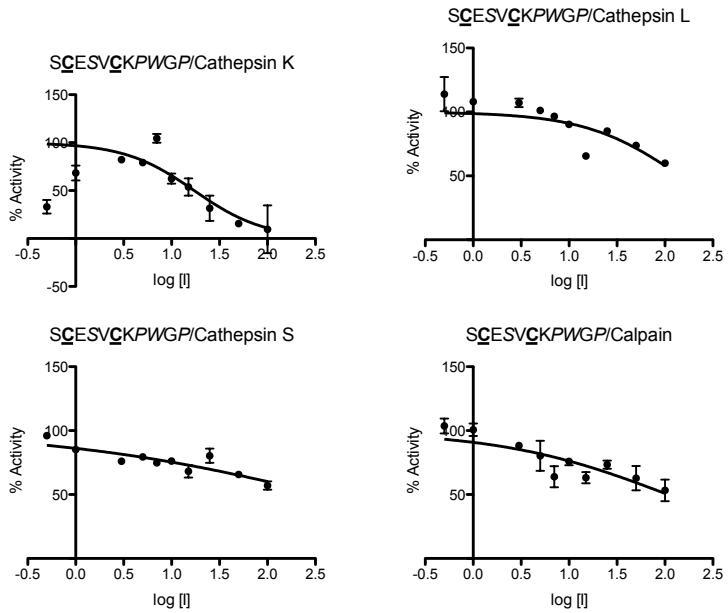

Figure S4.35: IC_{50} curves for S<u>C</u>E*S*V<u>C</u>K*PW*G*P*, 9m.

Michaelis-Menten Kinetics

To identify inhibition type we used standard Michaelis-Menten treatment. Initial velocities were calculated from the linear segment of the progress curves then plotted against their substrate concentration (~200-400 s).[142] Units were initially measured in RFU/sec then converted to μM/sec using the conversion factor 17567.8 RFU/μM for Z-FR-Amc and 5999.04 RFU/μM for Z-VVR-Amc. The conversion factor was obtained by the total hydrolysis of the substrate in a known concentration by papain. We then plotted velocity vs. substrate concentration and used GraphPadPrism program Michaelis-Menten (under kinetics) to determine the K_m^{app} and V_{max}^{app}.

[**7g**] (μM)	V_{max}^{app} (μM/sec)	K_m^{app}
0	0.002034 ± 0.0001	1.605
0.025	0.002058 ± 0.0001	2.022
0.05	0.002128 ± 0.0001	2.375

Table S4.2: Cathepsin L inhibitor 7g Michaelis-Menten results.

[**8k**] (μM)	V_{max}^{app} (μM/sec)	K_m^{app}
0	0.06344 ± 0.0106	29.96
0.5	0.07103 ± 0.0348	46.05
1	0.07114 ± 0.0137	50.16

Table S4.3: Cathepsin S inhibitor 8k Michaelis-Menten results.

[**9g**] (μM)	V_{max}^{app} (μM/sec)	K_m^{app}
0	0.006156 ± 0.0015	50.21
0.5	0.006261 ± 0.0012	53.65
1	0.006800± 0.0021	65.30

Table S4.4: Cathepsin K inhibitor 9g Michaelis-Menten results.

V_{max}^{app} is the same at all inhibitor concentrations while K_m^{app} increases with increasing inhibitor concentration. These results are indicative of competitive inhibition. To avoid weighting errors we used the values of K_m^{app} and V_{max}^{app} determined directly

from the non-linear least-squares best fits of the untransformed data and put these values into the reciprocal equation:

$$\frac{1}{v} = \left(\frac{K_m}{V_{\max}} \times \frac{1}{[S]}\right) + \frac{1}{V_{\max}} \quad 142$$

We then plotted the resulting reciprocal velocities against the respective reciprocal substrate concentrations creating a Lineweaver-Burk plot to further identify mode of inhibition. All lines intersected at the x-axis indicating competitive kinetics.

Lineweaver-Burk Plots

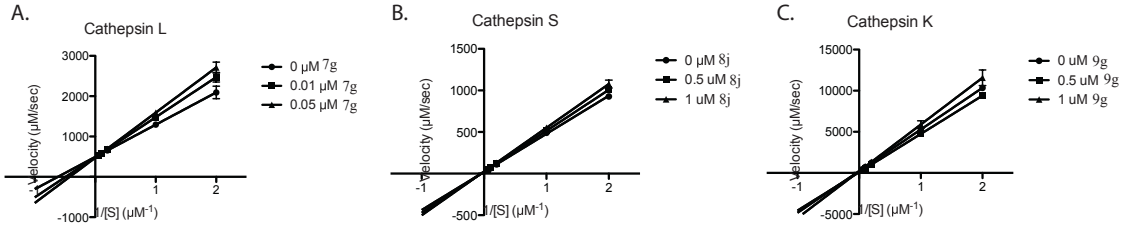

Figure S4.36: Lineweaver-Burke plots demonstrating that the α-helical inhibitors are all competitive inhibitors suggesting that it is likely they are binding at the active site.

α-Helical Inhibitors Modeled in Enzyme Active Sites

Using the zymogen crystal structures, the mutated, stabilized, α-helical inhibitors were modeled into the enzyme active site using Pymol as a visualization of their mode of inhibition.[31]

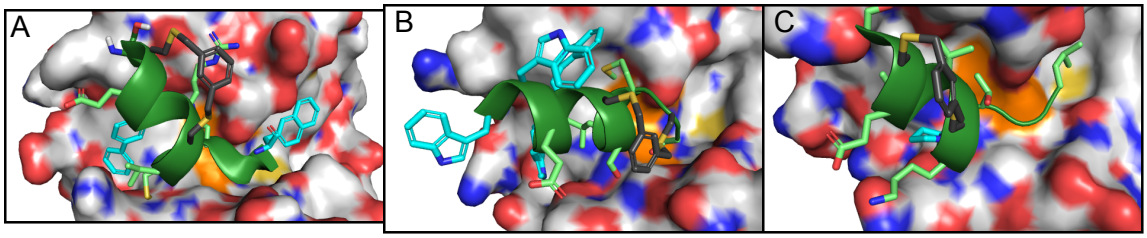

Figure S4.37: Models of a stabilized, α-helical inhibitor in the active site of its respective enzyme. (A) Cathepsin L, 7g, (B) Cathepsin S, 8k, (C) Cathepsin K, 9g.[31]

BIBLIOGRAPHY

(1) McGrath, M. E. *Annu Rev Biophys Biomol Struct* **1999**, *28*, 181.

(2) Pauly, T. A.; Sulea, T.; Ammirati, M.; Sivaraman, J.; Danley, D. E.; Griffor, M. C.; Kamath, A. V.; Wang, I. K.; Laird, E. R.; Seddon, A. P.; Menard, R.; Cygler, M.; Rath, V. L. *Biochemistry* **2003**, *42*, 3203.

(3) Coulombe, R.; Grochulski, P.; Sivaraman, J.; Menard, R.; Mort, J. S.; Cygler, M. *EMBO J* **1996**, *15*, 5492.

(4) Schechter, I.; Berger, A. *Biochem Biophys Res Commun* **1967**, *27*, 157.

(5) Schiefer, I. T.; Tapadar, S.; Litosh, V.; Siklos, M.; Scism, R.; Wijewickrama, G. T.; Chandrasena, E. P.; Sinha, V.; Tavassoli, E.; Brunsteiner, M.; Fa, M.; Arancio, O.; Petukhov, P.; Thatcher, G. R. *J Med Chem* **2013**, *56*, 6054.

(6) Biniossek, M. L.; Nagler, D. K.; Becker-Pauly, C.; Schilling, O. *J Proteome Res* **2011**, *10*, 5363.

(7) Goll, D. E.; Thompson, V. F.; Li, H.; Wei, W.; Cong, J. *Physiol Rev* **2003**, *83*, 731.

(8) Sorimachi, H.; Imajoh-Ohmi, S.; Emori, Y.; Kawasaki, H.; Ohno, S.; Minami, Y.; Suzuki, K. *J Biol Chem* **1989**, *264*, 20106.

(9) Guay, J.; Falgueyret, J. P.; Ducret, A.; Percival, M. D.; Mancini, J. A. *Eur J Biochem* **2000**, *267*, 6311.

(10) Reiser, J.; Adair, B.; Reinheckel, T. *J Clin Invest* **2010**, *120*, 3421.

(11) LaLonde, J. M.; Zhao, B.; Smith, W. W.; Janson, C. A.; DesJarlais, R. L.; Tomaszek, T. A.; Carr, T. J.; Thompson, S. K.; Oh, H. J.; Yamashita, D. S.; Veber, D. F.; Abdel-Meguid, S. S. *J Med Chem* **1998**, *41*, 4567.

(12) Riese, R. J.; Wolf, P. R.; Bromme, D.; Natkin, L. R.; Villadangos, J. A.; Ploegh, H. L.; Chapman, H. A. *Immunity* **1996**, *4*, 357.

(13) Cox, J. M.; Troutt, J. S.; Knierman, M. D.; Siegel, R. W.; Qian, Y. W.; Ackermann, B. L.; Konrad, R. J. *Anal Biochem* **2012**, *430*, 130.

(14) Baugh, M.; Black, D.; Westwood, P.; Kinghorn, E.; McGregor, K.; Bruin, J.; Hamilton, W.; Dempster, M.; Claxton, C.; Cai, J.; Bennett, J.; Long, C.; McKinnon, H.; Vink, P.; den Hoed, L.; Gorecka, M.; Vora, K.; Grant, E.; Percival, M. D.; Boots, A. M.; van Lierop, M. J. *J Autoimmun* **2011**, *36*, 201.

(15) Dana, D.; Davalos, A. R.; De, S.; Rathod, P.; Gamage, R. K.; Huestis, J.; Afzal, N.; Zavlanov, Y.; Paroly, S. S.; Rotenberg, S. A.; Subramaniam, G.; Mark, K. J.; Chang, E. J.; Kumar, S. *Bioorg Med Chem* **2013**, *21*, 2975.

(16) Chen, J. C.; Uang, B. J.; Lyu, P. C.; Chang, J. Y.; Liu, K. J.; Kuo, C. C.; Hsieh, H. P.; Wang, H. C.; Cheng, C. S.; Chang, Y. H.; Chang, M. D.; Chang, W. S.; Lin, C. C. *J Med Chem* **2010**, *53*, 4545.

(17) Torkar, A.; Lenarcic, B.; Lah, T.; Dive, V.; Devel, L. *Bioorg Med Chem Lett* **2013**, *23*, 2968.

(18) Panwar, P.; Du, X.; Sharma, V.; Lamour, G.; Castro, M.; Li, H.; Bromme, D. *J Biol Chem* **2013**, *288*, 5940.

(19) Saatman, K. E.; Creed, J.; Raghupathi, R. *Neurotherapeutics* **2010**, *7*, 31.

(20) Hong, S. C.; Goto, Y.; Lanzino, G.; Soleau, S.; Kassell, N. F.; Lee, K. S. *Stroke* **1994**, *25*, 663.

(21) Di Rosa, G.; Odrijin, T.; Nixon, R. A.; Arancio, O. *J Mol Neurosci* **2002**, *19*, 135.

(22) Dufty, B. M.; Warner, L. R.; Hou, S. T.; Jiang, S. X.; Gomez-Isla, T.; Leenhouts, K. M.; Oxford, J. T.; Feany, M. B.; Masliah, E.; Rohn, T. T. *Am J Pathol* **2007**, *170*, 1725.

(23) Vosler, P. S.; Brennan, C. S.; Chen, J. *Mol Neurobiol* **2008**, *38*, 78.

(24) Scott, C. J.; Taggart, C. C. *Biochimie* **2010**, *92*, 1681.

(25) Shaw, E.; Mohanty, S.; Colic, A.; Stoka, V.; Turk, V. *FEBS Lett* **1993**, *334*, 340.

(26) Frizler, M.; Lohr, F.; Furtmann, N.; Klas, J.; Gutschow, M. *J Med Chem* **2011**, *54*, 396.

(27) Kerns, J. K.; Nie, H.; Bondinell, W.; Widdowson, K. L.; Yamashita, D. S.; Rahman, A.; Podolin, P. L.; Carpenter, D. C.; Jin, Q.; Riflade, B.; Dong, X.; Nevins, N.; Keller, P. M.; Mitchell, L.; Tomaszek, T. *Bioorg Med Chem Lett* **2011**, *21*, 4409.

(28) Marquis, R. W.; Ru, Y.; LoCastro, S. M.; Zeng, J.; Yamashita, D. S.; Oh, H. J.; Erhard, K. F.; Davis, L. D.; Tomaszek, T. A.; Tew, D.; Salyers, K.; Proksch, J.; Ward, K.; Smith, B.; Levy, M.; Cummings, M. D.; Haltiwanger, R. C.; Trescher, G.; Wang, B.; Hemling, M. E.; Quinn, C. J.; Cheng, H. Y.; Lin, F.; Smith, W. W.; Janson, C. A.; Zhao, B.; McQueney, M. S.; D'Alessio, K.; Lee, C. P.; Marzulli, A.; Dodds, R. A.; Blake, S.; Hwang, S. M.; James, I. E.; Gress, C. J.; Bradley, B. R.; Lark, M. W.; Gowen, M.; Veber, D. F. *J Med Chem* **2001**, *44*, 1380.

(29) Kaulmann, G.; Palm, G. J.; Schilling, K.; Hilgenfeld, R.; Wiederanders, B. *Protein Sci* **2006**, *15*, 2619.

(30) Hanna, R. A.; Campbell, R. L.; Davies, P. L. *Nature* **2008**, *456*, 409.

(31) The Pymol Molecular Graphics System; Version 1.5.0.4.; Schrödinger, LLC.

(32) Kim, Y. W.; Grossmann, T. N.; Verdine, G. L. *Nat Protoc* **2011**, *6*, 761.

(33) Blackwell, H. E.; Grubbs, R. H. *Angew Chem Int Edit* **1998**, *37*, 3281.

(34) Schafmeister, C. E.; Po, J.; Verdine, G. L. *J Am Chem Soc* **2000**, *122*, 5891.

(35) Henchey, L. K.; Porter, J. R.; Ghosh, I.; Arora, P. S. *Chembiochem* **2010**, *11*, 2104.

(36) Patgiri, A.; Jochim, A. L.; Arora, P. S. *Acc Chem Res* **2008**, *41*, 1289.

(37) Patgiri, A.; Menzenski, M. Z.; Mahon, A. B.; Arora, P. S. *Nat Protoc* **2010**, *5*, 1857.

(38) Kushal, S.; Lao, B. B.; Henchey, L. K.; Dubey, R.; Mesallati, H.; Traaseth, N. J.; Olenyuk, B. Z.; Arora, P. S. *Proc Natl Acad Sci U S A* **2013**, *110*, 15602.

(39) Mahon, A. B.; Arora, P. S. *Chem Commun (Camb)* **2012**, *48*, 1416.

(40) Haney, C. M.; Loch, M. T.; Horne, W. S. *Chem Commun* **2011**, *47*, 10915.

(41) Haney, C. M.; Horne, W. S. *Chemistry* **2013**, *19*, 11342.

(42) Timmerman, P.; Beld, J.; Puijk, W. C.; Meloen, R. H. *Chembiochem* **2005**, *6*, 821.

(43) Muppidi, A.; Wang, Z.; Li, X.; Chen, J.; Lin, Q. *Chem Commun (Camb)* **2011**, *47*, 9396.

(44) Azzarito, V.; Long, K.; Murphy, N. S.; Wilson, A. J. *Nat Chem* **2013**, *5*, 161.

(45) Stewart, M. L.; Fire, E.; Keating, A. E.; Walensky, L. D. *Nat Chem Biol* **2010**, *6*, 595.

(46) Phillips, C.; Roberts, L. R.; Schade, M.; Bazin, R.; Bent, A.; Davies, N. L.; Moore, R.; Pannifer, A. D.; Pickford, A. R.; Prior, S. H.; Read, C. M.; Scott, A.; Brown, D. G.; Xu, B.; Irving, S. L. *J Am Chem Soc* **2011**, *133*, 9696.

(47) Baek, S.; Kutchukian, P. S.; Verdine, G. L.; Huber, R.; Holak, T. A.; Lee, K. W.; Popowicz, G. M. *J Am Chem Soc* **2012**, *134*, 103.

(48) Rao, T.; Ruiz-Gomez, G.; Hill, T. A.; Hoang, H. N.; Fairlie, D. P.; Mason, J. M. *PLoS One* **2013**, *8*, e59415.

(49) Zatz, M.; Starling, A. *N Engl J Med* **2005**, *352*, 2413.

(50) Polster, B. M.; Basanez, G.; Etxebarria, A.; Hardwick, J. M.; Nicholls, D. G. *J Biol Chem* **2005**, *280*, 6447.

(51) Janossy, J.; Ubezio, P.; Apati, A.; Magocsi, M.; Tompa, P.; Friedrich, P. *Biochem Pharmacol* **2004**, *67*, 1513.

(52) Sreenan, S. K.; Zhou, Y. P.; Otani, K.; Hansen, P. A.; Currie, K. P.; Pan, C. Y.; Lee, J. P.; Ostrega, D. M.; Pugh, W.; Horikawa, Y.; Cox, N. J.; Hanis, C. L.; Burant, C. F.; Fox, A. P.; Bell, G. I.; Polonsky, K. S. *Diabetes* **2001**, *50*, 2013.

(53) Franco, S. J.; Huttenlocher, A. *J Cell Sci* **2005**, *118*, 3829.

(54) Kulkarni, S.; Reddy, K. B.; Esteva, F. J.; Moore, H. C.; Budd, G. T.; Tubbs, R. R. *Oncogene* **2010**, *29*, 1339.

(55) Shintani-Ishida, K.; Yoshida, K. *Biochim Biophys Acta* **2011**, *1812*, 743.

(56) Liang, B.; Duan, B. Y.; Zhou, X. P.; Gong, J. X.; Luo, Z. G. *J Biol Chem* **2010**, *285*, 27737.

(57) Portbury, A. L.; Willis, M. S.; Patterson, C. *J Biol Chem* **2011**, *286*, 9929.

(58) Ma, J.; Wei, M.; Wang, Q.; Li, J.; Wang, H.; Liu, W.; Lacefield, J. C.; Greer, P. A.; Karmazyn, M.; Fan, G.; Peng, T. *J Biol Chem* **2012**.

(59) Ho, W. C.; Pikor, L.; Gao, Y.; Elliott, B. E.; Greer, P. A. *J Biol Chem* **2012**, *287*, 15458.

(60) Tan, Y.; Wu, C.; De Veyra, T.; Greer, P. A. *J Biol Chem* **2006**, *281*, 17689.

(61) Cuerrier, D.; Moldoveanu, T.; Campbell, R. L.; Kelly, J.; Yoruk, B.; Verhelst, S. H.; Greenbaum, D.; Bogyo, M.; Davies, P. L. *J Biol Chem* **2007**, *282*, 9600.

(62) Gil-Parrado, S.; Assfalg-Machleidt, I.; Fiorino, F.; Deluca, D.; Pfeiler, D.; Schaschke, N.; Moroder, L.; Machleidt, W. *Biol Chem* **2003**, *384*, 395.

(63) Ma, H.; Yang, H. Q.; Takano, E.; Hatanaka, M.; Maki, M. *J Biol Chem* **1994**, *269*, 24430.

(64) Sasaki, T.; Kikuchi, T.; Fukui, I.; Murachi, T. *J Biochem* **1986**, *99*, 173.

(65) Qian, J.; Cuerrier, D.; Davies, P. L.; Li, Z.; Powers, J. C.; Campbell, R. L. *J Med Chem* **2008**, *51*, 5264.

(66) Donkor, I. O. *Expert Opin Ther Pat* **2011**, *21*, 601.

(67) Li, Z.; Ortega-Vilain, A. C.; Patil, G. S.; Chu, D. L.; Foreman, J. E.; Eveleth, D. D.; Powers, J. C. *J Med Chem* **1996**, *39*, 4089.

(68) Ovat, A.; Li, Z. Z.; Hampton, C. Y.; Asress, S. A.; Fernandez, F. M.; Glass, J. D.; Powers, J. C. *J Med Chem* **2010**, *53*, 6326.

(69) Moldoveanu, T.; Gehring, K.; Green, D. R. *Nature* **2008**, *456*, 404.

(70) Donkor, I. O.; Korukonda, R. *Bioorg Med Chem Lett* **2008**, *18*, 4806.

(71) Pietsch, M.; Chua, K. C.; Abell, A. D. *Curr Top Med Chem* **2010**, *10*, 270.

(72) Abell, A. D.; Jones, M. A.; Coxon, J. M.; Morton, J. D.; Aitken, S. G.; McNabb, S. B.; Lee, H. Y.; Mehrtens, J. M.; Alexander, N. A.; Stuart, B. G.; Neffe, A. T.; Bickerstaffe, R. *Angew Chem Int Ed Engl* **2009**, *48*, 1455.

(73) Wendt, A.; Thompson, V. F.; Goll, D. E. *Biol Chem* **2004**, *385*, 465.

(74) Jackson, D. Y.; King, D. S.; Chmielewski, J.; Singh, S.; Schultz, P. G. *Journal of the American Chemical Society* **1991**, *113*, 9391.

(75) Leduc, A. M.; Trent, J. O.; Wittliff, J. L.; Bramlett, K. S.; Briggs, S. L.; Chirgadze, N. Y.; Wang, Y.; Burris, T. P.; Spatola, A. F. *P Natl Acad Sci USA* **2003**, *100*, 11273.

(76) Almeida, A. M.; Li, R.; Gellman, S. H. *J Am Chem Soc* **2012**, *134*, 75.

(77) Wang, D.; Liao, W.; Arora, P. S. *Angew Chem Int Ed Engl* **2005**, *44*, 6525.

(78) Dimartino, G.; Wang, D.; Chapman, R. N.; Arora, P. S. *Org Lett* **2005**, *7*, 2389.

(79) Schafmeister, C. E.; Po, J.; Verdine, G. L. *Journal of the American Chemical Society* **2000**, *122*, 5891.

(80) Walensky, L. D.; Kung, A. L.; Escher, I.; Malia, T. J.; Barbuto, S.; Wright, R. D.; Wagner, G.; Verdine, G. L.; Korsmeyer, S. J. *Science* **2004**, *305*, 1466.
(81) Wang, D.; Chen, K.; Kulp, J. L.; Arora, P. S. *Journal of the American Chemical Society* **2006**, *128*, 9248.
(82) Woolley, G. A. *Accounts of chemical research* **2005**, *38*, 486.
(83) Houston, M. E., Jr.; Gannon, C. L.; Kay, C. M.; Hodges, R. S. *Journal of peptide science : an official publication of the European Peptide Society* **1995**, *1*, 274.
(84) Phelan, J. C.; Skelton, N. J.; Braisted, A. C.; McDowell, R. S. *Journal of the American Chemical Society* **1997**, *119*, 455.
(85) Osapay, G.; Taylor, J. W. *Journal of the American Chemical Society* **1992**, *114*, 6966.
(86) Felix, A. M.; Heimer, E. P.; Wang, C. T.; Lambros, T. J.; Fournier, A.; Mowles, T. F.; Maines, S.; Campbell, R. M.; Wegrzynski, B. B.; Toome, V.; Fry, D.; Madison, V. S. *International journal of peptide and protein research* **1988**, *32*, 441.
(87) Fujimoto, K.; Kajino, M.; Inouye, M. *Chem-Eur J* **2008**, *14*, 857.
(88) Geistlinger, T. R.; Guy, R. K. *J Am Chem Soc* **2001**, *123*, 1525.
(89) Geistlinger, T. R.; Guy, R. K. *J Am Chem Soc* **2003**, *125*, 6852.
(90) Cabezas, E.; Satterthwait, A. C. *Journal of the American Chemical Society* **1999**, *121*, 3862.
(91) Haney, C. M.; Loch, M. T.; Horne, W. S. *Chemical communications* **2011**, *47*, 10915.
(92) Ghadiri, M. R.; Choi, C. *Journal of the American Chemical Society* **1990**, *112*, 1630.
(93) Ruan, F. Q.; Chen, Y. Q.; Hopkins, P. B. *Journal of the American Chemical Society* **1990**, *112*, 9403.
(94) Kawamoto, S. A.; Coleska, A.; Ran, X.; Yi, H.; Yang, C. Y.; Wang, S. *Journal of medicinal chemistry* **2012**, *55*, 1137.
(95) Holland-Nell, K.; Meldal, M. *Angew Chem Int Edit* **2011**, *50*, 5204.
(96) Freidinger, R. M. *J Med Chem* **2003**, *46*, 5553.
(97) Hruby, V. J. *Life Sci* **1982**, *31*, 189.
(98) Satterthwait, A. C.; Arrhenius, T.; Hagopian, R. A.; Zavala, F.; Nussenzweig, V.; Lerner, R. A. *Vaccine* **1988**, *6*, 99.
(99) Oneil, K. T.; Hoess, R. H.; Jackson, S. A.; Ramachandran, N. S.; Mousa, S. A.; Degrado, W. F. *Proteins* **1992**, *14*, 509.
(100) Bach, A. C.; Eyermann, C. J.; Gross, J. D.; Bower, M. J.; Harlow, R. L.; Weber, P. C.; Degrado, W. F. *Journal of the American Chemical Society* **1994**, *116*, 3207.
(101) Cheng, R. P.; Suich, D. J.; Cheng, H.; Roder, H.; DeGrado, W. F. *J Am Chem Soc* **2001**, *123*, 12710.
(102) Suich, D. J.; Mousa, S. A.; Singh, G.; Liapakis, G.; Reisine, T.; DeGrado, W. F. *Bioorgan Med Chem* **2000**, *8*, 2229.
(103) Cheng, R. P.; Scialdone, M. A.; DeGrado, W. F. *Abstr Pap Am Chem S* **1999**, *218*, U138.
(104) Nestor, J. J. *Curr Med Chem* **2009**, *16*, 4399.
(105) Szewczuk, Z.; Rebholz, K. L.; Rich, D. H. *International journal of peptide and protein research* **1992**, *40*, 233.
(106) Timmerman, P.; Beld, J.; Puijk, W. C.; Meloen, R. H. *Chembiochem* **2005**, *6*, 821.
(107) Lindman, S.; Lindeberg, G.; Gogoll, A.; Nyberg, F.; Karlen, A.; Hallberg, A. *Bioorgan Med Chem* **2001**, *9*, 763.
(108) Walker, M. A.; Johnson, T. *Tetrahedron Lett* **2001**, *42*, 5801.

(109) Blanco-Lomas, M.; Samanta, S.; Campos, P. J.; Woolley, G. A.; Sampedro, D. *Journal of the American Chemical Society* **2012**.

(110) Huang, R.; Holbert, M. A.; Tarrant, M. K.; Curtet, S.; Colquhoun, D. R.; Dancy, B. M.; Dancy, B. C.; Hwang, Y.; Tang, Y.; Meeth, K.; Marmorstein, R.; Cole, R. N.; Khochbin, S.; Cole, P. A. *Journal of the American Chemical Society* **2010**, *132*, 9986.

(111) Dewkar, G. K.; Carneiro, P. B.; Hartman, M. C. T. *Organic Letters* **2009**, *11*, 4708.

(112) Smeenk, L. E. J.; Dailly, N.; Hiemstra, H.; van Maarseveen, J. H.; Timmerman, P. *Organic Letters* **2012**, *14*, 1194.

(113) Johnson, W. C. *Proteins* **1990**, *7*, 205.

(114) Woody, R. W.; Koslowski, A. *Biophys Chem* **2002**, *101*, 535.

(115) Szyperski, T.; Guntert, P.; Otting, G.; Wuthrich, K. *J Magn Reson* **1992**, *99*, 552.

(116) Armstrong, D. a. Z., Raphael; v 1.4 ed. 2009.

(117) Greenfield, N. J. *Anal Biochem* **1996**, *235*, 1.

(118) Filippi, B.; Borin, G.; Moretto, V.; Marchiori, F. *Biopolymers* **1978**, *17*, 2545.

(119) MacArthur, M. W.; Thornton, J. M. *J Mol Biol* **1991**, *218*, 397.

(120) Marqusee, S.; Baldwin, R. L. *Proc Natl Acad Sci U S A* **1987**, *84*, 8898.

(121) Bradley, E. K.; Thomason, J. F.; Cohen, F. E.; Kosen, P. A.; Kuntz, I. D. *J Mol Biol* **1990**, *215*, 607.

(122) Shoemaker, K. R.; Kim, P. S.; York, E. J.; Stewart, J. M.; Baldwin, R. L. *Nature* **1987**, *326*, 563.

(123) Betts, R.; Weinsheimer, S.; Blouse, G. E.; Anagli, J. *J Biol Chem* **2003**, *278*, 7800.

(124) Cheng, Y.; Prusoff, W. H. *Biochem Pharmacol* **1973**, *22*, 3099.

(125) Turk, V.; Stoka, V.; Vasiljeva, O.; Renko, M.; Sun, T.; Turk, B.; Turk, D. *Biochim Biophys Acta* **2012**, *1824*, 68.

(126) Barlos, K.; Gatos, D.; Hatzi, O.; Koch, N.; Koutsogianni, S. *International journal of peptide and protein research* **1996**, *47*, 148.

(127) Benito, J. M.; Meldal, M. *Qsar Comb Sci* **2004**, *23*, 117.

(128) Adam, G. C.; Cravatt, B. F.; Sorensen, E. J. *Chem Biol* **2001**, *8*, 81.

(129) Cravatt, B. F.; Sorensen, E. J. *Curr Opin Chem Biol* **2000**, *4*, 663.

(130) Kidd, D.; Liu, Y.; Cravatt, B. F. *Biochemistry* **2001**, *40*, 4005.

(131) Puri, A. W.; Broz, P.; Shen, A.; Monack, D. M.; Bogyo, M. *Nat Chem Biol* **2012**.

(132) Albrow, V. E.; Ponder, E. L.; Fasci, D.; Bekes, M.; Deu, E.; Salvesen, G. S.; Bogyo, M. *Chem Biol* **2011**, *18*, 722.

(133) Yuan, F.; Verhelst, S. H.; Blum, G.; Coussens, L. M.; Bogyo, M. *J Am Chem Soc* **2006**, *128*, 5616.

(134) Gygi, S. P.; Rochon, Y.; Franza, B. R.; Aebersold, R. *Mol Cell Biol* **1999**, *19*, 1720.

(135) Greenbaum, D.; Medzihradszky, K. F.; Burlingame, A.; Bogyo, M. *Chemistry & Biology* **2000**, *7*, 569.

(136) Edelhoch, H. *Biochemistry-Us* **1967**, *6*, 1948.

(137) Wüthrich, K. *NMR of proteins and nucleic acids*; Wiley: New York, 1986.

(138) Delaglio, F.; Grzesiek, S.; Vuister, G. W.; Zhu, G.; Pfeifer, J.; Bax, A. *J Biomol NMR* **1995**, *6*, 277.

(139) Bartels, C.; Xia, T. H.; Billeter, M.; Guntert, P.; Wuthrich, K. *Journal of Biomolecular Nmr* **1995**, *6*, 1.

(140) Kelly, J. C.; Cuerrier, D.; Graham, L. A.; Campbell, R. L.; Davies, P. L. *Bba-Proteins Proteom* **2009**, *1794*, 1505.

(141) Pfizer, J.; Assfalg-Machleidt, I.; Machleidt, W.; Schaschke, N. *Biol Chem* **2008**, *389*, 83.

(142) Copeland, R. A. *Enzymes : a practical introduction to structure, mechanism, and data analysis*; VCH Publishers: New York, 1996.

(143) Cuerrier, D.; Moldoveanu, T.; Davies, P. L. *J Biol Chem* **2005**, *280*, 40632.

(144) Betts, R.; Anagli, J. *Biochemistry* **2004**, *43*, 2596.

(145) Blum, G.; von Degenfeld, G.; Merchant, M. J.; Blau, H. M.; Bogyo, M. *Nat Chem Biol* **2007**, *3*, 668.

(146) Verdoes, M.; Edgington, L. E.; Scheeren, F. A.; Leyva, M.; Blum, G.; Weiskopf, K.; Bachmann, M. H.; Ellman, J. A.; Bogyo, M. *Chem Biol* **2012**, *19*, 619.

(147) Verdoes, M.; Oresic Bender, K.; Segal, E.; van der Linden, W. A.; Syed, S.; Withana, N. P.; Sanman, L. E.; Bogyo, M. *J Am Chem Soc* **2013**, *135*, 14726.

(148) Schornberg, K.; Matsuyama, S.; Kabsch, K.; Delos, S.; Bouton, A.; White, J. *J Virol* **2006**, *80*, 4174.

(149) Hood, C. L.; Abraham, J.; Boyington, J. C.; Leung, K.; Kwong, P. D.; Nabel, G. J. *J Virol* **2010**, *84*, 2972.

(150) Chen, K. L.; Chang, W. S.; Cheung, C. H.; Lin, C. C.; Huang, C. C.; Yang, Y. N.; Kuo, C. P.; Kuo, C. C.; Chang, Y. H.; Liu, K. J.; Wu, C. M.; Chang, J. Y. *Cancer Lett* **2012**, *317*, 89.

(151) Joyce, J. A.; Hanahan, D. *Cell Cycle* **2004**, *3*, 1516.

(152) Stroup, G. B.; Lark, M. W.; Veber, D. F.; Bhattacharyya, A.; Blake, S.; Dare, L. C.; Erhard, K. F.; Hoffman, S. J.; James, I. E.; Marquis, R. W.; Ru, Y.; Vasko-Moser, J. A.; Smith, B. R.; Tomaszek, T.; Gowen, M. *J Bone Miner Res* **2001**, *16*, 1739.

(153) Ehmke, V.; Quinsaat, J. E.; Rivera-Fuentes, P.; Heindl, C.; Freymond, C.; Rottmann, M.; Brun, R.; Schirmeister, T.; Diederich, F. *Org Biomol Chem* **2012**, *10*, 5764.

(154) Kirschke, H.; Wikstrom, P.; Shaw, E. *FEBS Lett* **1988**, *228*, 128.

(155) Choe, Y.; Leonetti, F.; Greenbaum, D. C.; Lecaille, F.; Bogyo, M.; Bromme, D.; Ellman, J. A.; Craik, C. S. *J Biol Chem* **2006**, *281*, 12824.

(156) Coulombe, R.; Li, Y.; Takebe, S.; Menard, R.; Mason, P.; Mort, J. S.; Cygler, M. *Proteins* **1996**, *25*, 398.

(157) Chowdhury, S. F.; Joseph, L.; Kumar, S.; Tulsidas, S. R.; Bhat, S.; Ziomek, E.; Menard, R.; Sivaraman, J.; Purisima, E. O. *J Med Chem* **2008**, *51*, 1361.

(158) Chowdhury, S. F.; Sivaraman, J.; Wang, J.; Devanathan, G.; Lachance, P.; Qi, H.; Menard, R.; Lefebvre, J.; Konishi, Y.; Cygler, M.; Sulea, T.; Purisima, E. O. *J Med Chem* **2002**, *45*, 5321.

(159) Jo, H.; Meinhardt, N.; Wu, Y.; Kulkarni, S.; Hu, X.; Low, K. E.; Davies, P. L.; DeGrado, W. F.; Greenbaum, D. C. *J Am Chem Soc* **2012**, *134*, 17704.

(160) Lecaille, F.; Weidauer, E.; Juliano, M. A.; Bromme, D.; Lalmanach, G. *Biochem J* **2003**, *375*, 307.

(161) Lecaille, F.; Bromme, D.; Lalmanach, G. *Biochimie* **2008**, *90*, 208.

(162) Shin, M. C.; Zhang, J.; Min, K. A.; Lee, K.; Byun, Y.; David, A. E.; He, H.; Yang, V. C. *J Biomed Mater Res A* **2014**, *102*, 575.

(163) Koren, E.; Torchilin, V. P. *Trends Mol Med* **2012**, *18*, 385.

(164) Duchardt, F.; Fotin-Mleczek, M.; Schwarz, H.; Fischer, R.; Brock, R. *Traffic* **2007**, *8*, 848.

(165) Derossi, D.; Joliot, A. H.; Chassaing, G.; Prochiantz, A. *J Biol Chem* **1994**, *269*, 10444.

(166) Balhorn, R. *Genome Biol* **2007**, *8*, 227.

(167) Huntington, J. A. *Thromb Haemost* **2014**, *111*.

(168) Figueiredo, A. C.; de Sanctis, D.; Gutierrez-Gallego, R.; Cereija, T. B.; Macedo-Ribeiro, S.; Fuentes-Prior, P.; Pereira, P. J. *Proc Natl Acad Sci U S A* **2012**, *109*, E3649.

(169) Francischetti, I. M.; Valenzuela, J. G.; Ribeiro, J. M. *Biochemistry* **1999**, *38*, 16678.

(170) Walensky, L. D.; Kung, A. L.; Escher, I.; Malia, T. J.; Barbuto, S.; Wright, R. D.; Wagner, G.; Verdine, G. L.; Korsmeyer, S. J. *Science* **2004**, *305*, 1466.

(171) Flint, D. G.; Kumita, J. R.; Smart, O. S.; Woolley, G. A. *Chem Biol* **2002**, *9*, 391.

(172) Heinis, C.; Rutherford, T.; Freund, S.; Winter, G. *Nat Chem Biol* **2009**, *5*, 502.

(173) Wüthrich, K. *NMR of proteins and nucleic acids*; Wiley: New York, 1986.

(174) Delaglio, F.; Grzesiek, S.; Vuister, G. W.; Zhu, G.; Pfeifer, J.; Bax, A. *Journal of biomolecular NMR* **1995**, *6*, 277.

(175) Bartels, C.; Xia, T. H.; Billeter, M.; Guntert, P.; Wuthrich, K. *Journal of biomolecular NMR* **1995**, *6*, 1.

(176) Wishart, D. S.; Sykes, B. D.; Richards, F. M. *Biochemistry-Us* **1992**, *31*, 1647.

(177) Wishart, D. S.; Sykes, B. D. *Journal of biomolecular NMR* **1994**, *4*, 171.

(178) Chaudhury, S.; Lyskov, S.; Gray, J. J. *Bioinformatics* **2010**, *26*, 689.

(179) Kortemme, T.; Kim, D. E.; Baker, D. *Sci STKE* **2004**, *2004*, pl2.

(180) Luo, P.; Baldwin, R. L. *Biochemistry* **1997**, *36*, 8413.

(181) Mellgren, R. L.; Repetti, A.; Muck, T. C.; Easly, J. *J Biol Chem* **1982**, *257*, 7203.

(182) Liu, Y.; Kati, W.; Chen, C. M.; Tripathi, R.; Molla, A.; Kohlbrenner, W. *Anal Biochem* **1999**, *267*, 331.

(183) Melo, R. L.; Pozzo, R. C. B.; Alves, L. C.; Perissutti, E.; Caliendo, G.; Santagada, V.; Juliano, L.; Juliano, M. A. *Bba-Protein Struct M* **2001**, *1547*, 82.

(184) Dang, T. H. T.; de la Riva, L.; Fagan, R. P.; Storck, E. M.; Heal, W. P.; Janoir, C.; Fairweather, N. F.; Tate, E. W. *Acs Chem Biol* **2010**, *5*, 279.

(185) Johnson, W. C., Jr. *Proteins* **1990**, *7*, 205.

(186) Bohne, S.; Sletten, K.; Menard, R.; Buhling, F.; Vockler, S.; Wrenger, E.; Roessner, A.; Rocken, C. *J Pathol* **2004**, *203*, 528.

(187) Bromme, D.; Okamoto, K.; Wang, B. B.; Biroc, S. *J Biol Chem* **1996**, *271*, 2126.

(188) Turk, V.; Turk, B.; Turk, D. *EMBO J* **2001**, *20*, 4629.